INTERNATIONAL SCHOOL FOR ADVANCED STUDIES

Condensed Matter Theory Sector

Low temperature methane-to-methanol conversion on transition metal surfaces

An *ab initio* study

Thesis submitted for the degree of

Doctor Philosophiæ

Candidate

Guido Fratesi

Supervisor

Prof. Stefano de Gironcoli

October 2005

Contents

Introduction

The understanding of adsorption phenomena and chemical reactions occurring at surfaces is of central importance for many fields of research in Physics and Chemistry. In particular it is fundamental for heterogeneous catalysis. Our society heavily relies on the use of solid-state catalysts for the production of a great variety of chemical products including high-octane petrol, fertilizers, pharmaceutical chemicals, and margarine. The selectivity of these production processes critically depends on a careful choice of the catalyst, since reaction rates vary exponentially with the activation energy, and reductions in the latter with respect to the homogeneous non-catalysed phase can raise the reaction rate by several orders of magnitude.

In many cases catalysts consist of transition metal nanoparticles dispersed on a support such as silica or carbon. These nanoparticles expose different facets, among which the close-packed ones are probably the most common but other orientations are also present, as well as defects—e.g., steps or missing atoms. As a matter of fact, the truly active sites of a catalyst are often the defective ones. The study of adsorption and reactivity at low-index surfaces and defects thereon is therefore a model investigation of primary relevance and much closer to a real catalyst than one could imagine. Though many informations on this subject may be obtained by means of surface science experiments, a full understanding can often not be reached without the combined resort to numerical simulations.

The introduction of density-functional theory (DFT) in the 1960's [1, 2], together with the steadily increase of accessible computational power and the development of more and more efficient algorithms, has made possible the investigation by means of *ab initio* simulations of systems of continuosly increasing complexity, among which molecule-surface structures. DFT gener-

ally gives correct adsorption sites, binding energies in fair agreement with experiments and adsorption energy differences within few tenths of an eV from the experimental value. Most importantly, simulations disclose researcher's eye on a variety of additional details (e.g., bond-lengths, atomic orbitals occupation, binding energies decomposition into elemental contributions, and so on) which are difficult to obtain experimentally but whose knowledge adds significant insight. For example, for a class of simple reactions it has been possible to elucidate the electronic factors behind the reactivity, understanding its trend across the periodic table of the elements [3].

The second achievement which has made feasible the determination of the activation energy of a reaction has been the development of methods for the identification of saddle points of functions of many variables—in this case the energy of the system as a function of atomic coordinates. The combination of such methods with the *ab initio* calculation of the energy is a powerful tool but requires extensive numerical effort, made available only in very recent times.

Direct methane-to-methanol conversion is one of the current "dream" reactions for researchers in Chemistry and Chemical Physics. Large amounts of methane, whose reserves are enormous and compete with those of petroleum, are not exploited due to difficulties in transportation and storage of gaseous hydrocarbons. On the other hand methanol is a liquid molecule which has many applications in chemical synthesis and it has also been suggested as fuel alternative. Production of methanol from methane is a well established process; however, it proceeds through two high-temperature steps, and it is very energy consuming. It is not convenient for the production of methanol on a large scale. Direct low-temperature conversion of CH_4 to CH_3OH, being exothermic, could have the advantage that no wasted energy is required to drive the reaction. The expectations from this process are enormous, as methanol produced in a cheap way could lower the dependence on liquid petroleum, whose price is continously increasing and reserves are limited. Despite several attempts, no suitable environment/catalyst has been found in order to achieve the process more efficiently than in the traditional way.

In this thesis the possibility of direct low-temperature methane-to-methanol conversion by heterogeneous catalysis operated by transition metals has

been investigated by *ab initio* numerical simulations based on DFT. Two main issues will be addressed: i) since defects may be determinant, as it was mentioned above, attention will be devoted to understand their role, taking as an example the surface of Rh; ii) the effect of the local chemical composition of the substrate will then be studied to point out electronic factors behind the catalytic properties observed towards three simple reactions.

This thesis is organized as follows. In Chapter 1 the problems behind the utilization of many methane reserves will be presented. Methanol potentials will be described. The traditional production scheme and alternative attempts for direct conversion reported in the literature will be reviewed. In Chapter 2 the theoretical framework and tools are introduced. An introduction to methods based on the calculation of the electronic structure for the first-principles determination of species–species and species–catalyst interactions will be given. The special tools required for the evaluation of activation energies will also be described. Chapter 3 addresses the possibility of direct methane-to-methanol conversion on Rh surfaces. The analysis will proceed through the detailed examination of two particular reaction sites on Rh, the clean (111) terrace and a Rh adatom thereon. The motivations underlying this particular choice will be given in detail. From these two cases, the possibility of extending the results to generic Rh surfaces will be assessed. It will be found that other competing processes are more probable than methanol synthesis. Chapter 4 proceeds then through a systematic analysis across the periodic table of the elements, considering three adjacent transition metals in a period (Rh, Pd, Ag), and three in a group (Cu, Ag, Au). None of the clean (111) surfaces of the elements considered here favors methanol formation with respect to competing reactions. However, from the analysis which will be presented, some guidelines in the search for candidate catalysts will be proposed by extrapolation of these results. A model system will be identified for which the activation energy for methanol formation is the lowest among the processes considered, and a possible experimental confirmation will be suggested.

Chapter 1

Prospects and challenges for methane employment

In this chapter the scientific and technological interests towards the conversion of methane to methanol will be presented. Direct conversion would be particularly desirable and currently known attempts for achieving the process will be overviewed.

1.1 Methane: a valuable resource for the future

At present consumption rate, known liquid petroleum reserves can be expected to last for roughly 40 years only. Even though new oil fields are continuosly being discovered, and improved techniques allow recovery from previously exploited ones, production has increased even faster, and it is of primary importance to optimize the use of energy sources minimizing all waste.

In particular, large amount of methane are flared or reinjected due to difficulties in trasportation and storage. Methane (CH_4) is the main component of natural gas, and it is used in domestic and industrial burners for heating and electricity generation, but it also represents a large potential for chemical synthesis. It is frequently produced along with liquid petroleum, from reserves which are often located far from industrial complexes and potential

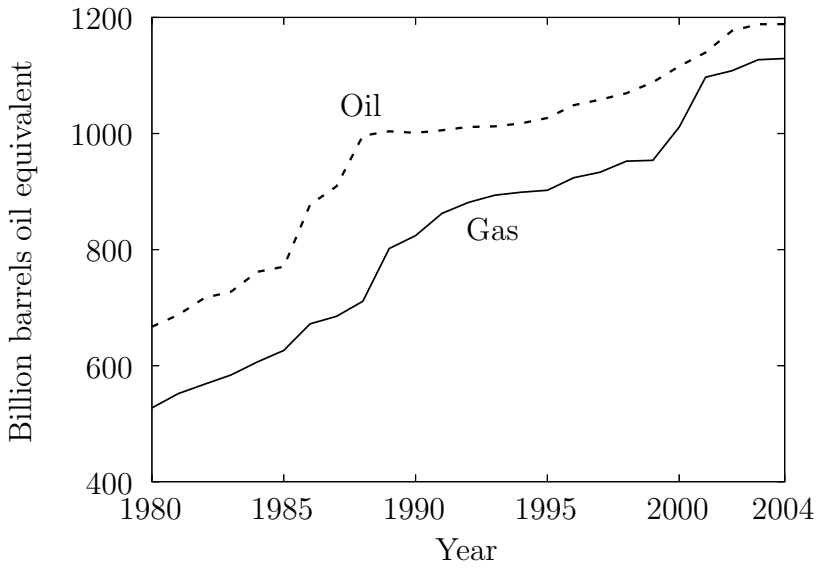

Figure 1.1: Proven world oil and gas reserves. Data taken from Ref. [4].

markets, possibly off-shore. Whereas the displacement of large amount of oil is easy and cheap, it is not always convenient to exploit the natural gas, since liquefaction for shipping requires expensive compression and/or refrigeration, and pipelines may not be available. The wasteful flaring practice has become illegal in many countries, and the gas is mostly reinjected for possible later recovery of the field.

Altogether, methane reserves are comparable with those of liquid petroleum, and their rate of increase is even higher owing to continuous developments and improved technologies (see Fig. 1.1). According to 2004's reserve/production ratio, natural gas would last some 30 years more than oil. For an efficient utilization of this resource, and to avoid the inconvenient reinjection of methane at oil production plants, big efforts are being devoted at the conversion of CH_4 to more useful and easy-to-transport liquid fuels and chemicals. For example, heavier hydrocarbons can be obtained via Fischer-Tropsch synthesis. This is a well established technology already applied on a large scale and has the advantage of producing low-sulphur fuel, but it is limited by high costs.

1.2 Conversion of methane to methanol

Among the different candidate products of methane conversion, methanol (CH_3OH) is probably the one which is recently attracting more interest. It is the simplest alcohol, light, volatile, flammable, and liquid (boiling point: 64.7 °C). This section is devoted to the description of methanol uses and an overview of production methods.

1.2.1 Methanol uses

CH_3OH is commonly used as solvent and antifreeze in pipelines, and as a denaturant for ethyl alcohol, but mainly as:

Raw material

The largest use of methanol is in making other chemicals. The most important of these is formaldehyde, from which many products as various as plastics, plywood, paints, and explosives are obtained. Other derivatives of CH_3OH include dimethyl ether, used as a spray propellant, and acetic acid.

Fuel

Methanol is also a good fuel for internal combustion engines, even though its volumetric power density is half that of gasoline. However, with present production techniques (Sec. 1.2.2), the use as fuel on a large scale is not economically convenient with respect to gasoline. For some special applications, methanol is nevertheless used as fuel, e.g., for drag races: since it is miscible with H_2O, its fires can be extinguished with plain water. Improved methanol synthesis technologies, or the further increase of crude oil costs, would raise interest in the application of CH_3OH for internal combustion engines. Early technoeconomical analysis were even suggesting that CH_3OH would start being competitive with transportation fuels when the crude oil price raised above $\approx$ 27 \$/bbl [5], and this value has largely been passed (higher than 70 \$/bbl at the time of writing).

Hydrogen carrier

For the foreseeable future, many governments and major industries have devoted increasing efforts to develop the so-called "hydrogen economy"—the generation of hydrogen and its use as a clean fuel. (It's worth remembering that H_2 is an energy *carrier* and not an energy *source*, as frequently misunderstood.) In these terms, CH_3OH is an efficient and easy way to store H_2. Hydrogen could be converted into methanol via the traditional methanol synthesis process (see Sec. 1.2.2, where also the production of H_2 will be addressed) at the production site, and then delivered more conveniently in liquid form to the place of usage. There, H_2 can be obtained via a suitable combination of endothermic steam reforming and exothermic partial oxidation ($CH_3OH + H_2O \rightarrow 3H_2 + CO_2 - 131$ kJ/mol and $CH_3OH + 1/2O_2 \rightarrow 2H_2 + CO_2 + 155$ kJ/mol, respectively). An hydrogen vehicle can store methanol and reform it on-board to feed its fuel cell.

Fuel for fuel cells

Perhaps the most tempting application of methanol is the direct use as fuel for the so-called direct methanol fuel cells (DMFC) [6], operative also at low temperature and atmospheric pressure. The electrochemicals reactions at the electrodes are

$$\text{anode:} \quad CH_3OH + H_2O \rightarrow CO_2 + 6H^+ + 6e^-, \tag{1.1}$$

$$\text{catode:} \quad 1.5O_2 + 6H^+ + 6e^- \rightarrow 3H_2O, \tag{1.2}$$

$$\text{overall:} \quad 1.5O_2 + CH_3OH \rightarrow CO_2 + 2H_2O. \tag{1.3}$$

At 25 °C and 1 atm, free energy favors the products of the overall reaction by 686 kJ/mol; the open-circuit voltage is 1.18V. Both reactions are commonly catalyzed by carbon-supported platinum catalysts. For CH_3OH oxidation, candidate better catalysts include Ru-Pt and Pt-Sn alloys. Electrodes are separated by a proton exchange membrane made of, e.g., nafion (a polymer). A schematic design of a DMFC is presented in Fig. 1.2. We will not enter in detail in this rapidly evolving field, but just mention some key differences between hydrogen and methanol fuel cells. The electro-oxidation of hydrogen is a much faster reaction than the oxidation of methanol. Hence, to achieve

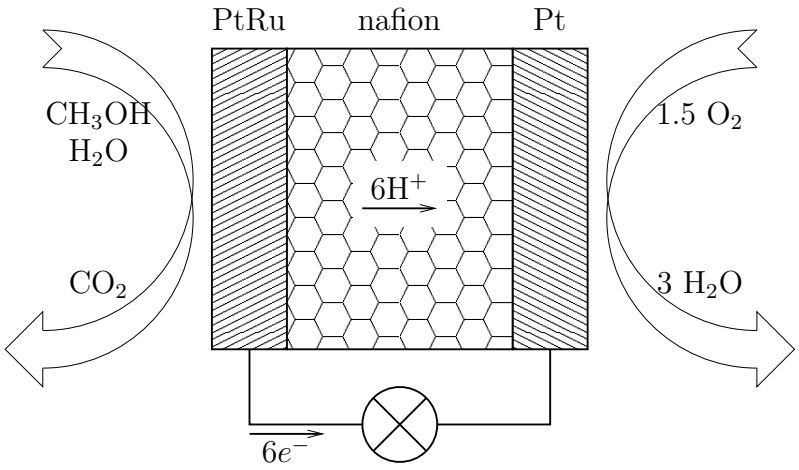

Figure 1.2: Schematic design of a direct methanol fuel cell.

comparable power densties, it's necessary to use improved and/or high Pt loading catalysts (with sensible consequences for the costs of the device). Power densities about one tenth of that of hydrogen loaded fuel cells have been achieved [7]. A further disadvantage is the methanol crossover through the membrane, for which a definite solution has not been found yet, thus lowering fuel efficiency and the cell potential. On the other hand, DMFCs have specific advantages regarding costs, simplicity of design, availability, distribution and easy handling. For example, they can also operate in "passive mode" i.e., with no forced fuel flow and hence no mechanical parts. Nowadays they are rising particular interest as power suppliers for portable applications such as mobile phones or laptop computers.

Towards a methanol economy?

Considering the many difficulties of the hydrogen economy [8], some researchers are incentivating the shift towards a methanol economy—the Nobel laureate George Olah [9] among them.

In this hypothetical scenario, methanol is meant as a convenient energy carrier. It would be produced by oxidation of methane (Sec 1.2.3) and, in the longer term, by carbon dioxide recycling of CO_2 with hydrogen, with the additional benefit of reducing the amount of green-house gases. Carbon

dioxide could be obtained from power or industrial plants, or filtered from the atmosphere if some new efficient way to filter the low-concentration CO_2 (0.037%) are developed. The seas are unlimited sources of H_2, through electrolysis of water. In this way, nuclear energy and energy from all suitable alternate sources would be stored as liquid CH_3OH.

Methanol would then replace fossil fuels. It would be used as fuel in internal-combustion engines. Hydrocarbons and their products would be synthesized from it. Electric energy could be obtained from fuel cells with very high efficiency.

With respect to hydrogen, methanol has also other advantages. The volumetric power density of methanol is 50% higher than that of liquid hydrogen. Moreover, the infrastructures required for distribution of compressed or refrigerated H_2 are extremely expensive, whereas no such large investment would be required for the liquid CH_3OH.

1.2.2 Traditional indirect production of methanol

Methanol is currently produced from methane in a two step process: syngas—a mixture of H_2 and CO—is produced, then methanol is synthesized from it. This process, in particular the first step, is quite expensive and limiting the large scale application of methanol.

Methane is now the most common source for syngas production, originally obtained from coal. Different methods are available, but each of them has its disadvantages. Steam and carbon dioxide reforming ($CH_4 + H_2O \rightarrow CO + 3H_2 - 206$ kJ/mol and $CH_4 + CO_2 \rightarrow 2CO + 2H_2 - 247$ kJ/mol) are highly endothermic and affected by heat transfer limitations. They proceed at high temperatures (900 °C), the heat being supplied by large amounts of fuel fired near the reaction tubes. Partial oxidation ($CH_4 + 1/2O_2 \rightarrow CO + 2H_2 + 35$ kJ/mol) is slightly exothermic and usually requires low investments. However, the need of nearly pure oxygen can be fulfilled only by expensive air separation units. In autothermal reforming, the required heat for steam reforming is produced by combustion of part of the methane with supplied oxygen ($CH_4 + 3/2O_2 \rightarrow CO + 2H_2O + 520$ kJ/mol). This has been indicated as the cheapest solution with current technologies [10], but it still requires

the oxygen separation unit.

The synthesis of CH_3OH from syngas dates back to 1923, when the technology to hydrogenate CO was commercialized by BASF. The reaction is

$$CO + 2H_2 \rightarrow CH_3OH + 91 \text{ kJ/mol.} \tag{1.4}$$

The process is limited to low conversion per pass and it's strongly exothermic, thus implying large recycle of the unconverted gas and considerable cooling effort. Both factors affect significantly production costs. At that time, a ZnO-Cr_2O_3 catalyst working at 240–300 bar and 350–400 °C was used. Modern methanol production has been made more efficient through the use of the more active copper/zinc/alumina catalyst, introduced in 1966. Owing to the higher activity, this catalyst is capable of operating at lower temperatures and pressures, 60–80 bar and 250–280 °C respectively. The lower temperature also enhances methanol selectivity by suppressing side reactions. Remarkably, on Cu-based catalysts, reaction (1.4) does not take place directly. Instead, the synthesis proceeds through the formation of carbon dioxide via the water-gas shift reaction followed by CO_2 hydrogenation: $CO + H_2O \rightarrow CO_2 + H_2$, $CO_2 + 3H_2 \rightarrow CH_3OH + H_2O$ [11].

1.2.3 Attempts for direct methane-to-methanol conversion

The direct oxidation of methane to methanol would avoid the expensive syngas generation. Conceptually, it is the sum of partial oxidation of CH_4 to CO and H_2 and the hydrogenation of CO:

$$CH_4 + 1/2O_2 \rightarrow CH_3OH + 126 \text{ kJ/mol.} \tag{1.5}$$

The process is exothermic and no wasted energy is required to drive the reaction. In principle, methods based on reaction (1.5) should be preferrable with respect to indirect ones, but to date the low yields obtained are preventing their large scale commercial application.

Gas-phase partial oxidation of methane to methanol has been investigated by several groups. To our knowledge, the best results have been obtained by Zhang *et al.* [12]. They reported 7–8% CH_3OH yield at 430–470 °C

and 5.0 MPa, too low to compete with the indirect process. This process, operated by a free radical mechanism, is difficult to control. It is therefore expected that large improvements in selectivity and yield could be achieved by finding a suitable catalyst. This is indeed a formidable challenge, since catalysts may favor competing reaction and reduce the yield of methanol. For example, the heterogeneous catalysis operated by the steel walls of the reactor enhances total oxidation [13] (the results quoted above refer to the use of a quartz-lined reactor).

The homogeneous catalysis by gas-phase transition metal oxide cations, MO^+, has also been investigated, following the observation that gas-phase FeO^+ converts methane to methanol [14]. It is believed that the reaction proceeds through the formation of a metastable hydroxo intermediate OH–M^+–CH_3 [15]. The studies on the magnetic FeO^+ are also of theoretical interest, because spin-orbit coupling can be important: the potential energy surfaces corresponding to quartet and sextet states lie close, and involve three junctions that can provide a chance of spin-forbidden transition, leading to a significant decrease of the activation energies [16].

In a completely different approach, more aimed at achieving the conversion in relatively mild conditions, promising results have been obtained by Periana *et al.* [17] by using a bipyramidil platinum (II) complex in concentrated H_2SO_4. At 220 °C, methyl bisulfate (CH_3OSO_3) is produced at high conversion (90%) and selectivity (81%). Subsequent hydrolysis could then form methanol and regenerate H_2SO_4. The 73% yield is impressively higher than the ones achieved with other methods, but there are still concerns about costs, environmental aspects, and the use of relatively high temperatures.

It should also be mentioned that direct methane-to-methanol conversion is already operated in nature by the methane mono-oxygenase enzyme found in methanotrophic bacteria. The enzyme contains iron centers in the active site, and at the key intermediate it has a $Fe_2^{IV}O_2$ diamond-shaped structure [18]. Researchers have also tried following this example, but low methane conversions have been obtained.

In this overview of the attempts for direct methane-to-methanol conversion, the absence of studies on heterogeneous catalysis is considerable. The present thesis, reporting results of numerical simulations of the conversion on Rh and other transition metal surfaces, is a contribution in this area.

Chapter 2

Numerical simulations for the study of catalysis

To investigate the activity of a catalyst towards a given reaction, the knowledge of some physical quantities is of fundamental importance. Adsorption energies and sites of the various species, reaction enthalpies, and activation energies are certainly among them. Though these quantities can in many cases be measured, numerical simulations are useful for several aspects, starting from the interpretation of experimental results, up to the study of systems for which the experiment is difficult or even impossible to be performed, and to the determination of quantities which are not directly experimentally measurable.

Since in this thesis the result of numerical simulations for the catalytic activity of transition metals in direct methane-to-methanol conversion will be presented, the theoretical methods used will be described in this chapter.

2.1 *Ab initio* electronic structure calculations

The Born-Oppenheimer approximation has been adopted for the separation of the electronic and ionic degrees of freedom. Then density-functional theory was used for the solution of the electronic problem. The approach chosen has the advantage that interatomic interactions are evaluated in a fully *ab initio* framework with no adjustable parameters, i.e., no empirical atom-atom

potential is used.

2.1.1 The Born-Oppenheimer approximation

For determining the properties of a system of interacting $N_{\rm el}$ valence electrons and $N_{\rm I}$ ions[1] one has to solve the Schrödinger equation for the wavefunction $\Psi(\mathbf{R},\mathbf{r})$ and the hamiltonian

$$\begin{aligned} H &= -\sum_{I=1}^{N_{\rm I}} \frac{\hbar^2}{2M_I}\nabla^2_{\mathbf{R}_I} - \sum_{i=1}^{N_{\rm el}} \frac{\hbar^2}{2m_e}\nabla^2_{\mathbf{r}_i} \\ &\quad + \sum_{i<j} \frac{e^2}{|\mathbf{r}_i-\mathbf{r}_j|} - \sum_{i,I} \frac{Z_I e^2}{|\mathbf{r}_i-\mathbf{R}_I|} + \sum_{I<J} \frac{Z_I Z_J e^2}{|\mathbf{R}_I-\mathbf{R}_J|}, \end{aligned} \tag{2.1}$$

where i and I are indexes for the electrons and ions, respectively, M_I and eZ_I are the mass and charge of the I-th ion, m_e and $-e$ the electron mass and charge, and $\mathbf{R} = \{\mathbf{R}_1,\ldots,\mathbf{R}_{N_{\rm I}}\}$ and $\mathbf{r} = \{\mathbf{r}_1,\ldots,\mathbf{r}_{N_{\rm el}}\}$ are the ionic and electronic coordinates. Spin indexes are implicitely understood where needed. The basic approximation under a practical treatment of this hamiltonian is in most cases the separation of the electronic and ionic degrees of freedom, proposed by Born and Oppenheimer in 1927. It consists in writing the wavefunction $\Psi(\mathbf{R},\mathbf{r})$ in the factorized form

$$\Psi(\mathbf{R},\mathbf{r}) = \Phi(\mathbf{R})\psi_{\mathbf{R}}(\mathbf{r}), \tag{2.2}$$

where the electronic wavefunction ψ depends parametrically on the ionic positions, and in neglecting the non-adiabatic terms which arise from the ionic kinetic operator acting on the electronic wavefunction. The Schrödinger equation $H\Psi = \mathcal{E}\Psi$ then factorizes into two separate equations for the ions and the electrons:

$$\left(-\sum_{I=1}^{N_{\rm I}} \frac{\hbar^2}{2M_I}\nabla^2_{\mathbf{R}_I} + E(\mathbf{R})\right)\Phi(\mathbf{R}) = \mathcal{E}\Phi(\mathbf{R}), \tag{2.3}$$

$$\left(-\sum_{i=1}^{N_{\rm el}} \frac{\hbar^2}{2m_e}\nabla^2_{\mathbf{r}_i} + V_{\text{el-el}} + V_{\text{el-I}} + V_{\text{I-I}}\right)\psi_{\mathbf{R}}(\mathbf{r}) = E(\mathbf{R})\psi_{\mathbf{R}}(\mathbf{r}), \tag{2.4}$$

[1] It is assumed that the most relevant chemical properties of the system are determined by the valence electrons, whereas the core electrons can be thought as fixed in their atomic configuration.

where we have abbreviated with $V_{\text{el-el}}$, $V_{\text{el-I}}$, and $V_{\text{I-I}}$ the third, fourth, and fifth term in Eq. (2.1), respectively. The electronic hamiltonian in Eq. (2.4) will be indicated in the following as $H_{\text{el}}(\mathbf{R})$. Equations (2.3) and (2.4) are coupled via the term $E(\mathbf{R})$, which acts as a potential term in the ions hamiltonian and is determined by the solution of the electronic problem at fixed ionic positions. $E(\mathbf{R})$ is known as the Born-Oppenheimer *potential energy surface* (PES).[2]

The Born-Oppenheimer approximation is physically grounded because of the large mass difference between the two classes of particles. Since electrons are much lighter than ions, their motion is much faster and their excitation energy is much larger, so one can assume the electronic configuration to be relaxed in the ground state of Eq. (2.4) for any position of the ions, hence the parametric dependence of $\psi_{\mathbf{R}}(\mathbf{r})$ on $\mathbf{R}$.

Once the PES has been evaluated, Eq. (2.3) can be solved either quantum-mechanically or approximated by its classical counterpart $M_I\ddot{\mathbf{R}}_I = \mathbf{F}_I$, with the forces $\mathbf{F}$ given by the Hellmann-Feynman theorem:

$$\mathbf{F}_I = -\frac{\partial E(\mathbf{R})}{\partial \mathbf{R}_I} = -\left\langle \psi_{\mathbf{R}}(\mathbf{r}) \left| \frac{\partial H_{\text{el}}(\mathbf{R})}{\partial \mathbf{R}_I} \right| \psi_{\mathbf{R}}(\mathbf{r}) \right\rangle . \tag{2.5}$$

Stable and metastable ionic configurations reported in this thesis have been obtained within a classical treatment of the ions, minimizing $E(\mathbf{R})$ with respect to $\mathbf{R}$.

Thanks to the simplification provided by the Born-Oppenheimer separation of the degrees of freedom, the major difficulty is confined to the solution of the electronic equation (2.4). This, however, is still a formidable task because of the electron-electron interaction: $\psi_{\mathbf{R}}(\mathbf{r})$ depends on the coordinates of all the electrons and cannot be factorized in single-particle contributions. A solution is provided by density-functional theory.

[2]Since $H_{\text{el}}(\mathbf{R})$ has many eigenvalues, $\{E_\mu(\mathbf{R})\}$, a PES can be defined for each of them. One is usually interested in the one corresponding to the lowest eigenvalue, $\mu = 0$, called "ground-state PES". In the following, only this specific choice, $E(\mathbf{R}) = E_0(\mathbf{R})$, will be considered.

2.1.2 Density-functional theory

The ground state energy $E(\mathbf{R})$ and wavefunction $\psi_{\mathbf{R}}(\mathbf{r})$ of the electronic hamiltonian $H_{\text{el}}(\mathbf{R})$ of Eq. (2.4) at fixed ionic positions can formally be found by minimizing $\langle\psi_{\mathbf{R}}|H_{\text{el}}(\mathbf{R})|\psi_{\mathbf{R}}\rangle$ subject to the normalization requirement on $\psi_{\mathbf{R}}$. The problem is that $\psi_{\mathbf{R}}$ is a function of the $3N_{\text{el}}$ variables $\{\mathbf{r}_1,\ldots,\mathbf{r}_{N_{\text{el}}}\}$. The important advantages provided by density-functional theory (DFT) are the reformulation of this problem in terms of the electronic density, depending on three space coordinates only, and the introduction of an easy-to-handle single-particle formalism.

Hohenberg and Kohn [1] have demonstrated that there is a one-to-one relationship between the external potential V_{ext} ($V_{\text{ext}} = V_{\text{el-I}}$) and the ground state electron density $n_0(\mathbf{x})$.[3] Furthermore, they have stated that there exists a unique universal[4] functional $F[n(\mathbf{x})]$ of the electron density such that the total energy functional defined by

$$E[n(\mathbf{x})] = F[n(\mathbf{x})] + \int V_{\text{ext}}(\mathbf{x})n(\mathbf{x})\mathrm{d}\mathbf{x} \tag{2.6}$$

is minimized for $n(\mathbf{x}) = n_0(\mathbf{x})$, with the requirement that the total number of electrons is preserved. So in order to determine the ground state energy and density it is sufficient to minimize a functional of the electronic density, which depends on three variables only. The problem is that the functional dependence of $E[n]$ must be determined.

The second development was introduced by Kohn and Sham [2], and consists in mapping the original interacting problem into an auxiliary non-interacting one, constructed such as to have the same electron density as the real system. In this way, $n_0(\mathbf{x})$ can be rather easily evaluated taking advantage of the ficticious system,

$$n_0(\mathbf{x}) = \sum_i f_i|\varphi_i(\mathbf{x})|^2, \tag{2.7}$$

where i labels the non-interacting states $\{\varphi_i\}$, and f_i is the occupation of the state according to Fermi-Dirac distribution. The wavefunctions $\{\phi_i\}$ are the

[3] $\mathbf{x} = (x, y, z)$ is chosen as the label for the spatial coordinate, to make clear the distinction with the electronic coordinates $\mathbf{r} = \{\mathbf{r}_1,\ldots,\mathbf{r}_{N_{\text{el}}}\}$. The parametrical dependence on $\mathbf{R}$ is implicitely understood.

[4] That is, not depending on the specific form of the external potential.

solutions of a single particle Schrödinger equation:

$$H_{\rm KS}\varphi_i(\mathbf{x}) = \left(-\frac{\hbar^2\nabla^2}{2m_e} + V_{\rm KS}(\mathbf{x})\right)\varphi_i(\mathbf{x}) = \epsilon_i\varphi_i(\mathbf{x}). \tag{2.8}$$

The problem has thus been converted in the identification of the effective Kohn-Sham (KS) potential $V_{\rm KS}$, acting on the electrons of the ficticious system. To this end, one observes that the Hohenberg-Kohn theorem can be applied to the auxiliary problem, and in this case the density functional $F[n]$ corresponds to the kinetic energy of non-interacting electrons $T_0[n]$. This suggests to write the universal functional for the interacting system as

$$F[n(\mathbf{x})] = T_0[n(\mathbf{x})] + \frac{e^2}{2}\int\frac{n(\mathbf{x})n(\mathbf{x}')}{|\mathbf{x}-\mathbf{x}'|}{\rm d}\mathbf{x}{\rm d}\mathbf{x}' + E_{\rm xc}[n(\mathbf{x})], \tag{2.9}$$

where the classical Coulomb interaction has been put in evidence, and all many-body effects not described by the first two terms enter the so called exchange-correlation energy, $E_{\rm xc}[n(\mathbf{x})]$, discussed below in greater detail. The KS potential is then determined by requiring that the functional of Eq. (2.9) and the non-interacting one are minimized by the same electron density n_0, and is

$$V_{\rm KS}(\mathbf{x}) = V_{\rm ext}(\mathbf{x}) + e^2\int\frac{n(\mathbf{x})}{|\mathbf{x}-\mathbf{x}|}{\rm d}\mathbf{x} + V_{\rm xc}(\mathbf{x}), \tag{2.10}$$

$$V_{\rm xc}(\mathbf{x}) = \frac{\delta E_{\rm xc}[n]}{\delta n(\mathbf{x})}. \tag{2.11}$$

Finally, making use of Eq. (2.8), the total energy can be expressed as

$$\begin{aligned} E[n(\mathbf{x})] &= \sum_i f_i\epsilon_i - \frac{e^2}{2}\int\frac{n(\mathbf{x})n(\mathbf{x}')}{|\mathbf{x}-\mathbf{x}'|}{\rm d}\mathbf{x}{\rm d}\mathbf{x}' + E_{\rm xc}[n(\mathbf{x})] \\ &\quad - \int V_{\rm xc}(\mathbf{x})n(\mathbf{x}){\rm d}\mathbf{x} + \sum_{I,J}\frac{Z_IZ_Je^2}{|\mathbf{R}_I-\mathbf{R}_J|}. \end{aligned} \tag{2.12}$$

This is how PESs have been evaluated in this thesis.

The formalism presented so far is *exact*. However, the true functional form of the exchange-correlation energy is not known. As a matter of fact, Eq. (2.9) is not much more than a formal definition of $E_{\rm xc}[n(\mathbf{x})]$. All our ignorance about the many-body problem has been just moved into this term

and the above derivation is useful whenever the third term in Eq. (2.9) is small or some suitable approximation can be found. The earliest and simplest of such approximations is to replace $E_{\rm xc}$ locally by the one of an homogeneous electron gas of the same point-wise density. This is known as the local-density approximation (LDA) [2]. The exchange correlation energy and potential are expressed as

$$E_{\rm xc}^{\rm LDA}[n] = \int \varepsilon_{\rm xc}^{\rm hom}(n(\mathbf{x}))n(\mathbf{x})\mathrm{d}\mathbf{x}, \tag{2.13}$$

$$V_{\rm xc}^{\rm LDA}(\mathbf{x}) = \frac{\delta E_{\rm xc}^{\rm LDA}}{\delta n(\mathbf{x})} = \left.\frac{\partial \varepsilon_{\rm xc}^{\rm hom}(n)n}{\partial n}\right|_{n=n(\mathbf{x})}, \tag{2.14}$$

where $\varepsilon_{\rm xc}^{\rm hom}(n)$ is the exchange-correlation energy density of the homogeneous electron gas of density n. LDA is exact in the limit of high density or of a slowly varying density distribution, and works quite well also for the description of weakly correlated materials. A possible improvement upon LDA is the inclusion of the dependence of the gradient of the density, the so called generalized gradient approximation (GGA):

$$E_{\rm xc}^{\rm GGA}[n] = \int \varepsilon_{\rm xc}^{\rm GGA}(n(\mathbf{x}), |\nabla n(\mathbf{x})|)n(\mathbf{x})\mathrm{d}\mathbf{x}, \tag{2.15}$$

where $\varepsilon_{\rm xc}^{\rm GGA}$ can be described in several forms. The GGA usually provides binding energies in closer agreement to experiments than LDA, and has been adopted in this work in the formulation of Perdew, Burke, and Ernzherof [19].

Implementation

The solution of the KS equation (2.8) is by no means trivial since the wavefunctions $\{\phi_i\}$ enter the expression of the effective potential in Eq. (2.10) via the charge density. To solve the system an iterative method is usually adopted, starting from some initial guess for the wavefunctions and potential, and updating both up to self-consistency. One also takes advantage from the variational principle, which states that errors in the total energy depend quadratically on errors in the wavefunction. To this purpose, a slightly modified form of Eq. (2.12), equivalent at self-consistency but quadratic in the error at all the steps of the iterative procedure, is customary adopted.

As for the application to extended systems, it is often convenient to assume that they form periodically repeated infinite structures. Surfaces are then modelled by slabs of finite thickness, embedded in boxes with periodic boundary conditions in the three dimensions. Eq. (2.8) is conveniently expanded in a plane wave basis set, taking advantage from efficient algorithms such as the Fast Fourier Transform. Moreover, the evaluation of the forces in this framework is rather direct and almost costless [20].

The expansion is done on a finite number of basis functions corresponding to a given maximum kinetic energy. Since the accurate description of the wavefunctions close to the ionic cores would require an enormous number of plane waves, the pseudopotential method in the Vanderbilt's ultrasoft flavour is used [21]. This consists in replacing the ionic potential with some smoothened form which gives the same atomic eigenvalues and, outside a chosen core region, the same eigenvectors as the original atomic potential. The requirement of norm conservation of the wavefunctions is released and the true charge density is restored by the use of an overlap operator.

These procedures are implemented in the ESPRESSO simulation package [22] used for the numerical simulations presented in the forthcoming chapters. Further details on the computational tools are provided in appendix B.

2.2 Methods for the study of thermally activated processes

Chemical reactions are often thermally activated processes, events occurring on time scales which are exponentially longer as the temperature is lowered, but for which the microscopic dynamics is temperature-indipendent and characterized by large frequencies. At low temperatures, they are macroscopically perceived as slow phenomena, but the reason for this is that the process (a barrier overcoming) is a microscopically fast but rare event.

A simplified picture of a thermally activated process is given in Fig. 2.1. The system is characterized by two stable configurations, henceforth referred as reactants or initial state (IS) and products or final state (FS), which are

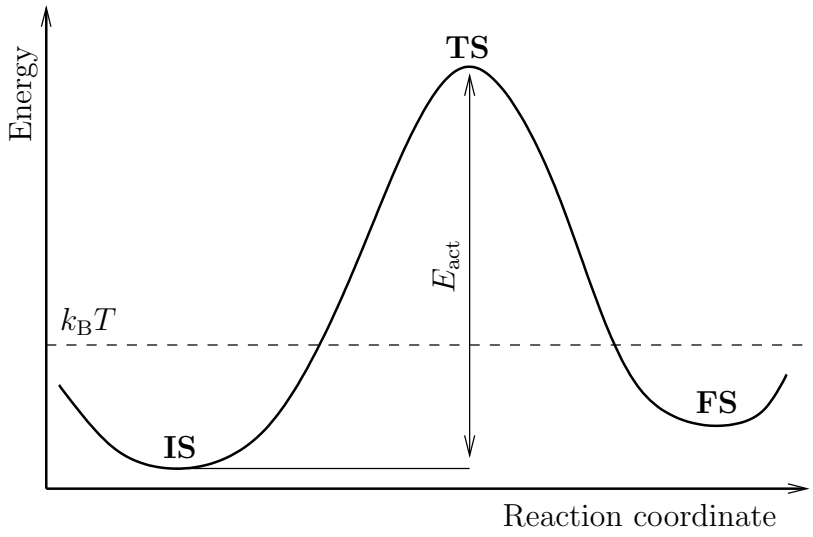

Figure 2.1: Simplified picture of a thermally activated process in one dimension. Whenever the thermal energy $k_{\mathrm{B}}T$ is much lower than the activation energy E_{act} the barrier crossing is a rare event.

represented as local minima in the PES. IS and FS are separated by an energy barrier whose height is called activation energy, E_{act}. The activated transition from the IS to the FS occurs with a probability of the order of $\mathrm{e}^{-E_{\mathrm{act}}/k_{\mathrm{B}}T}$ (see below). Hence, whenever $E_{\mathrm{act}} \gg k_{\mathrm{B}}T$, jumps would occur rarely, while the system will spend most of the time either in the IS or the FS.[5] For these reasons the simulation of thermally activated processes requires special tools which will be overviewed in the remaining of this chapter.

2.2.1 Transition-state theory

The time evolution of a system can be probed in a direct way by molecular dynamics (MD) simulations. In MD, Newton equation is solved iteratively by determining the atomic position at the subsequent step according to the velocities and the forces, the latter evaluated either by *ab initio* methods or by empirical interatomic potentials. For an accurate integration of the

[5]For example, for a reaction with an activation energy of 1 eV and a typical frequency of 10–100 THz, at 300K a transition will occur on the average every $\approx$ 40–400 minutes.

equation of motion, the time step must be chosen smaller than any time scale of the system in order to follow the fastest oscillations. Typically, vibration frequencies are of the order of 10^{14} Hz, and the time step cannot be chosen much longer than 10^{-15} s. As a consequence, the maximum length of a MD simulation is $\approx 10^{-15}$ s $\times N_{\text{step}}$, where N_{step} is the number of iterations one can afford to do, depending on the available computational power, on the system size and on the method used to compute the forces. Generally, simulations in a range between 10^{-13} and 10^{-8} s are accessible. For the method to be fruitful, the MD simulation must be longer than the time scales of the phenomena under study. It's then evident that MD cannot be applied to the time evolution of systems characterized by length scales spanning several order of magnitudes, since the ratio between the largest and the smallest frequency roughly determines the minimum number of steps of a useful simulation.

Thermally activated processes belong to this class of problems. Referring again to Fig. 2.1, MD can be applied to the description of the oscillations around the two minima, but not to the jumps from one side of the barrier to the other. An unreasonably long simulation would be necessary for the evaluation of the transition probability, since jumps would occur rarely whenever $E_{\text{act}} \gg k_{\text{B}}T$.

The transition rate can be more easily evaluated by a statistical approach known as *transition-state theory* (TST). This neglects all deviations from the thermodynamic equilibrium distribution, and rely on the assumption of the existence of a dividing surface between the reactants and products—the transition state (TS).

The TST rate k for the process IS→TS→FS is given by the probability of being at the TS with the velocity pointing towards the FS. In the one dimensional picture of Fig. 2.1, one has

$$\begin{aligned} k &= \frac{\langle \frac{p}{m}\delta(q-q^{\text{TS}})\theta(p)\rangle}{\langle\theta(q-q^{\text{TS}})\rangle} \\ &= \frac{1}{\langle\theta(q-q^{\text{TS}})\rangle}\frac{\mathrm{e}^{-\beta E(q^{\text{TS}})}}{\beta}, \end{aligned} \tag{2.16}$$

where $\{q,p\}$ are the generalized position and momentum, and $E(q)$ is the Born-Oppenheimer PES. The denominator $\langle\theta(q-q^{\text{TS}})\rangle$ can be evaluated

easily if one also assumes that the PES can be described around the IS within the harmonic approximation. Expanding the PES as $E(q) = E(q^{\mathrm{IS}}) + \frac{1}{2}E''(q^{\mathrm{IS}})(q - q^{\mathrm{IS}})^2$ one obtains

$$\langle \theta(q - q^{\mathrm{TS}}) \rangle = \frac{2\pi \mathrm{e}^{-\beta E(q^{\mathrm{IS}})}}{\beta \omega(q^{\mathrm{IS}})}, \tag{2.17}$$

where the frequency $\omega(q)$ is defined as $\sqrt{\frac{E''(q)}{m}}$. For the rate constant one finally has the celebrated Van't Hoff-Arrhenius law:

$$k = \frac{1}{2\pi} \omega(q^{\mathrm{IS}}) \mathrm{e}^{-\beta E_{\mathrm{act}}}. \tag{2.18}$$

To generalize the result to $3N$ coordinates, one notices that a saddle point separates two minima.[6] The $3N - 1$ surface dividing the IS and TS can be chosen orthogonal to the normal mode with imaginary frequency at the saddle point. As a consequence, the saddle point is a local minimum of the PES on the dividing surface and plays the role of TS. Assuming that the harmonic approximation holds for all $3N$ coordinates around the IS and for the $3N - 1$ coordinates on the dividing surface around the TS, Eq. (2.18) becomes

$$k = \frac{1}{2\pi} \frac{\prod_{\mu=1}^{3N} \omega(q^{\mathrm{IS}})_\mu}{\prod_{\mu=1}^{3N-1} \omega(q^{\mathrm{TS}})_\mu} \mathrm{e}^{-\beta E_{\mathrm{act}}}. \tag{2.19}$$

Eq. (2.19) indicates that only zero-temperature, local properties of the PES around the IS and TS are necessary for the evaluation of the transition rate. Moreover, only the energy difference between the TS and the IS is crucial in determining the temperature dependece of k. Summarizing, it has been shown that the problem of characterizing a rare event can be transformed into the search for the saddle points of the PES of the system. This still is an uneasy task, since locating saddle points is much more difficult than locating minima because methods based on the first derivatives only do not converge to unstable stationary points, and evaluating second derivatives is generally expensive and not convenient. A different, more appropriate, approach will be described in the forthcoming section.

[6] In general, more than one saddle points might separate the two minima, as is the case for different mountain passes from one side to the other of a chain of mountains. The following discussion applies to each of them separately.

2.2.2 The nudged elastic band method

The saddle point between two minima IS and FS of the PES can be identified by noticing that it is the highest point of the so called *minimum energy path* (MEP). This is a path $\mathbf{R}(s)$ in the space of configurations, with extrema at IS and FS, with the property of being everywhere parallel to the gradient of the PES or, in other words, that the components of the forces orthogonal to the path are zero:[7]

$$\boldsymbol{\nabla} E\left(\mathbf{R}(s)\right) - \big(\boldsymbol{\tau}(s) \cdot \boldsymbol{\nabla} E\left(\mathbf{R}(s)\right)\big)\boldsymbol{\tau}(s) = 0. \tag{2.20}$$

Here s is an arbitrary reaction coordinate parametrizing the MEP, and $\boldsymbol{\tau}(s)$ is the tangent vector. All the activation energies reported in this thesis have been evaluated solving Eq. (2.20) by means of the nudged elastic band method (NEB) proposed by Jóhnsson, Mills, and Jacobsen [23], recently implemented by Sbraccia [24] in the ESPRESSO simulation package [22], and briefly described in the following.

For practical purposes, the continuous path is discretized into a finite sequence of "images" of the system (chain) $\{\mathbf{R}^{(i)}\}_{i=1}^{N_{\text{imag}}}$, where the subscript (i) labels the images. One writes Eq. (2.20) for each image in the chain,

$$\boldsymbol{\nabla} E\left(\mathbf{R}^{(i)}\right) - \big(\boldsymbol{\tau}^{(i)} \cdot \boldsymbol{\nabla} E\left(\mathbf{R}^{(i)}\right)\big)\boldsymbol{\tau}^{(i)} = -\mathbf{F}_{\perp}(\mathbf{R}^{(i)}) = 0, \quad i = 1, \ldots, N_{\text{imag}}, \tag{2.21}$$

where the tangent is approximated as $\tau^{(i)} = \frac{\mathbf{R}^{(i+1)} - \mathbf{R}^{(i-1)}}{|\mathbf{R}^{(i+1)} - \mathbf{R}^{(i-1)}|}$ or other more accurate expression, and the symbol $\mathbf{F}_{\perp}(\mathbf{R}^{(i)})$ is introduced for the projection of the forces orthogonal to the path tangent. Solving the above set of equations is equivalent to minimizing for each image the energy on the hyperplane orthogonal to the path. Given an initial estimate of the MEP e.g., a linear interpolation between IS and FS, the solution can be reached iteratively by evolving each image according to a ficticious dynamics with forces given by $\mathbf{F}_{\perp}(\mathbf{R}^{(i)})$, until these are zero to the desired accuracy (see Fig. 2.2 for a simple example). Though in principle converging to the MEP, the approach described so far would be unusable in practice: in general, images

[7] For the case of several saddle points mentioned in the note at page 24, a path with the properties required for being a MEP can be identified for each of them. Usually, the most interesting one is then the one with the lowest activation energy.

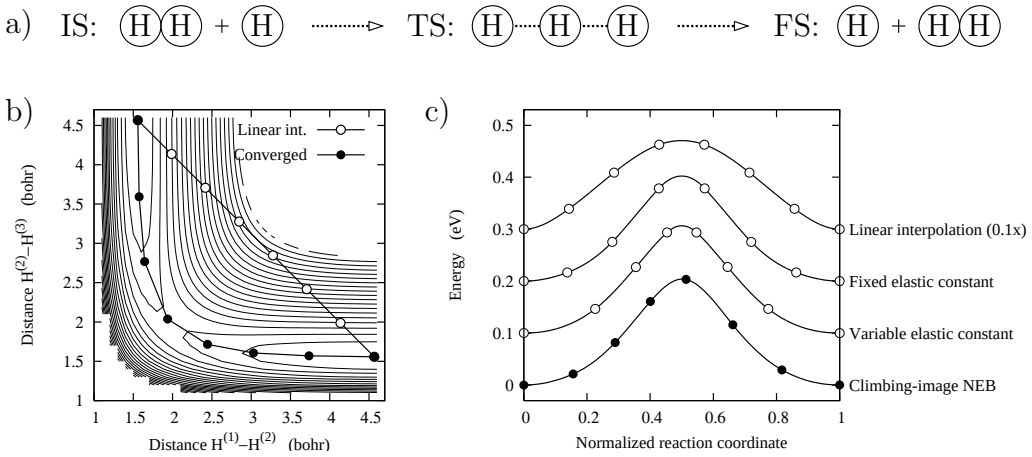

Figure 2.2: Simple example of the application of the NEB method to the determination of the energy barrier of a thermally activated process—the collinear proton transfer in H_2+H→H+H_2. a) Reaction mechanism. b) Contour lines of the two-dimensional PES. The straight line with empty symbols is the initial guess for the discretized path as obtained from linear interpolation. The curved line with filled symbols is the minimum-energy path. Isolines refer to values spaced by 0.1 eV. c) Potential energy profile along the path. The origin of the energy axis for the different curves is shifted for clarity. From top to bottom: the linear interpolation guess (×0.1); after convergence; after convergence, with springs stiffer close to the saddle point (images get closer to the TS); after convergence, with the climbing-image procedure (one image "climbs" up to the TS).

will eventually collapse to the minima, since the evaluation of the tangent is approximated and a residual component of the forces parallel to the path would anyhow be present.

To avoid the sliding down of the images, in NEB virtual springs of zero rest-length are also introduced. The path is described as an elastic band, called *nudged* because the elastic forces are projected along the path's tangent so that images are kept approximatively equispaced without deforming the path. The total force acting on the image i during the ficticious dynamics is

thus

$$\begin{aligned}\mathbf{F}(\mathbf{R}^{(i)}) &= \mathbf{F}_{\perp}(\mathbf{R}^{(i)}) + \mathbf{F}_{\parallel}^{\text{springs}}(\mathbf{R}^{(i)}) \\ &= -\left[\boldsymbol{\nabla} E\left(\mathbf{R}^{(i)}\right) - \left(\boldsymbol{\tau}^{(i)} \cdot \boldsymbol{\nabla} E\left(\mathbf{R}^{(i)}\right)\right)\boldsymbol{\tau}^{(i)}\right] \\ &\quad -k\left[\boldsymbol{\tau}^{(i)} \cdot \left(\mathbf{R}^{(i+1)} + \mathbf{R}^{(i-1)} - 2\mathbf{R}^{(i)}\right)\right]\boldsymbol{\tau}^{(i)}, \end{aligned} \tag{2.22}$$

where k is the elastic constant of the springs. The value of k may significantly affect the speed of the algorithm, but does not influence the result. At convergence $\mathbf{F}(\mathbf{R}^{(i)}) = 0$, thus Eq. (2.21) is satisfied for any positive value of k. As a matter of fact, it is also possible to set different elastic constants for the various springs without modifying the shape of the path. This can be used to tune the inter-image distance: for example, by adopting stiffer springs near points of higher energy, images become denser close to the saddle point than at the path extrema, thus increasing the resolution at the most important points (Figure 2.2c).

Unless very special cases, none of the N_{imag} images will be located *at* the saddle point. Increasing N_{imag} could be a way for reducing the distance between TS and the closest image, but it's expensive and not fully satisfying since the true saddle point will not be reached. To locate rigorously the saddle point, Henkelman *et al.* have introduced the climbing-image NEB [25], an important improvement of the NEB method. After some iterations of NEB an image, usually the highest in energy, is chosen for "climbing" up to the saddle. During the ficticious dynamics, this image evolves according to the force due to the PES with the component parallel to the path reverted, and is not subject to the spring forces:

$$\mathbf{F}(\mathbf{R}) = -\boldsymbol{\nabla} E(\mathbf{R}) + 2\big(\boldsymbol{\tau} \cdot \boldsymbol{\nabla} E(\mathbf{R})\big)\boldsymbol{\tau}. \tag{2.23}$$

The algorithm then proceeds as described above. At almost the same computational effort as standard NEB, climbing-image NEB provides the activation energy and the coordinates at the saddle point (filled points in Fig. 2.2c).

Chapter 3

Methane-to-methanol conversion on Rh surfaces

In this chapter the possibility of direct methane-to-methanol conversion catalyzed by Rh surfaces is sistematically investigated by means of numerical simulations. The need for single C–H bond activation, and the difficulties commonly encountered on transition metals, will be first overviewed. A possible solution to these problems has recently been suggested in under-coordinated reaction sites as Rh adatoms on Rh(111), motivating the choice of the Rh substrate for the present study.

Activation energies along the possible pathways will be reported for the clean Rh(111) terrace and the Rh adatom. The validity of these results will then be extended to more generic Rh catalysts, discussing the sentitivity of activation barriers to reaction site. Based on this analysis one can conclude that Rh systems are not expected to be suitale catalyst for low temperature methane-to-methanol conversion. A different approach will then be discussed in Chapter 4.

3.1 Methane activation on transition metal surfaces

Methane is a very stable molecule. The cleavage of a C–H bond to neutral CH_3 and H costs as much as 4.49 eV [26]. Chemical processes involving

methane are therefore generally difficult to occur spontaneously. Reactions either proceed in the homogeneous phase by a free-radical mechanism, which however is hard to control, or one C–H bond can be weakened and possibly broken (an approach know as "methane activation") using a variety of methods, such as photochemical, electrochemical, eletrical, and catalytic activation. Among them, the use of an appropriate catalyst for methane dehydrogenation seems a very convenient choice. In this section the common problems in CH_4 activation on transition metal surfaces are discussed, together with a possible solution which has recently been suggested—the use of under-coordinated reaction sites. This motivated the study of methane-to-methanol conversion at a Rh adatom on a Rh(111) surface.

3.1.1 Problems for CH_4 on transition metals

The search for a convenient catalyst for methane activation is particularly hard because on many of the transition metals commonly used as catalysts the dehydrogenation of methane does not stop at CH_3 but proceeds further to CH or atomic C. This opens the way to the formation of carbon deposits, which are a source of major problems because they inactivate the catalyst by the formation of graphitic sheets. Moreover, poisoning substances usually bind selectively at steps and other defects which are the active sites of the catalyst, thus inactivating it already at relatively low coverages.

On the "dream" catalyst, the first dehydrogenation of methane,

$$CH_4 \rightarrow CH_3 + H, \tag{3.1}$$

has a low activation energy whereas the further dissociation of methyl (CH_3),

$$CH_3 \rightarrow CH_2 + H, \tag{3.2}$$

is blocked either because energetically unfavorable or because the activation energy is extremely high. In contrast to this ideal picture, on real transition metals reaction (3.2) is more convenient than, or at best roughly as convenient as, reaction (3.1). Subsequent CH_2 dehydrogenation to CH and H occurs usually very fast. This problem has been highlighted by several studies in which the energy of CH_x ($x = 0, 1, \ldots, 4$) species and corresponding activation energies for their dehydrogenation have been determined.

Watwe and coworkers [27] have investigated by density functional theory simulations the adsorption of CH_x on Ni(111) surfaces. The calculated activation energies for CH_x–H bond breaking are 1.32, 0.71, 0.29, and 1.44 eV for $x = 3, \ldots, 0$. With the exception of the barrier for CH dehydrogenation, the activation energy is thus decreasing along the dehydrogenation pathway. Moreover CH was found to be the most stable species. The authors also reported the result of kinetic analyses showing that CH is indeed the most abundant species on the surface.

Michaelides and Hu [28] concentrated on catalytic reactions taking place on Pt(111) surfaces. A situation similar to the one of Ni(111) was presented: the activation energies for CH_4 and CH_3 dehydrogenation are rather similar, 0.66 and 0.82 eV respectively. The least stable species is CH_2, which dissociates to CH and H with a barrier of 0.14 eV only. CH is then stable against hydrogenation or further dehydrogenation.

As for the activation of a single C–H bond, Ru(0001) surface is even worse, as reported by Ciobîcă *et al.* [29]. On this surface, not only the calculated activation energies is decreasing when passing from the CH_4 to the CH_3 and to the CH_2 dehydrogenation (0.88, 0.51, and 0.16 eV respectively), but also the dissociated products are getting more and more stable. The series ends at CH, for which 1.12 eV are required to activate complete dehydrogenation.

Perhaps even more significant is the case of Pd(100) investigated by Zhang and Hu [30]. There, the activation energy for CH_x dissociation decreases monotonically for decreasing x (0.79, 0.52, 0.20 eV for $x = 4, 3, 2$). CH dissociation (0.52 eV) is again an exception in this trend, being the activation energy higher than that for CH_2 dissociation, but atomic carbon formation is in this case energetically favored by 0.42 eV with respect to CH. If methane is activated, dehydrogenation would proceed up to completion.

The energy profile along the dehydrogenation pathway for these systems is indicated in Fig. 3.1. Results are consistent with experiments, when these are available. The reader interested in experimental results can refer to the papers cited above and references therein.

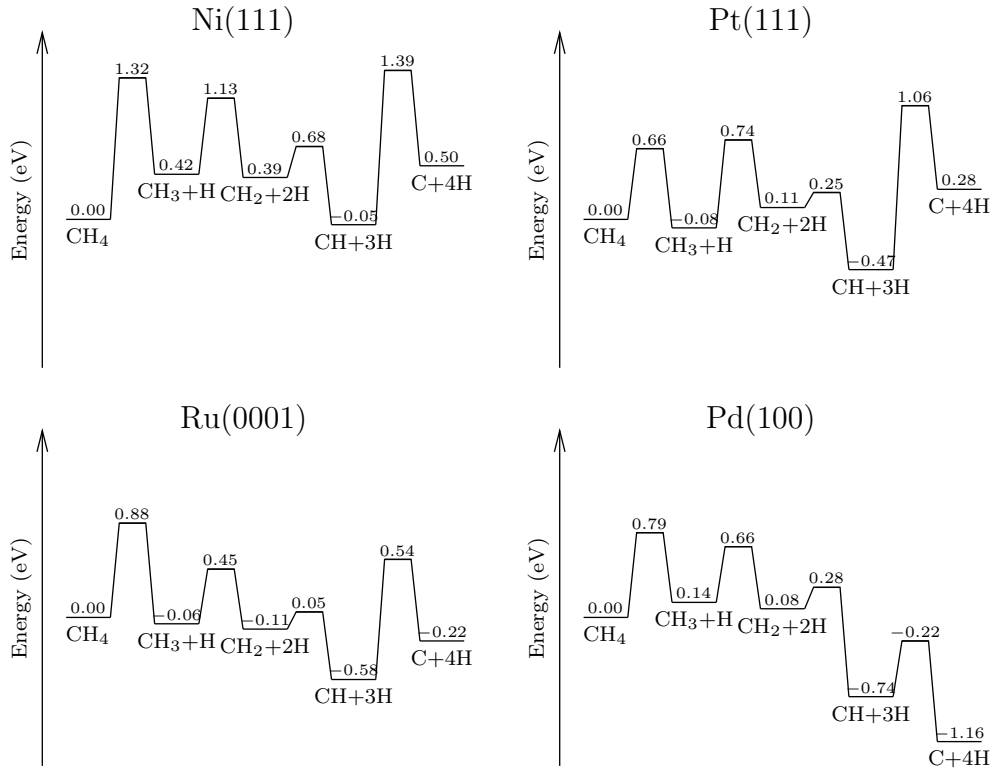

Figure 3.1: Complete dehydrogenation pathways for methane on transition metal surfaces by *ab initio* calculations. Data taken from: Ni(111), Ref. [27]; Pt(111), Ref. [28]; Ru(0001), Ref. [29]; Pd(100), Ref. [30].

3.1.2 Expectations for under-coordinated surface sites

From the analysis of the investigation presented above it is noticed that transition states for methane dissociation are coordinated to just one surface atom, while during methyl dehydrogenation two metal atoms are involved, and three for methylene dissociation.[1] Hence it is expected that the transition state for reaction (3.2) and subsequent steps is destabilized if the catalyst's geometry does not provide sufficiently high-coordinated reaction sites—thus raising the activation energy and making these processes unfavored with

[1]It has been established and veryfied also for different molecules that the higher the valence of the heavier dissociation product, the higher the coordination number of the reactant complex at the transition state [28].

respect to CH_4 dissociation.

The limiting case of an isolated metal atom as reaction site for methane activation has been investigated by Zhang and Hu [31]. They calculated the activation energy for the first dehydrogenation on a Pt atom adsorbed on a $MoO_3(010)$ surface to be 0.3 eV, much lower than that for the same reaction occurring on Pt(111) (0.7 eV according to Ref. [28]). On this system, the dehydrogenation of methyl is energetically prohibeted, being endothermic by ≈ 2 eV.

A systematic study of the activation energy for the first and the second C–H bond activation as a function of the coordination number of the catalyst's atoms involved has been assessed by Kokalj *et al.* [32]. The barriers for reactions (3.1) and (3.2) have been calculated for several reaction sites on the Rh(111) surface, namely at the (111) terrace (coordination $N_C = 9$), at a step edge ($N_C = 7$), at an added row ($N_C = 5$), and at an adatom ($N_C = 3$). Their results are summarized in Fig. 3.2. Both reactions are favored when moving from the terrace to the step edge and the added row: the barrier for the first dehydrogenation lowers from 0.69 to 0.50 and 0.48 eV, and the one for the second changes from 0.42 to 0.40 and 0.35 eV [in all three cases the barrier for (3.2) is lower than the one for (3.1)]. This trend can be explained by the different electronic structure of the metal atoms (d-band narrower and higher), and should not be misinterpreted as due to changes in the coordination of the reactant complex at the transition state since for each reaction the TS geometrical structure is similar on the three sites. Instead, it's remarkable that at the adatom the barrier for reaction (3.2) is much higher than on all the other sites (0.63 eV), while process (3.1) follows the above trend (0.47 eV). For the explanation of the exceptional behavior of methyl dissociation at the adatom several effects have to be taken into account: The initial state CH_3–Rh bond is stabilized at the adatom site by ≈ 0.3 eV, and three centers C–H–Rh bonds, which are weakening the C–H interaction, are not formed since H–Rh distances are too large; CH_2 forms two bonds with the surface, only one of the two becoming stronger at the adatom whereas the other one with the surface is not enhanced; The location of H at the TS (top site) is very unfavorable at the adatom.

Coming back to the possibility of single C–H bond activation, the results

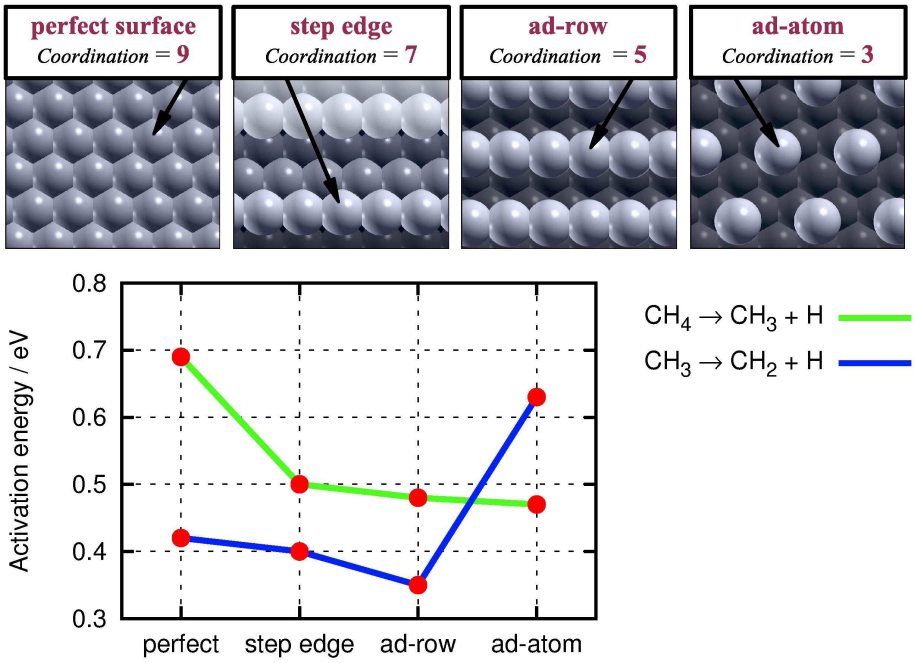

Figure 3.2: Different local geometries of the reaction site on Rh(111), and activation energies for the first two steps of methane dehydrogenation on a perfect surface (coordination $N_C = 9$), step edge ($N_C = 7$), added row ($N_C = 5$), and adatom ($N_C = 3$). Adapted from Ref. [32].

of Ref. [32] indicate that the presence of Rh adatoms on Rh(111) surfaces can enhance the first dehydrogenation of CH_4 while hindering the further decomposition of CH_3. The activation energies for these two processes were estimated to be 0.69 and 0.42 eV on the clean surface, and 0.47 and 0.63 eV at the adatom site. Moreover methane was found to preferentially adsorb at the adatom site by as much as 0.2 eV. Hence, if it were possible to let the reaction selectively occur at adatom sites, methane activation would be favored with respect to following methyl decomposition and it should be possible to tune the temperature so that methane is activated at an adatom site, but no further dehydrogenation occurs. This is the observation which motivated the choice of the Rh adatom as model catalyst.

Detailed analysis of the results reported in Ref. [32] also allowed the authors to extend the investigation focusing on the dependence of the catalyst's reactivity

on the local chemical composition and to design a new reaction site—a reactive rhodium adatom on a less reactive copper substrate—that effectively activates the dehydrogenation of methane, and effectively hinders the dehydrogenation of methyl, even to a larger extent: the calculated activation energies for these two reactions are 0.35 and 0.91 eV, respectively. This work, to which I contributed, will be briefly presented in Appendix A.

3.2 Methane-to-methanol: Reaction mechanisms

The net reaction for methane-to-methanol conversion reads

$$CH_4 + 1/2O_2 \rightarrow CH_3OH + 126 \text{ kJ/mol.} \tag{3.3}$$

Hence methanol could form by reactions of activated CH_4 and atomic oxygen. On Rh surfaces, the latter would be readily available in presence of O_2 in the gas phase since oxygen molecules adsorb dissociatively and desorb with a large activation energy (2.42 eV [33]). A number of studies have characterized the O/Rh system either by experimental [33, 34, 35], theoretical [36, 37], or combined approaches [38, 39]. If exposure to oxygen is high (above $\approx 10^{-3}$ mbar at 800 K [38]), the formation of a thin oxide layer is observed. Only the case of Rh under low oxygen exposure, hence still retaining the metallic character, will be considered in the following.

Let us examine schematically the reaction mechanisms that could lead to methanol synthesis. In presence of atomic O, methane could in principle form directly methanol by "insertion" of an O atom in one of its four C–H bonds. However, the calculated value for the corresponding activation barrier is very high (2.06 eV) and this process is therefore not convenient with respect to methane decomposition. Alternatively, CH_4 could dissociate at a surface site to form CH_3 and H, or do the same on top of an adsorbed oxygen giving adsorbed CH_3 and OH. In the former case CH_3 could then combine with adsorbed oxygen to give a methoxy intermediate (CH_3O). Methanol could be subsequently formed by recombination of CH_3O and H, or OH and CH_3. These reactions, leading to methanol formation, are pictorially represented

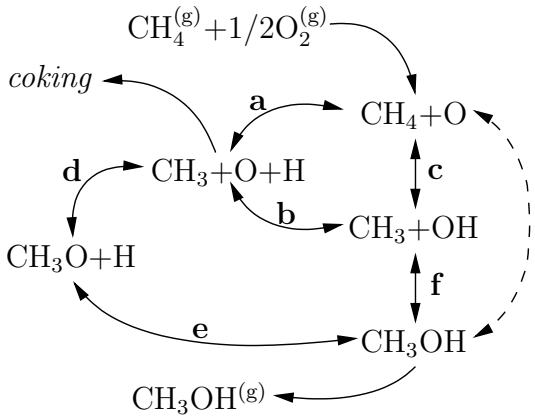

Figure 3.3: (a)-(f): Processes leading to methanol formation starting from methane in the gas phase and atomic oxygen adsorbed on the surface.

in Fig. 3.3, where the different processes are labeled from (a) to (f) for future reference.

These reactions are in competition with other processes leading to the complete dissociation of methane and eventually to coking and inactivation of the substrate. As reported in Sec. 3.1.2, Kokalj and coworkers [32] have found that the activation barrier for deprotonation of CH_3 radical is 0.63 eV on an adatom site, higher than its value on the clean Rh(111) surface (0.42 eV). For direct methanol synthesis to be achievable on Rh surfaces it is necessary that for at least one path in Fig. 3.3 all intermediate and transition states involved have lower energies.

3.3 Reactions on Rh(111) and Rh adatoms on Rh(111)

3.3.1 Adsorption sites and energies

Three layer slabs were used to model the Rh(111) surfaces. The bottom two layers were kept fixed at the bulk truncated positions, while the upper one was allowed to relax. Molecules were placed on this side of the slabs and relaxed together with the upper layer. The analysis was restricted to a coverage of 0.25 ML (corresponding to an O_2 partial pressure up to $\approx 10^{-8}$ mbar at

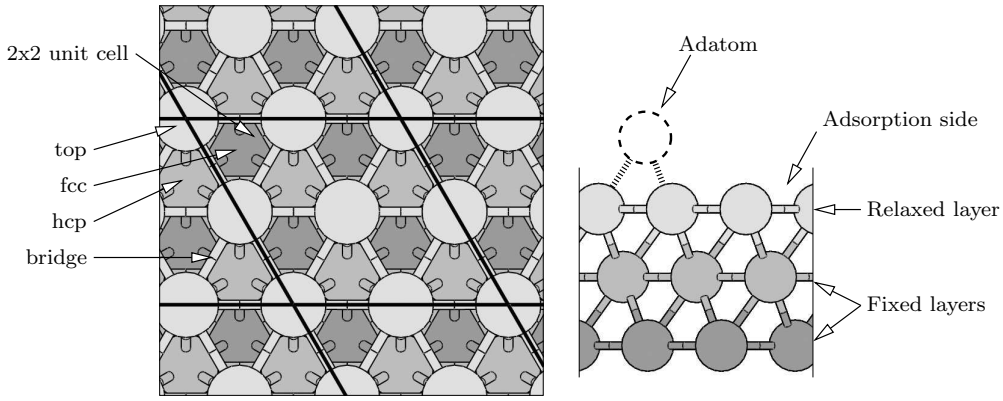

Figure 3.4: The surface (2×2) unit cell used for the calculations referred to in this chapter. The high-symmetry sites have also been indicated: top; fcc, threefold face-center cubic hollow; hcp, threefold hexagonal close packed hollow; bridge.

800 K [38]) using a periodically repeated (2×2) surface unit cell. This cell, together with high simmetry sites, is depicted in Fig. 3.4. For the study of the Rh adatom on the Rh(111) terrace, henceforth referred to as Rh/Rh(111), a further Rh atom is added in the fcc site and its coordinates optimized together with the topmost layer. Adsorption energies have been obtained by means of density-functional theory calculations, as indicated in Chapter 2, and are defined as

$$E_{\mathrm{A}} = E_{\mathrm{A/m}} - E_{\mathrm{A}}^{(\mathrm{g})} - E_{\mathrm{m}}, \tag{3.4}$$

where E_{A} is the adsorption energy of species A to the substrate m, and $E_{\mathrm{A/m}}$, $E_{\mathrm{A}}^{(\mathrm{g})}$, and E_{m} are the total energies of the A/m complex, gas phase A, and the clean m surface in their relaxed atomistic configurations. Following the notation chosen, more negative values of E_{A} correspond to stronger bonds. Further details on the computational method can be found in Appendix B.

The density of states (DOS) projected on the atomic orbitals of a surface Rh atom at the (111) terrace and on the Rh adatom on Rh(111) is reported in Fig. 3.5. No large differences are found as far as the *s* electrons are concerned, but the *d*-projected DOS is remarkably narrower at the undercoordinated adatom, and shifted at higher energies closer to the Fermi E_{F} level since both the surface and the adatom are neutral—thus the integral of the DOS

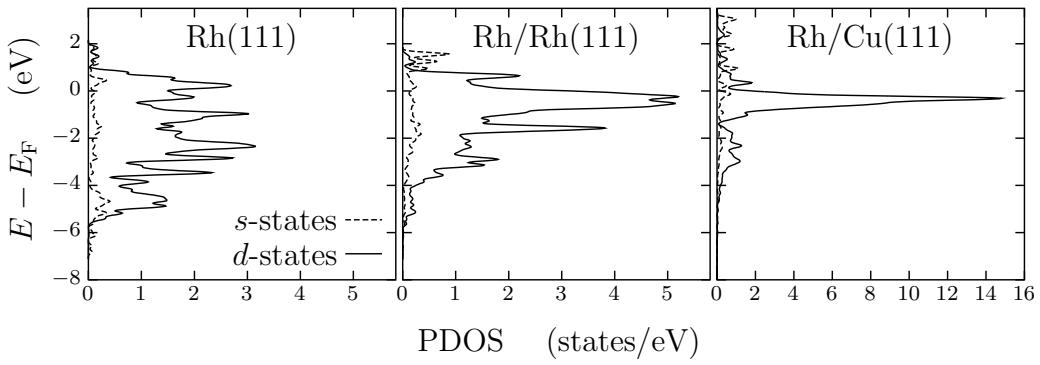

Figure 3.5: From left to right, density of states (PDOS) of atoms at the (111) surface of Rh, a Rh adatom on Rh(111), a Rh adatom on Cu(111). E_F is the Fermi level.

Substrate	CH_4	O	CH_3	CH_3O	CH_3OH	H	OH
Rh(111)	−0.10	−4.96	−1.78	−2.19	−0.38	−2.80	−2.88
	–	fcc	fcc	fcc	top	fcc	fcc
Rh/Rh(111)	−0.30	−4.89	−2.18	−2.62	−0.59	−2.89	−3.30
	top	bridge	top	top	top	bridge	top

Table 3.1: Binding energies (in eV) and adsorption sites of relevant molecules, radicals, and atoms on Rh(111) and the Rh adatom on Rh(111). For Rh/Rh(111), "bridge" stands for species bridging between the adatom and a surface atom.

up to E_F must be invariant. For comparison with the newly designed reaction site mentioned at page 34, the DOS of a Rh adatom on Cu(111), whose d-band is even narrower, is also plotted in Fig. 3.5. Peaks at energies between −4 and −2 eV are derived from the hybridization with the Cu d states.

Binding energies for molecules, radicals, and atoms involved in this study are reported in Table 3.1. The narrowing of the d-band at the adatom explains, following Hammer and Nørskov argument [3], the generally observed stronger binding on Rh/Rh(111). The only exception is oxygen, for which adsorption on the terrace would be slightly more favorable than at the adatom (−4.96 and −4.89 eV, respectively). The reason for this deviation is geometrical: the adsorption site close to the adatom is bridging between the

adatom itself and a surface atom, whereas adsorption is in fcc on the terrace. Would the O be in the bridge site also on the (111) surface, its adsorption energy would be −4.48 eV, thus 0.41 eV less stable than on Rh/Rh(111).[2] An individual analysis of adsorption of all the species considered is delayed to Chapter 4, where a comparison among chemically different substrates will be presented.

3.3.2 Reaction pathways

Clean Rh(111) terrace

The energy profile for the reactions indicated in Fig. 3.3 occuring on the clean Rh(111) surface is reported in Fig. 3.6a. The energy of desorbed methanol is chosen as reference for this diagram. This is done by computing adsorption energies as

$$E'_{\mathrm{A}} = E_{\mathrm{A/m}} - E^{(\mathrm{g})}_{\mathrm{CH_3OH}} - E_{\mathrm{m}}, \tag{3.5}$$

noticing that all configurations in Fig. 3.3 have the same atomic composition as CH_3OH.

The activation energy for the recombination of CH_3 and O (process (d) in Fig. 3.3) has been calculated without the additional hydrogen atom nearby, since H and CH_3 are very mobile on the surface (my estimate for H and CH_3 diffusion barriers is 0.11 and 0.13 eV, respectively). In a similar way, the formation of OH group from O and H [process (b) in Fig. 3.3] has been computed in absence of spectator CH_3 radical.

The transition state (TS) geometries of these reactions are shown in Fig. 3.7a-f. From the results of Fig. 3.6a, one sees that the highest activation energies are those associated to CH_3–O and CH_3–OH bond formation. Hence, C–O bond formation is the most difficult step in methanol synthesis. The first barrier is lower than the second one (1.56 and 1.80 eV respectively), and so the minimum energy pathway connecting methane to methanol on Rh(111) involves the following elementary steps: dissociation

[2]The reader might at this point wonder why H is not another exception, being the adsorption sites the same as for O. However, one can notice that the on-bridge hydrogen adsorption on the terrace is only 0.11 eV less stable than the fcc one.

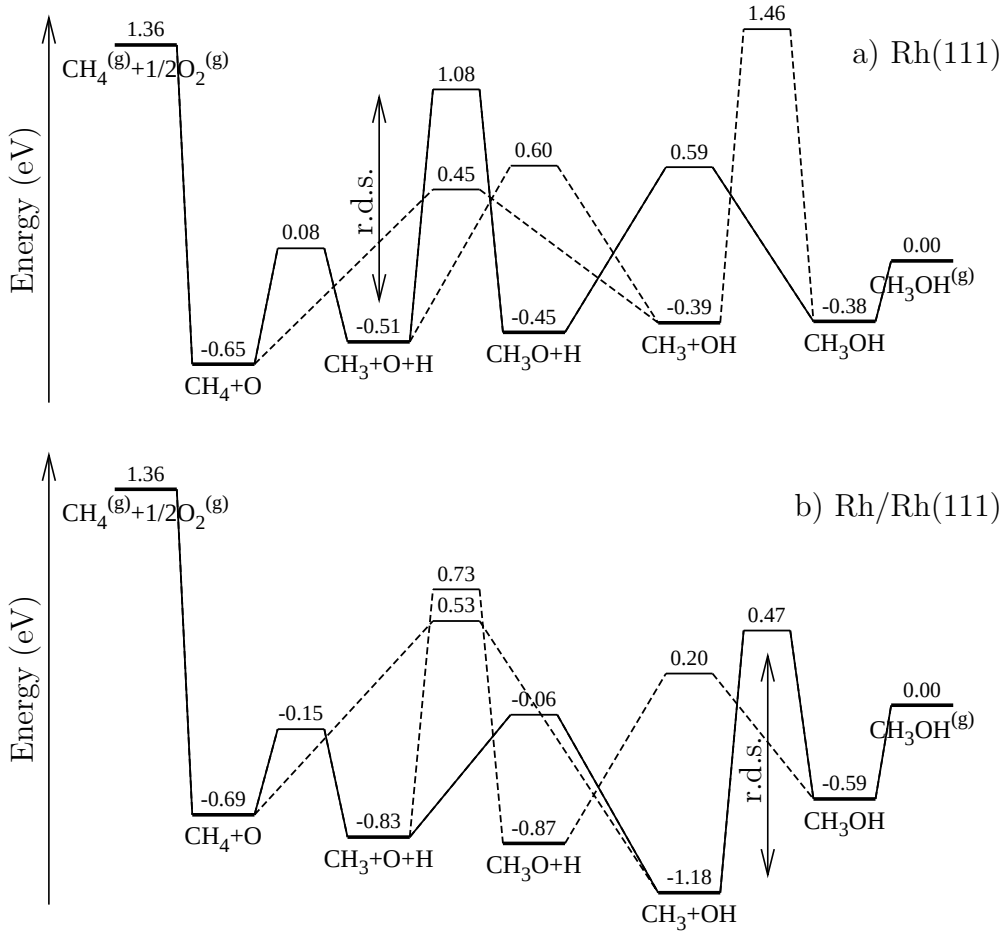

Figure 3.6: Metastable configurations and transition states for the reactions connecting methane to methanol, schematically indicated in Fig. 3.3. Energies are expressed in eV with respect to desorbed methanol. Solid lines indicate the minimum energy pathway going from CH_4 to CH_3OH, and vertical arrows marked "r.d.s." the rate-determining step along the minimum-energy pathway. a) reactions occurring on the perfect Rh(111) surface. b) the same on a Rh adatom on Rh(111).

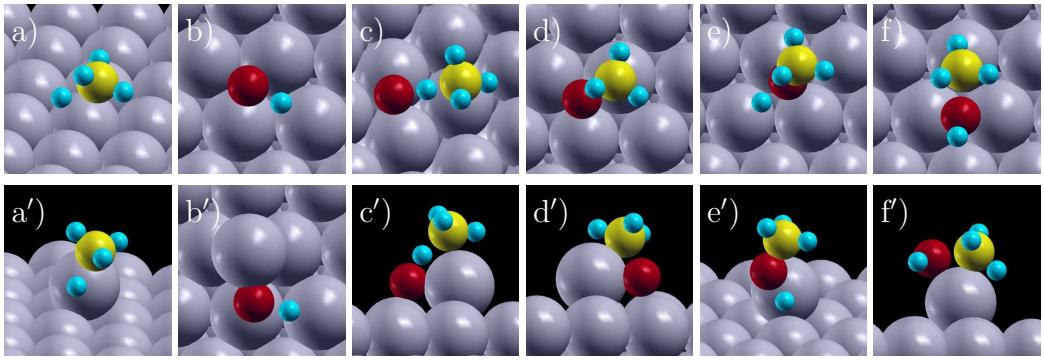

Figure 3.7: Geometry of the transition states for the reactions considered in this study. On the perfect surface: a) $CH_4 \rightleftharpoons CH_3+H$; b) $OH \rightleftharpoons O+H$; c) $CH_4+O \rightleftharpoons CH_3+OH$; d) $CH_3O \rightleftharpoons CH_3+O$; e) $CH_3OH \rightleftharpoons CH_3O+H$; f) $CH_3OH \rightleftharpoons CH_3+OH$. Panels a′)-f′): the same as a)-f) on a Rh adatom.

of CH_4, recombination of CH_3 and preadsorbed O, recombination of CH_3O and H [(a)-(d)-(e) pathway].

Rh adatom on Rh(111)

The results for the same reactions occuring at an adatom site have been collected in Fig. 3.6b, and the corresponding TS geometries can be found in Fig. 3.7a′-f′.

The larger reactivity of the low-coordinated Rh atom causes an increase in the binding strength of the various configurations, and the reaction pathways are lowered in energy. Moving to the adatom site, the first dehydrogenation barrier of methane decreases by 0.2 eV, in agreement with Ref. [32]. Again, CH_3–O association reaction has been studied in absence of a spectator hydrogen atom, while for O–H recombination the presence of a CH_3 group at the adatom site has been considered since CH_3 strongly binds to it (adsorption stronger by 0.40 eV with respect to terrace site). In the initial configuration for this reaction, oxygen atom was bound to the adatom while H came from the terrace. This required the use of a larger (2×3) surface unit cell.

As in the case of reactions occurring at terrace sites, also in this case the highest activation energies are associated to C–O bond formation: the barrier for CH_3–O recombination is almost unaffected by the different geom-

etry (from 1.57 to 1.56 eV), and the one for CH_3–OH lowers from 1.80 to 1.65 eV. Even if this second activation barrier is higher than the first one, this is compensated by the fact that the CH_3+OH configuration has lower energy than CH_3+O+H. As a consequence, the minimum energy pathway for methane to methanol on an adatom site goes through (a)-(b)-(f) steps: dissociation of CH_4, recombination of H and O, and recombination of CH_3 and OH.

Rh adatom on Cu(111)

It was suggested that, as far as the relative height of the activation barriers for CH_4 and CH_3 dehydrogenation is concerned, the model catalyst composed of a reactive Rh adatom on a less reactive surface like Cu(111), Rh/Cu(111), could be even better than Rh/Rh(111) (see page 34). It is therefore also interesting to investigate methane-to-methanol pathways on Rh/Cu(111). One can reasonably assume that the minimum energy pathway and the rate-determining step could be the same as for the similar Rh adatom on Rh(111). Thus only the activation energy of process (f) has been evaluated here. With respect to methanol in the gas phase, the energy of the initial state CH_3+OH is -0.96 eV, and that of the transition state 0.39 eV (-1.18 and 0.47 eV on Rh/Rh(111), respectively). The barrier is then 1.35 eV, 0.30 eV lower than on Rh/Rh(111). This reduction is the result of the combination of two effects. The first one is the stabilization of the TS due to the narrower d band of Rh adatom on Cu(111) compared to Rh/Rh(111) (see Fig. 3.5), and it is very small (-0.08 eV). The second one, also quite weak, is the destabilization of the initial state, due to the weaker bond formed by OH (-3.16 eV) with respect to the Rh/Rh(111) case (-3.30 eV).[3]

[3]At variance with the adatom case, the adsorption on clean (111) terraces, vertical in the hollow site, is stronger on Cu than on Rh (-3.11 and -2.88 eV, respectively). Hence moving from terrace to Rh adatom OH is stabilized by 0.42 eV on Rh/Rh(111), but only by 0.05 eV on Rh/Cu(111).

The difference might be explained as follows: on Cu(111), the bond is formed mainly to the jellium-like s electrons, whereas on Rh(111) also the not completely filled d states contribute and the interaction may be interpreted also as the sum of bonding with individual metal atoms. Moving to the adatom OH is farther from the surface s electrons. Bond is instead formed in bridge position among the adatom and a surface atom, thus in a configuration which is not optimal for Cu. To support the above argument, one can

Conclusions for methane-to-methanol on Rh(111) and Rh/Rh(111)

Coming now to the comparison with the competing CH_3 deprotonation process it is clear that in spite of the observed stabilization of the intermediates and general reduction of most of the barriers at the adatom site, the activation energies for CH_3–O and CH_3–OH recombination are too high with respect to those of CH_3 dehydrogenation, both at the terrace and adatom site (0.42 and 0.63 eV, respectively).[4]

As a consequence, the perfect Rh(111) surface and the adatom of Rh on Rh(111) are not good candidate catalysts for methane to methanol conversion. In particular, for the Rh/Rh(111) system, it would be possible to choose a temperature for which CH_4 dissociates and CH_3 does not, but then methyl would not be able to react with O or OH.

3.4 Extension of the results to generic Rh surfaces

In the preceding section it was found that methanol formation is not a competitive process on the clean Rh(111) surface nor on Rh adatom sites on Rh(111). Since any theoretical analysis is necessarily limited in the number of systems addressed, an important issue to be understood is whether and how much results could change considering different orientations of the substrate, some other defected structure (like for instance stepped surfaces) or higher oxygen coverage.

compare the adsorption energy of OH in the fcc hollow position with the one in bridge site: on Rh(111) bridge site is as favorable as fcc, whereas for Cu(111) it is less stable by 0.15 eV.

[4]On Rh/Cu(111) the situation would be slightly better, but still the activation energy for $CH_3 \rightarrow CH_2+H$ (0.91 eV) is lower than the one for methanol formation (1.35 eV).

3.4.1 General considerations on dissociation and association reactions

This issue has been addressed recently by Liu and Hu in Ref. [40] where some general rules for predicting the reaction-site sentitivity or insensitivity for association/dissociation reactions have been proposed, based on the analysis of two simple reactions: methane first dehydrogenation and carbon monoxide dissociation. Here the arguments presented in Ref. [40] are critically reanalysed and applyied to all the six reactions previously described with the exception of

$$\text{(c)} \qquad CH_4 + O \rightleftharpoons CH_3 + OH, \tag{3.6}$$

which is not an association/dissociation reaction.

In their analysis, Liu and Hu [40] noticed that many important dissociation reactions of generic form

$$AB \rightleftharpoons A + B \tag{3.7}$$

have late-TSs, that is transition states close to the dissociated final state (FS). Inspection of Fig. 3.7 shows that this is indeed the case for the reactions considered here [with the already mentioned exception of reaction (c)]. For late-TS reactions Liu and Hu suggest that the direct (dissociation) reaction is in general reaction-site sensitive while the inverse (association) reaction is rather reaction-site insensitive. Their argument goes as follows.

The adsorption energy of the A+B activated complex at the TS is decomposed as

$$E^{\mathrm{TS}}_{\mathrm{A+B}} = E^{\mathrm{TS}}_{\mathrm{A}} + E^{\mathrm{TS}}_{\mathrm{B}} + E^{\mathrm{TS}}_{\mathrm{int}} = \Sigma E^{\mathrm{TS}} + E^{\mathrm{TS}}_{\mathrm{int}}, \tag{3.8}$$

where $E^{\mathrm{TS}}_{\mathrm{A}}$ ($E^{\mathrm{TS}}_{\mathrm{B}}$) is the adsorption energy of A (B) in the geometry of the TS without B (A), and the interacion energy, $E^{\mathrm{TS}}_{\mathrm{int}}$, is defined by the above equation and is due to bond sharing, Pauli repulsion, and electrostatic interaction between A and B in the TS geometry. Similarly the energy of the FS can be decomposed as

$$E^{\mathrm{FS}}_{\mathrm{A+B}} = E^{\mathrm{FS}}_{\mathrm{A}} + E^{\mathrm{FS}}_{\mathrm{B}} + E^{\mathrm{FS}}_{\mathrm{int}} = \Sigma E^{\mathrm{FS}} + E^{\mathrm{FS}}_{\mathrm{int}}, \tag{3.9}$$

where $E_{\mathrm{A}}^{\mathrm{FS}}$ ($E_{\mathrm{B}}^{\mathrm{FS}}$) are the relaxed adsorption energies of A and B on the substrate and $E_{\mathrm{int}}^{\mathrm{FS}}$ describes the correction due to co-adsorpition in the FS geometry and is usually small. For the initial state (IS) the AB molecule in the gas phase has been assumed in Ref. [40].

The dissociation reaction barrier is therefore

$$E_{\mathrm{act}}^{\mathrm{diss}} = \Sigma E^{\mathrm{TS}} + E_{\mathrm{int}}^{\mathrm{TS}} - \Delta E_{\mathrm{A–B}}^{(\mathrm{g})}, \tag{3.10}$$

where $\Delta E_{\mathrm{A–B}}^{(\mathrm{g})} = E_{\mathrm{AB}}^{(\mathrm{g})} - E_{\mathrm{A}}^{(\mathrm{g})} - E_{\mathrm{B}}^{(\mathrm{g})}$ is the A–B bond energy in the gas phase.[5] As adsorption energies may strongly depend on the adsorption site, dissociation reactions are expected to be surface sensitive and particularly favoured at defected sites. At defects, undercoordinated substrate-atom are present and their *d*-band is narrower and, for late transition metals, shifted to higher energies than at the perfect surface. Thus, according to Hammer-Nørskov chemisorption model [3], adsorbates generally bind more strongly to defects: ΣE^{TS} decreases, reducing the dissociation barrier on defects. Notice however that the choice of a gas-phase reference in Ref. [40] ignores completely the adsorption energy of AB molecule that could be substantial and site dependent. A more appropriate definition of the dissociation barrier could be

$$E_{\mathrm{act}}^{\mathrm{diss}} = \Sigma E^{\mathrm{TS}} + E_{\mathrm{int}}^{\mathrm{TS}} - E_{\mathrm{AB}}^{\mathrm{IS}} - \Delta E_{\mathrm{AB}}^{(\mathrm{g})}, \tag{3.11}$$

where $E_{\mathrm{AB}}^{\mathrm{IS}}$ is the molecular adsorption energy in the initial state. This point will be discussed in detail also later.

The association reaction barrier is instead defined as

$$E_{\mathrm{act}}^{\mathrm{ass}} = \Sigma E^{\mathrm{TS}} - \Sigma E^{\mathrm{FS}} + E_{\mathrm{int}}^{\mathrm{TS}} - E_{\mathrm{int}}^{\mathrm{FS}}. \tag{3.12}$$

For late-TS reactions, the first two terms in this espression should be similar and largely compensate each other, while the last term is usually small. Surface sensitivity of association reactions depends therefore mainly on $E_{\mathrm{int}}^{\mathrm{TS}}$, which increases with the number of chemical bonds which are formed by reactants [40]. Most species concerned here form only single bonds (e.g., –CH_3, CH_3O–, ...), so this term should be generally small. Associations are then expected to be surface insensitive.

[5] Consistently with the notation adopted for adsorption energies, Eq. (3.4), more negative numbers means stronger bonds.

3.4.2 Analysis of individual reactions

The five dissociation/association reactions involved in methane to methanol conversion will now be analysed in detail on the basis of the above arguments. The relevant quantities are collected in Table 3.2. In order to simplify the comparison between terrace and adatom sites, for both sites "spectator" radicals will not be included when examining (b) and (d) elementary processes. As a consequence, activation energies reported in Table 3.2 for these reaction are sometimes marginally different from the ones used in Fig. 3.6.

a) $\mathbf{CH_4 \rightleftharpoons CH_3 + H}$

The dissociation of CH_4 to CH_3 and H, and the corresponding association reaction, is one of the two reactions investigated by Liu and Hu [40] to assess their "general rules". They reported a strong reduction of the dissociation barrier, computed according to Eq. (3.10), on Rh steps (0.32 eV) as compared to (111) terrace sites (0.67 eV). According to their calculation, at the step edge ΣE^{TS} decreases by 0.3 eV, whereas $E_{\mathrm{int}}^{\mathrm{TS}}$ is small and almost unchanged (0.20 eV on the flat surface and 0.16 eV at the step). My calculated value for the dissociation barrier, according to Eq. (3.11), on the flat Rh(111) surface is 0.73 eV. Had one followed Ref. [40] and taken as a reference methane in the gas phase, the molecular adsorption energy should be added to this result, obtaining 0.63 eV, in excellent agreement with Liu and Hu's result.

In analogy with the reported result for step edge, I find a significant reduction of the activation energy at the adatom site (0.41 eV) that would be even stronger (0.11 eV) by taking the gas-phase as a reference. It should be stressed however that in the adatom case, reported here, the reason for site sensitivity of the activation barrier seems different from the one occuring at the step: as it was found for the step case the TS is stabilized at the adatom (ΣE^{TS} decreases by 0.24 eV), but this contribution to the barrier is compensated by a similar increase in CH_4 adsorption energy (0.20 eV). An essential contribution to site sentitivity for this reaction barrier comes from product interaction energy at the TS, $E_{\mathrm{int}}^{\mathrm{TS}}$, which, although small in absolute terms (0.12 and -0.17 eV for the terrace and the adatom, respectively), is not constant and changes by as much as 0.29 eV favouring the adatom site.

Reaction	Substrate	$E_{\mathrm{act}}^{\mathrm{diss}}$	$E_{\mathrm{act}}^{\mathrm{ass}}$	$E_{\mathrm{AB}}^{\mathrm{IS}}$	ΣE^{TS}	$E_{\mathrm{int}}^{\mathrm{TS}}$	ΣE^{FS}	$E_{\mathrm{int}}^{\mathrm{FS}}$
(a) $CH_4 \rightleftharpoons CH_3+H$	Rh(111)	0.73	0.42	−0.10	−4.11	0.12	−4.58	0.17
	Rh/Rh(111)	0.41	0.39	−0.30	−4.35	−0.17	−5.07	0.16
(b) $OH \rightleftharpoons O+H$	Rh(111)	0.99	0.96	−2.88	−7.17	0.52	−7.76	0.15
	Rh/Rh(111)	1.03	0.66	−3.20	−7.11	0.18	−7.58	−0.02
(d) $CH_3O \rightleftharpoons CH_3+O$	Rh(111)	1.53	1.57	−2.19	−5.76	0.61	−6.74	0.03
	Rh/Rh(111)	1.60	1.56	−2.62	−6.21	0.71	−7.06	0.00
(e) $CH_3OH \rightleftharpoons CH_3O+H$	Rh(111)	0.97	0.89	−0.38	−4.25	0.29	−4.99	0.15
	Rh/Rh(111)	0.79	1.08	−0.59	−4.90	0.55	−5.51	0.08
(f) $CH_3OH \rightleftharpoons CH_3+OH$	Rh(111)	1.84	1.80	−0.38	−3.24	0.43	−4.66	0.05
	Rh/Rh(111)	1.06	1.65	−0.59	−4.35	0.55	−5.48	0.03

Table 3.2: Activation energies and their decomposition for the dissociation/association reactions under investigation. Values in eV. See the text for explanation of symbols. The products bonding energy in the gas phase is, from top to bottom, $\Delta E^{(\mathrm{g})}$=−4.62, −4.76, −4.48, −4.55, and −4.27 eV.

The peculiar negative sign of $E_{\rm int}^{\rm TS}$ at the adatom means that, at the TS geometry, the interaction is attractive. This can be understood in terms of direct electrostatic interaction between CH_3 and H. At the adatom, the H is located 2.53 Å outside the outermost Rh layer (0.69 Å more than the H-Rh bond in the FS), and its positive charge is expected to be little screened by the metal electrons (see Fig. 3.7a′). A rough estimate of the electrostatic interaction between the two fragments can be obtained by approximating C and the four H atoms with point charges, whose value is determined by Lowdin population analysis. An attraction ≈ 0.1 eV stronger at the adatom than at the terrace site is obtained in this way, a result consistent at least in sign with the observed lowering by 0.29 eV of $E_{\rm int}^{\rm TS}$.

As for the association barrier, Ref. [40] reports very small difference in the association barrier for step (0.59 eV) and terrace (0.65 eV) sites. The increased TS binding energy, more negative $\Sigma E^{\rm TS}$, at the step is compensated by a similar change in the FS, $\Sigma E^{\rm FS}$. Interaction between fragments plays minor role in their case.

Also from my results one finds that this association raction is site insensitive but again for somewhat different reasons. The association barrier at the (111) terrace site is 0.42 eV while it is 0.39 eV on the adatom. The adatom/terrace differences in adsorption energy for the fragments at the TS and in the FS are -0.24 and -0.49 eV respectively favoring in both cases the lower coordination site as expected, but not compensating each other exactly as the "late-TS reaction" argument would imply. Nearly complete compensation is obtained only when the already mentioned site-dependent fragment interaction energy at the TS is included. Site insensitivity in the association barrier results therefore from a cancellation of different contributions. Whether such cancellation is accidental or might have deeper origin is not clear to me. Fragment interaction energy in the FS, included in this thesis and neglected in Ref. [40], explains the discrepancy in the reported numerical values for the terrace site but plays no role in determining site sensitivity of this reaction.

b) OH ⇌ O + H

According to my calculations, reaction-site sensitivity of OH dissociation and O+H recombination is opposite to proposed "general rules". The dissociation is insensitive (with 0.99 and 1.03 eV activation energies for terrace and adatom site, respectively) while association reaction is site sensitive (with 0.96 and 0.66 eV barriers).

As for dissociation, its insensitivity comes again from cancellation of two distinct effects. On one hand, OH is strongly adsorbed to the terrace site (−2.88 eV), and selectively binds to adatoms (−3.20 eV).[6] This term was not considered in Ref. [40], but one can notice that using Eq. (3.10) instead of Eq. (3.11) would incorrectly result in negative activation barriers. On the other hand, the fragment interaction energy at the TS, $E_{\rm int}^{\rm TS}$, decreases from 0.52 to 0.18 eV going from the terrace to the adatom, compensating the IS binding energy change. Binding energies of O and H at the TS are instead quite insensitive to the substrate change: $\Sigma E^{\rm TS}$ is −7.17/−7.11 eV for terrace/adatom site.

Association is sensitive ($E_{\rm act}^{\rm ass}$ = 0.96/0.66 eV on terrace/adatom). Final state contributions, $\Sigma E^{\rm FS} + E_{\rm int}^{\rm FS}$, and $\Sigma E^{\rm TS}$ have little effect on the activation energy, and the difference of 0.30 eV is mainly due to TS interaction energy, $E_{\rm int}^{\rm TS}$, which is strongly reduced at the adatom. This decrease is of electrostatic origin, mediated by the substrate. Oxygen attracts electrons from the surrounding Rh atoms, which are then positively charged and repel the positive H. On the perfect surface (see Fig. 3.7b), O is close to a hollow site and H is close to a neighbouring one, disturbed by the two Rh atoms in between which aquire a positive charge of 0.16 e each. On Rh/Rh(111) the situation is more favorable (Fig. 3.7b′): the oxygen atom sits in a bridge position between the adatom and a surface atom. These two atoms become positive by 0.22 e and 0.16 e respectively, but H has to overcome the repulsion of the second one only before meeting O; as a result, the substrate-mediated repulsion

[6] The adsorption energy for Rh/Rh(111) is slightly different from the −3.30 eV reported in Table 3.1 because there adsorption was on top of the adatom site, whereas here the bridge site has been chosen since it is closer to the TS and it is the preferred one in presence of CH_3 coadsorbed on the adatom. After formation, hydroxil may then migrate to the top site with some presumably small activation energy (not evaluated).

between O and H is much lower. This analysis also explains why the search for a TS with H close to the positively charged adatom was unsuccessful.

d) $CH_3O \rightleftharpoons CH_3 + O$

Dissociation of CH_3O into CH_3 and O is site-insensitive ($E_{act}^{diss} = 1.53/1.60$ eV for terrace/adatom site), the reason being the similar preferential adsorption to the adatom of both CH_3 in TS and CH_3O in the IS. Notice that if Eq. (3.10) were used instead of Eq. (3.11), the activation energy would result site-sensistive but negative. The former expression thus appears of little use in case of strongly adsorbed ISs. The TS interaction term does not play a significant role ($E_{int}^{TS} = 0.61/0.71$ eV for terrace/adatom). The association is also nonsensitive ($E_{act}^{ass} = 1.57/1.56$ eV), in agreement with the general analysis: both $\Sigma E^{TS} - \Sigma E^{FS}$ and E_{int}^{TS} have little effect.

e) $CH_3OH \rightleftharpoons CH_3O + H$

Methanol dissociation to CH_3O and H is surface sensitive ($E_{act}^{diss} = 0.97$-/0.79 eV), in agreement with the general rules discussed above. The change in barrier height is mostly due to a change in the adsorption energies of CH_3O and H at the TS, whose sum decreases (they become more bound) by 0.65 eV going from terrace to adatom. This is only partly compensated by the increases of methanol-substrate bond and of the TS interaction energy. The latter determines the surface sensitivity of the association reaction. Notice that in this case, somehow at variance with the general feeling that defect sites should enhance reactivity, the barrier increases from 0.89 to 1.08 eV going from the terrace to the adatom site, due to the strong increase (from 0.29 to 0.55 eV) in the E_{int}^{TS}. To explain qualitatively this unusual behaviour one can again resort to some electrostatic argument combined with Lowdin population analysis of the fragments: CH_3O is negatively charged and has withdrawn electrons from the closest Rh atom which becomes slightly positive. On the perfect surface (see Fig 3.7e), this atom is farther than CH_3O from the approaching H atom, whereas on Rh/Rh(111) (see Fig 3.7e′) the positively charged Rh is the adatom itself, which strongly repels H .

f) $CH_3OH \rightleftharpoons CH_3 + OH$

In agreement with the argument presented in Ref. [40], dissociation of CH_3OH to CH_3 and OH is sensitive to the change of reaction site (1.84/1.06 eV for terrace/adatom). As expected from the general analysis, the major contribution to the sensitivity is the change of ΣE^{TS} ($-3.24/-4.35$ eV). Also for the association barrier there is good agreement with the general analysis being much less sensitive than the dissociation barrier (1.80/1.65 eV). When going from the perfect surface to the adatom, the changes in $\Sigma E^{\mathrm{TS}} - \Sigma E^{\mathrm{FS}}$ and E_{int} are both small with respect to the large activation energy, and partly compensate each other.

Review of the general arguments for surface sensitivity/insensitivity

It's interesting to summarize the above discussion and compare with the arguments of Ref. [40], in order to extend these considerations. Three out of five of the dissociation reactions considered here are site sensitive as expected. These are the reactions where the associated molecules [CH_4 in (a) and CH_3OH in (e) and (f)] are weakly bound to the surface. The other two dissociation reactions (OH and CH_3O) are site insensitive because the adsorption energy of the reactant is comparable to the one of the products, and similarly site-dependent. Assuming a gas phase reference, as in Ref. [40], would make then more site sensitive but the corresponding activation energies would then be unphysically negative. Therefore in general, $E_{\mathrm{AB}}^{\mathrm{IS}}$ should not be neglected and, when large, can reduce site sensitivity.

For association reactions, the expected compensation in the changes of TS and FS adsorption energies, ΣE^{TS} and ΣE^{FS} was generally found. However, the interaction term can then become the determining contribution. It does not necessarily lower the barrier when moving to defects and, for example, CH_3+OH→CH_3OH becomes less favorable at the adatom. In many cases substrate-mediated repulsion between fragments is fairly dependent on the reaction site and, in general, $E_{\mathrm{int}}^{\mathrm{TS}}$ should be carefully taken into account.

3.4.3 Is methane-to-methanol conversion on Rh surfaces possible?

Coming back to the main issue of this chapter, to assess the possibility of using Rh catalysts for direct methane-to-methanol conversion, recall that the rate-limiting steps for these process on Rh(111) and Rh/Rh(111) are the association steps of reactions (e) and (f). According to previous analysis they are both *site-insensitive* and this is not due to occasional cancellation of contributions, but to the compensation between changes in ΣE^{TS} and ΣE^{FS}, and the minor part taken by $E_{\mathrm{int}}^{\mathrm{TS}}$.

Even if the precise behavior of this last term is difficult to predict, in this case it is of the order of 0.5 eV, and it's very unlikely that its site dependence can lower the activation energy by more than a fraction of an eV. This is not sufficient to make methanol formation preferred to further deprotonation of methyl radical.

Chapter 4

Guidelines for the search for a new catalyst

In Chapter 3 it was shown that tuning the geometry of the reaction site may not be sufficient to favor methane-to-methanol conversion. Here the reactivity of different transition metal surfaces will be investigated, with the purpose of extracting the overall characteristics of selected processes and of identifying trends across the periodic table of the elements.

By this approach useful relations between activation energies and more readily accessible quantities (e.g., linear combinations of adsorption energies) will be established. Such relations will then be used to screen rather large sets of substrates, detecting the most interesting ones. For those only, the detailed and expensive calculations needed to determine the energy barriers will indeed be performed.

A candidate catalyst will finally be proposed, and a possible experimental confirmation suggested.

4.1 Methane and oxygen on transition metal surfaces

In this section results for the (111) surface of rhodium, palladium, silver, copper, and gold will be presented, with the aim of understanding trends in the reactivity. The power of numerical simulations will be exploited by

examining also situations which are difficult—maybe impossible—to probe experimentally (for example, the reactions of oxygen dissociatively adsorbed on gold). The results obtained in these cases are not intended to directly mimic the reality, but to push to the limit the effect of specific contributions so that their relevance for the phenomenon under investigation is better highlighted.

4.1.1 Selection of the reactions

Investigating all the possible reactions which could occur at a catalyst's surface is a formidable and generally undesirable task. Also restricting to some smaller set—as the reactions connecting methane to methanol through the most probable intermediate steps, as we did for Rh in the previous chapter—but considering many different catalysts requires a considerable effort without necessarily adding significant information. It is therefore necessary to identify a few key processes to be analyzed in detail in order to get some insight on the overall process of interest.

After CH_4 dissociation it's very difficult to form methanol because of the possibility of further dehydrogenation, at least on Rh as it was seen in Chapter 3. Hence I decided to concentrate on the direct pathway converting methane to methanol (which on Rh required a very large activation energy). Then one should also investigate the competing processes which can occur directly from the same starting point ($CH_4^{(g)}$+O/metal). Hence the following reactions will be discussed: (a) The direct formation of methanol by insertion of oxygen in a C-H bond, which on the Rh surface was very unlikely; (b) The dehydrogenation of methane to CH_3+H on the terrace, without the participation of oxygen; (c) The hydrogen transfer from CH_4 to O, forming OH and CH_3; (d) The transfer of an H to the surface, and the simultaneous binding of methyl to the oxygen, forming CH_3O. These processes have been indicated pictorially in Fig. 4.1.

Of course, (a)-(d) are not the only reactions which could occur, or which could be of interest, but they are the ones for which the reactant configuration is promptly available. Other processes can then follow. Just to mention a few, after (c) methanol can form from methyl and hydroxyl, or

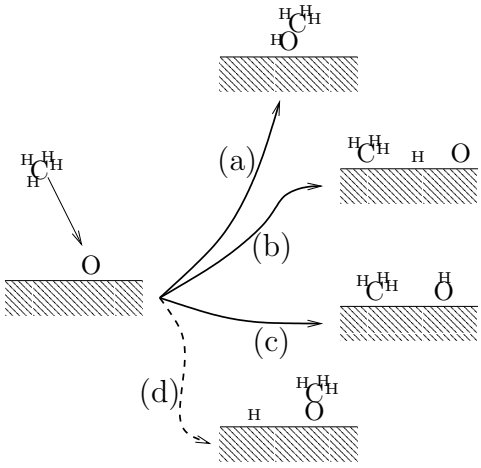

Figure 4.1: Reactions investigated in this chapter. The dashed line for (d) indicates that this reaction is not likely to occur directly. See the text for details.

from methoxy and hydrogen after (d). Or methanol can dissociate. It's easily found that the number of possibilities is even greater if the study is not limited to the model system consisting of *one* oxygen atom and *one* methane molecule. In this respect, a noteworthy case of particular interest is methanol decomposition to formaldehyde (CH_2O) on silver: it has been indicated that CH_3OH first dissociates to CH_3O and H, and then to CH_2O with the help of oxygen/hydroxyl extracting further hydrogen and forming H_2O. In any case, those just mentioned are "n^{th}-order" processes. Some of them could certainly be the interesting subject of further study, but this would require first the understanding of 1^{st}-order ones. The present discussion will address this point, and concentrate on the 1^{st}-order reactions depicted in Fig. 4.1.

4.1.2 Adsorption sites and energies

The molecules, radicals, and atoms involved in the selected reactions are CH_4, O, CH_3, CH_3O, CH_3OH, H, and OH. It is instructive to start by briefly reviewing and commenting on the adsorption geometries and energies of these species.

Three layer slabs were used to model the (111) surfaces. The bottom two

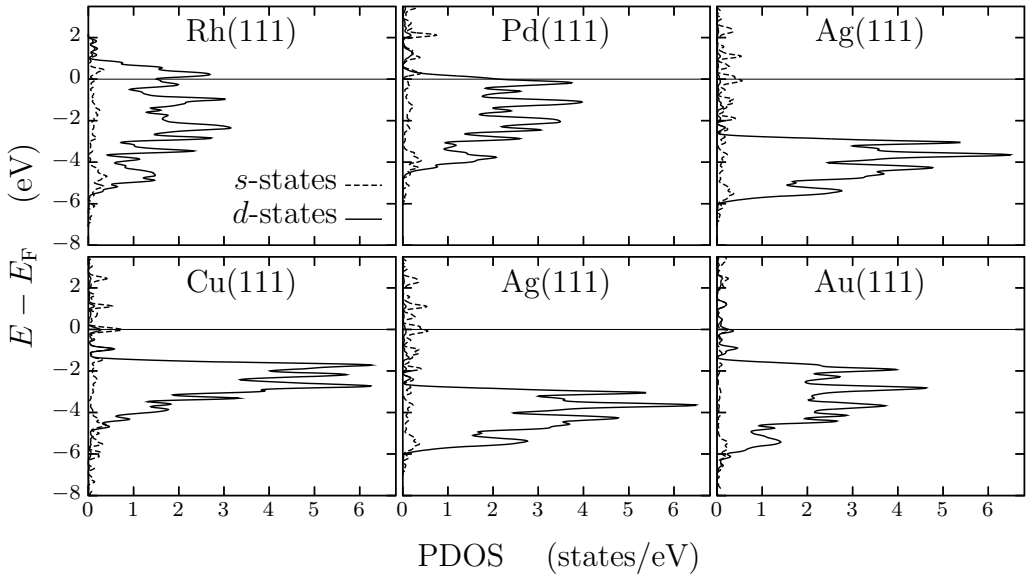

Figure 4.2: Density of states (PDOS) of atoms at the (111) surface of Rh, Pd, Ag, Cu, and Au. E_{F} is the Fermi level.

layers were kept fixed at the bulk positions, while the upper one was allowed to relax. Molecules were placed on this side of the slabs and relaxed together with the upper layer. We restricted our analysis to a coverage of 0.25 ML, using a periodically repeated (2×2) surface unit cell. This cell, together with high simmetry sites, was depicted in Fig. 3.4. Adsorption energies, which were defined in Eq. (3.4), have been obtained by means of density-functional theory calculations, as indicated in Chap. 2. More details on the computational method can be found in Appendix B.

Clean (111) surfaces

The density of states projected to the atomic orbitals of the surface atoms is a very useful quantity for the understanding of surface adsorption, and is reported in Fig. 4.2. When moving from left to right in the periodic table across the $4d$ metals (top row in Fig. 4.2), the d band shifts at lower energies and becomes more populated because of the additional electrons, and shrinks due to the increased lattice constant. For the noble metals of the IB group (bottom row in Fig. 4.2), the d band is completely filled. The position and

		left-to-right in the periodic table			*top-to-bottom in the periodic table*		
Species	Site	Rh	Pd	Ag	Cu	Ag	Au
CH_4	–	−0.10	−0.11	−0.09	−0.09	−0.09	−0.09
O	fcc	−4.96	−4.20	−3.63	−4.83	−3.63	−3.12
CH_3	fcc	−1.78	−1.45	−0.85	−1.37	−0.85	−0.58
	top	−1.74	−1.66	−0.91	−1.19	−0.91	−1.21
CH_3O	fcc	−2.19	−1.75	−1.75	−2.31	−1.75	−1.06
CH_3OH	top	−0.38	−0.29	−0.16	−0.20	−0.16	−0.15
H	fcc	−2.80	−2.79	−2.15	−2.51	−2.15	−2.24
OH	fcc	−2.88	−2.47	−2.57	−3.11	−2.57	−1.80

Table 4.1: Adsorption sites and energies of relevant molecules, radicals, and atoms on selected transition metal surfaces. All values in eV.

population of the s band, instead, is very similar for all the metals considered.

The adsorption of the various species are now examied individually. The results for the adsorption energy are collected in Table 4.1. Following the sign convention chosen, more negative numbers refer to stronger adsorption: see Eq. (3.4).

Methane, CH_4

Methane is a closed-shell molecule with a very wide HOMO-LUMO gap (our DFT estimate: 8.5 eV). It cannot form chemical bonds with the metal surface, nor electrostatic bonds since it is a non-polar molecule. Instead, the interaction is mainly of Van der Walls kind, and thus outside the current realm of DFT because of approximated exchange-correlation functionals. The present calculations indicate no binding, with a C–metal distance as large as possible: relaxing the structure resulted in having methane in the middle of the vacuum region. The adsorption energies obtained ($E_{\rm ads} \leq 0.1$ eV) are zero within the accuracy which can be expected from this kind of calculation.

Oxygen, O

The adsorption of oxygen is the prototypical system on which adsorption models have been developed and tested. Two general observations, which remain valid for a large amount of adsorbates, are the increasing of the adsorption energy when moving rightwards in the periodic table, and the same behavior when moving downwards. These trends have been reported by many authors. My results for O in the most stable fcc site are $E_{\mathrm{O}} = -4.96$, -4.20, and -3.63 eV for Rh, Pd, and Ag and -4.83, -3.63, and -3.12 eV for Cu, Ag, and Au. Gold owes its unique nobleness to the most positive E_{O}: the O–Au bond is weaker than half the O–O bond in O_2 (from my calculations, the latter quantity is estimated to be -3.06 eV, and O adsorption would be marginally exothermic).

Perhaps the most famous and succesful adsorption model was developed by Hammer and Nørskov [3]. They proposed that bond formation takes place in two conceptual steps. First, oxygen $2p$ states interact with metal s electrons, giving rise to a broad resonance shifted at lower energies. Then these hybridized states couple with d electrons. Since the d band is narrow, splitting between bonding and antibonding states is observed. The first trend observed moving rightwards in the periodic table is easily explained: the d band shifts to lower energies, and antibonding states become more populated. A first parameter for a general understanding is thus the position of the d band ε_d. As for the second trend the authors observed that for IB transition metals the d band is anyhow filled. Accordingly, no significant contribution should be expected from the emptying of antibonding orbitals. Nevertheless the requirement that adsorbate states are orthogonal to the metal d states raises the kinetic energy by a quantity proportional to the square of the adsorbate-metal coupling matrix element squared, V_{ad}^2, the second parameter of the model. Since the $5d$ are more extended than the $4d$ and $3d$ states, V_{ad}^2 is larger for Au than for Ag and Cu thus explaining the differences within the same group.

Methyl, CH_3

Methyl adsorption is made of two components: in addition to the C–surface bond there can also be another bonding, usually referred to as agostic-bonding in organometallic chemistry. This is a three center C–H–metal bonding which occurs when the H–metal distance is small. Its presence is responsible, for example, for the different adsorption energy of methyl to Rh(111) in the fcc site when the hydrogen atoms point towards a top or a hcp site. In the former case, the H–metal distance is 0.5 Å smaller and E_{CH_3} is 0.4 eV lower.

Agostic bonding has been explained by a mixing of CH bonding orbitals with the *d* states of the surface [41], and it is expected to be attractive on Rh and Pd where the *d* band is not completely full. On the contrary, it has been recently proposed that on the noble metals it could be repulsive [42]. Since the extent of the *d* orbitals increases from top to bottom in the periodic table, one may expect that the repulsion between H and the metal surface atoms becomes larger accordingly, thus explaining the destabilization of methyl in the fcc site when passing from Cu to Ag and Au [42]. On Ag and Au, in particular, this effect is so large to disfavor the fcc site with respect to the top.

For the top site, the adsorption energy does not follow the periodic table in a trivial way, $E^{top}_{CH_3}$ being slightly lower for gold than for silver. The origin of this non usual behavior is still unclear to me.[1] Different factors which are non-monotonic on the Cu-Ag-Au series could affect the methyl binding in a concerted manner: (i) *d* wavefunctions become steadily more extended moving from Cu to Ag and Au, and the same trend would be expected for the *s* wavefunctions. However, in gold *s* wavefunctions are more contracted than in silver and even in copper, due to relativistic effects which are stronger in heavier atoms; (ii) Being the *d* states more extended, the *d* coupling matrix element V^2_{ad} for Au could be large enough to push antibonding states above the Fermi level, if the adsorbate has sufficiently high-lying valence states;

[1] In the already cited work of Wang *et al.* [42], the authors reported a different yet still unusual result, that is CH_3 being the most stable on Ag followed by Cu and Au. The origins of this trend, different than the one for fcc adsorption, was not discussed.

(iii) The d band of Ag is very deep, so the effect (ii) is less probable on it. Remind that a combination of (ii) and (iii) has been invoked to explain why for atomic C and N adsorption silver is more noble than gold [3].

Methoxy, CH_3O

While this work was in progress, the adsorption of methoxy on transition metals has been examined by Wang *et al.* [43] by means of *ab initio* calculations and interpreted in terms of the Hammer-Nørskov chemisorption model. Adsorption energies have been correlated to the d band center ε_d and the coupling matrix element squared V_{ad}^2. The results obtained are similar to those reported there both concerning the atomistic configurations—CH_3O vertical with O pointing toward the surface in a fcc site—and adsorption energies.

Methanol, CH_3OH

Methanol is another closed-shell molecule (DFT HOMO-LUMO gap: 5.2 eV), and interacts very weakly with all the surfaces considered. The interaction is slightly larger than for methane, since CH_3OH is a polar molecule (dipolar moment: 1.7 D). The preferred adsorption site is on-top of a metal atom, via an O $2p$ orbital. The oxygen–metal-atom distance is quite large, ranging from 2.34 Å for Rh(111) to 2.78 Å for Au(111); the sum of the covalent radii, for comparison, is 2.08 Å and 2.17 Å, respectively. The precise value of the binding energy has to be taken with care because of the difficult description of exchange and correlation at such large distances.

Hydrogen, H

As for hydrogen, the fcc site was found to be the most stable adsorption site. H is less stable passing from Rh and Pd to Ag, or from Cu to Ag and Au. Our estimated adsorption energy on gold is slightly lower than on silver, but the difference is of the order of the accuracy which is expected from DFT calculations. For both these surfaces, E_{H} is higher than half the calculated binding energy of H_2 (-2.28 eV) so that atomic H would quickly recombine and desorb.

Hydroxyl, OH

OH preferentially adsorbs vertically, with the O atom in a fcc hollow site and the H on top of it. It could be of interest mentioning that on Rh(111) and Pd(111) the adsorption in the bridge site is also possible, with an almost indistinguishable binding energy.

4.1.3 Reaction pathways

Activation energies and reaction pathways for the elemental processes shown in Fig. 4.1 have then been determined by the NEB algorithm described in Sec. 2.2.2. The energetics for the CH_4+O system and its derivatives after possible diffusion of the components has been collected in Fig. 4.3, together with the energies of the transition states. There, the energy of desorbed CH_3OH is chosen as reference energy for all the diagrams. With respect to the initial state, CH_4+O, the desired process (a) leading to methanol is indicated on the left hand side and the competing reactions (b), (c), and (d) on the right hand side. For reaction (d), the transition state has not been reported since no direct pathway was found, but rather proceeds by passing through the dissociation of methane [process (b)] and then the formation of methoxy: process (d), in principle among the 1^{st}-order reactions, is instead a 2^{nd}-order one and will not be discussed any more.

Some considerations can be drawn on the basis of the adsorption energies only. When moving rightwards in the periodic table metals bind adsorbates less and less strongly. On the Rh surface all the metastable configurations have comparable energies, but for the less reactive Pd dissociated adsorbates are less stable. This is even more evident in the case of Ag. In particular, the dissociation of methane on the terrace is discouraged from the energetic point of view, since the strong C–H bond is replaced by two weak surface-adsorbate bonds. The same trend is found when moving downwards from Cu to Au. The energy of adsorbed methanol, instead, is quite constant among the different substrates, since the interaction is always weak.

These considerations suggest that the least reactive metals may be the best for direct CH_3OH formation from CH_4 and O, at least for the energetics of the metastable states. Also the activation energies will matter because,

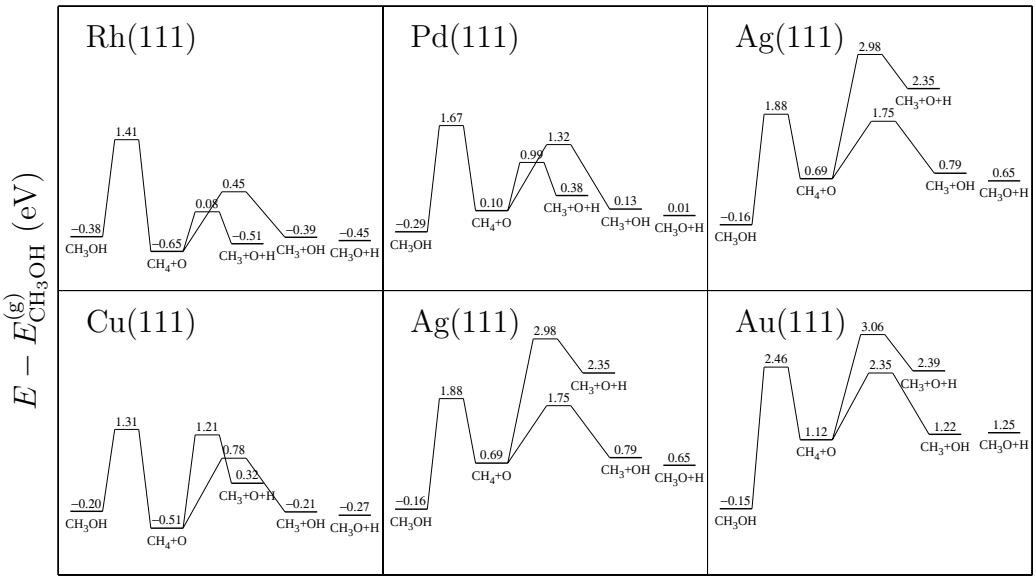

Figure 4.3: Pathways for the "1st-order" reactions of the CH_4+O system. The panel containing data on silver has been repeated for convenience. All energies in eV, taking as reference the energy of desorbed methanol.

for instance, on silver CH_3+OH is less stable than CH_3OH by 0.95 eV, but the barrier for (c) is lower than that for (a) by 0.39 eV. When CH_3 and OH will be available, methanol can also form from their combination, but the presence of these radicals on the surface would open the way to all those 2nd-order processes mentioned above.

As for the transition states, we find the same expected trend, that is the energy increases when going right-down in the periodic table. Since the reaction barriers are the balance between the energy of the transition and metastable states, both following the same trend, the behavior of the activation energy is not easily predictable *a priori*. For example, when moving to less reactive substrate the barrier for reaction (b) increases, but the one for reaction (c) is almost constant and the one for (a) even decreases (numerical values in Fig. 4.4).

It should be noticed that changes in activation energies are mostly due to the electronic structure of the substrate, and not to changes in the geometry of the transition state, as it could instead be the case for the adatom-*vs*-

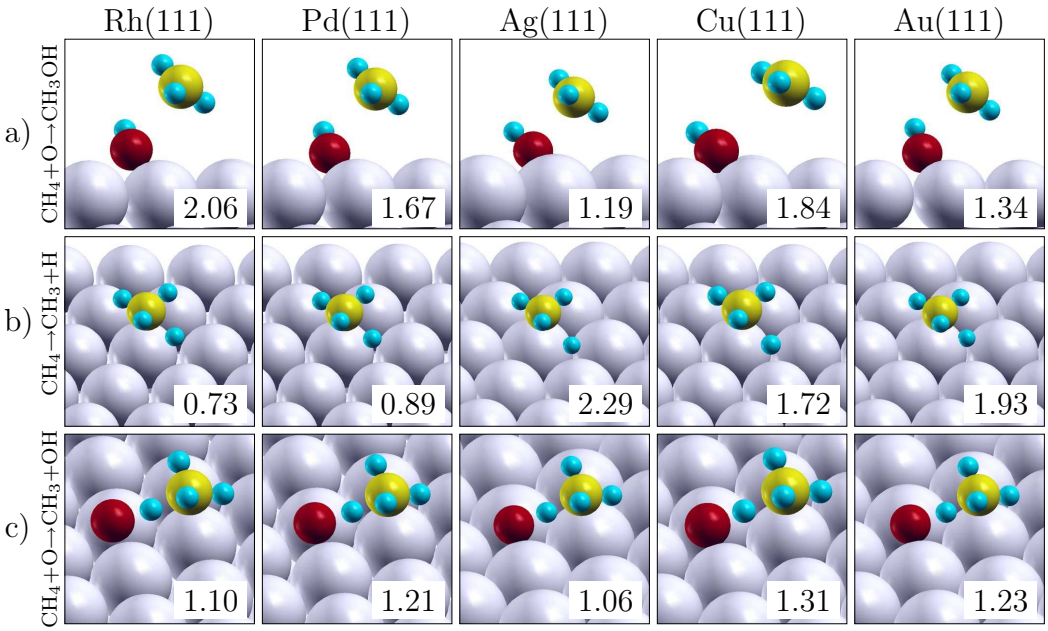

Figure 4.4: Transition state geometries and activation energies (in eV) of the 1st-order reactions shown in Fig. 4.1 on the (111) surface of the five transition metals studied in this thesis.

terrace study of Chapter 3. The transition state geometries are indeed very similar for the five metals considered, as shown in Fig. 4.4.

The magnetic structure of the adsorbed species should also be discussed. Initial and final states of all the reactions considered do not present spin magnetization, as well as the transition states of reactions (b) and (c). On the contrary, the TS for reaction (a) is magnetic by $\approx 1\ \mu_B$ per cell. Hence spin-polarized calculations were performed for the evaluation of the activation energy of this process—otherwise values incorrectly higher by 0.31 eV on the average would have been obtained. The case of Rh(111) is now taken as example to illustrate the features of this configuration. The spin polarization of the TS of reaction (a), reported in Fig. 4.5a, clearly indicates that magnetism occurs only at the C atom of methyl. This atom is coordinated to three hydrogens, far from both the dissociated H and the reacting O (2.58 and 2.73 Å respectively), and sp^2 hybridized. The out-of-plane p_z orbital is splitted between the two spin components, the minority one being shifted at energies above the Fermi level and thus unoccupied. This is evident from the

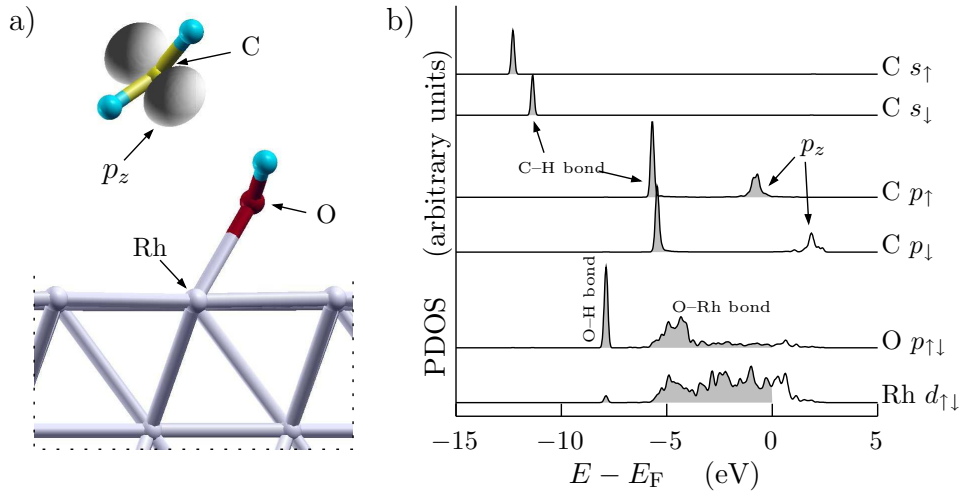

Figure 4.5: a) Spin polarization at the TS of reaction (a), CH_4+O→CH_3OH, on Rh(111): Only the majority-spin component of the p_z orbital of C is occupied. b) Density of states projected on selected valence atomic orbitals. The "spin-down" component of the p_z orbital is located at energies above the Fermi level and empty.

density of states projected on selected atomic orbitals, shown in Fig. 4.5b.

For the large interatomic distances reported above, current approximations of the exchange-correlation functional based on the local value and gradient of the density (Sec. 2.1.2) are generally not strictly reliable due to the wrong description of Van der Waals interactions. Activation energies for reaction (a) might be affected. Nevertheless, this chapter is more concerned with trends of the energy barriers than with absolute values. It is expected that the large variations of the activation energy observed on different substrates are not sensitive to this problem.

4.2 Identification of indicators

For the convenience of the forthcoming discussion, the activation energies for processes (a), (b), and (c) on the (111) surfaces of Rh, Pd, and Ag are resumed in Fig. 4.6. As already mentioned, by filling the d orbital the

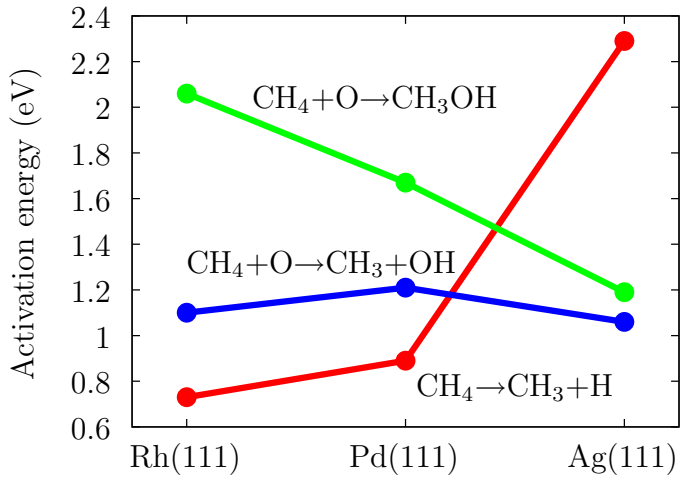

Figure 4.6: Activation energies of selected reaction as a function of the 4*d* orbital occupation of the transition metal atoms composing the (111) surface.

direct formation of methanol from methane and atomic oxygen is favored, whereas the dehydrogenation of methane on the terrace is hindered and the dehydrogenation to the oxygen atom is almost unaffected. On silver, process (b) is clearly not competitive, but the formation of methanol is still more difficult than reaction (c).

If Fig. 4.6 could be extended more to the right, one could imagine process (a) having a lower activation energy than (c). However, this cannot be done since silver already fills the 4*d* orbitals, and further electrons would be added to the 5*s* states. Moving from silver to the less reactive gold, the situation is controversial: both the barriers for (a) and (c) increase. To understand these trends, simple discussions based on the position in the periodic table only, such as the one sketched previously in Sec. 4.1.3, are not sufficient. Moreover, they would not help except for the special case of surfaces of elements.

More quantitative insight can be gained by detailed examination of the activation energies. In particular, their decomposition in elemental terms, guided by physical intuition, will help identifying relations between energy barriers and simple quantities such as sums and differences of adsorption energies, called *indicators* in the following. The usefulness of this approach is that indicators are rather easily evaluated for large sets of substrates, and

can be used to select the interesting ones by having a rough estimate of the activation energies *a priori*. In this section indicators will be identified and their quality discussed. In the next section they will be used in the search for a better catalyst.

4.2.1 (a) CH_4+O→CH_3OH

The direct pathway for partial oxydation of methane to methanol is an association reaction, but it's not characterized by a late-TS.[2] Looking at Fig. 4.4, it's evident that the TS is not similar to CH_4 and O, but more to an almost desorbed CH_3 and an adsorbed OH. The O–H distance is within 0.01 Å the one in gas phase OH. In Sec. 3.4.1 the activation energies were analyzed under the assumption of late-TS. Now a different analysis is required, and should be based on this observation on the TS structure.

Taking again desorbed methanol as reference energy, the energy of CH_4+O (IS) may be written as

$$E^{\mathrm{IS}} = E_{\mathrm{CH_4}} + E_{\mathrm{O}} + E^{\mathrm{IS}}_{\mathrm{int}} - \Delta E^{(\mathrm{g})}_{\mathrm{CH_4–O}}, \tag{4.1}$$

where $E_{\mathrm{CH_4}}$ (E_{O}) is the adsorption energy of CH_4 (O), $E^{\mathrm{IS}}_{\mathrm{int}} = E_{\mathrm{CH_4+O}} - E_{\mathrm{CH_4}} - E_{\mathrm{O}}$, and $\Delta E^{(\mathrm{g})}_{\mathrm{CH_4–O}} = E^{(\mathrm{g})}_{\mathrm{CH_3OH}} - E^{(\mathrm{g})}_{\mathrm{CH_4}} - E^{(\mathrm{g})}_{\mathrm{O}} = -4.41$ eV. For the TS a slightly different decomposition has been adopted. If we consider the TS as made of OH bound to the surface and CH_3 adsorbing to OH, its energy can be interpreted as

$$E^{\mathrm{TS}} = E^{\mathrm{TS}}_{\mathrm{OH}} + \tilde{E}^{\mathrm{TS}}_{\mathrm{CH_3}} + \Delta E^{(\mathrm{g})}_{\mathrm{CH_3–OH}}, \tag{4.2}$$

where $E^{\mathrm{TS}}_{\mathrm{OH}}$ is the adsorption energy of OH in the TS geometry without CH_3, $\tilde{E}^{\mathrm{TS}}_{\mathrm{CH_3}} = E^{\mathrm{TS}}_{\mathrm{CH_3+OH/metal}} - E^{(\mathrm{g})}_{\mathrm{CH_3}} - E_{\mathrm{metal}}$ is the adsorption energy of methyl in the TS geometry to the OH/metal system,[3] and $\Delta E^{(\mathrm{g})}_{\mathrm{CH_3–OH}} = E^{(\mathrm{g})}_{\mathrm{CH_3OH}} - E^{(\mathrm{g})}_{\mathrm{CH_3}} - E^{(\mathrm{g})}_{\mathrm{OH}} = -4.27$ eV. It's useful to further split $E^{\mathrm{TS}}_{\mathrm{OH}}$ into

[2] A late-TS reaction is one for which the TS is similar to the dissociated state. For further discussion refer to Sec. 3.4.1.

[3] Instead of $\tilde{E}^{\mathrm{TS}}_{\mathrm{CH_3}}$ one could have written $E^{\mathrm{TS}}_{\mathrm{CH_3}} + E^{\mathrm{TS}}_{\mathrm{int}}$, a notation closer to the one adopted for the IS and elsewhere in the text. However, the adsorption of methyl to the surface in the geometry of the TS without OH has not a deep physical meaning since the interaction of CH_3 to the surface in this case is mostly mediated by OH (see Fig. 4.4).

Substrate	$E_{\mathrm{act}}^{(\mathrm{a})}$	$E_{\mathrm{OH}} - E_{\mathrm{O}}$	ΔE_{OH}	$\tilde{E}_{\mathrm{CH_3}}^{\mathrm{TS}}$	$-E_{\mathrm{CH_4}}$	$-E_{\mathrm{int}}^{\mathrm{IS}}$	$-\Delta E^{(\mathrm{g})}$
Rh(111)	2.06	2.08	0.02	−0.01	0.10	0.00	−0.13
Pd(111)	1.67	1.71	0.04	−0.05	0.11	−0.01	−0.13
Ag(111)	1.19	1.05	0.14	0.04	0.09	0.00	−0.13
Cu(111)	1.84	1.71	0.19	−0.05	0.09	0.02	−0.13
Au(111)	1.34	1.40	0.00	−0.02	0.09	0.00	−0.13

Table 4.2: Decomposition of the activation energy for CH_4+O→CH_3OH. Energies in eV. See the text for the definition of the symbols.

$E_{\mathrm{OH}} + (E_{\mathrm{OH}}^{\mathrm{TS}} - E_{\mathrm{OH}}) = E_{\mathrm{OH}} + \Delta E_{\mathrm{OH}}$. The activation energy for the reaction is then:

$$E_{\mathrm{act}}^{(\mathrm{a})} = (E_{\mathrm{OH}} - E_{\mathrm{O}}) + \Delta E_{\mathrm{OH}} + \tilde{E}_{\mathrm{CH_3}}^{\mathrm{TS}} - E_{\mathrm{CH_4}} - E_{\mathrm{int}}^{\mathrm{IS}} - \Delta E^{(\mathrm{g})}, \qquad (4.3)$$

where $\Delta E^{(\mathrm{g})} = \Delta E_{\mathrm{CH_3–OH}}^{(\mathrm{g})} - \Delta E_{\mathrm{CH_4–O}}^{(\mathrm{g})} = 0.13$ eV.

The quantities composing $E_{\mathrm{act}}^{(\mathrm{a})}$ according to Eq. 4.3 are reported in Table 4.2. The major contribution to the barrier is given by the difference $E_{\mathrm{OH}} - E_{\mathrm{O}}$. The other terms are much smaller and relatively more constant with respect to changes in the activation energy. We also notice that the hydroxyl binding energy at the TS geometry roughly equals that in the relaxed geometry, the difference being lower than 0.2 eV with respect to a binding energy ranging from −3.1 to −1.8 eV. These considerations lead us to conclude that a linear relation should exist between the activation energy and the binding energy difference $E_{\mathrm{OH}} - E_{\mathrm{O}}$, which is thus chosen as indicator for this reaction. The validity of this statement is particularly evident from Fig. 4.7a, where $E_{\mathrm{act}}^{(\mathrm{a})}$ is plotted versus $E_{\mathrm{OH}} - E_{\mathrm{O}}$. A linear fit of the data gives $E_{\mathrm{act}}^{(\mathrm{a})} \approx E_{\mathrm{OH}} - E_{\mathrm{O}} + 0.02 \pm 0.08$ eV.

Of course, the chosen decomposition of E^{TS} is somewhat arbitrary, as well as any other possible choice. Nevertheless, the one made here is in my opinion preferrable since it is the most close to the nature of the transition state and the most helpful to understand the trends in the activation energies.

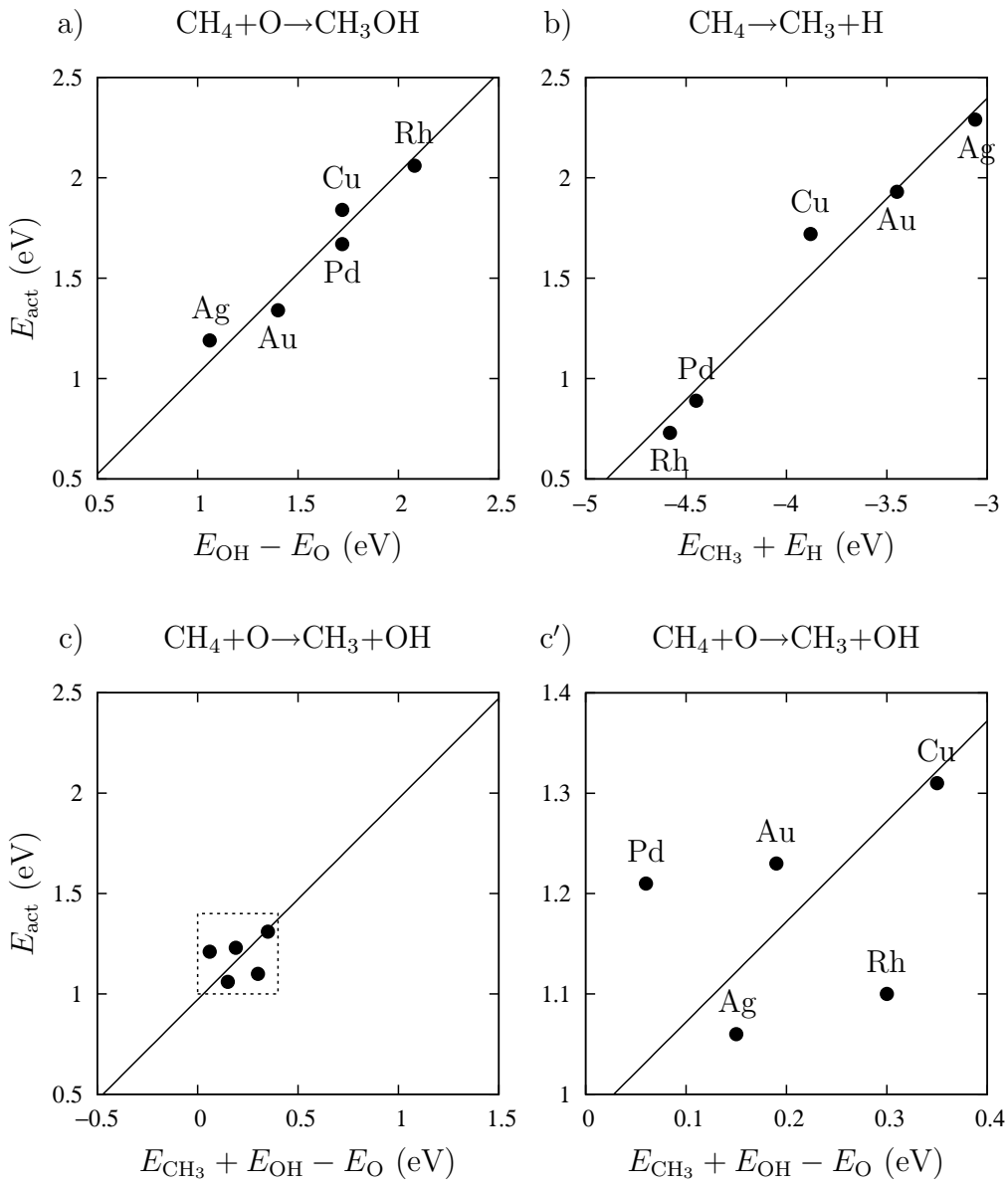

Figure 4.7: a), b), and c): activation energies of corresponding reactions plotted against the indicators proposed in the text. Points refer to values for Rh, Pd, Ag, Cu, and Au (111) surfaces. Lines are fits through the points with functions of the form $y(x) = x + b$. The scale of the graph is the same to evidenciate the different variations observed for the three reactions. c′) is an enlargement of the region delimited by the dotted square in c).

Substrate	$E_{\mathrm{act}}^{(\mathrm{b})}$	$E_{\mathrm{act}}^{(\mathrm{b})\leftarrow}$	$E_{\mathrm{CH_4}}^{\mathrm{IS}}$	ΣE^{TS}	$E_{\mathrm{int}}^{\mathrm{TS}}$	ΣE^{FS}	$E_{\mathrm{int}}^{\mathrm{FS}}$	$d_{\mathrm{C-H}}^{\mathrm{TS}}$
Rh(111)	0.73	0.42	−0.10	−4.11	0.12	−4.58	0.17	1.56
Pd(111)	0.89	0.46	−0.11	−3.95	0.11	−4.46	0.15	1.63
Ag(111)	2.29	0.55	−0.09	−2.79	0.37	−3.06	0.08	1.91
Cu(111)	1.72	0.72	−0.09	−3.40	0.40	−3.88	0.16	1.76
Au(111)	1.93	0.49	−0.09	−3.07	0.29	−3.44	0.18	1.75

Table 4.3: Decomposition of the activation energy for $CH_4 \rightarrow CH_3+H$ according to the discussion of Sec. 3.4.1. Energies in eV. $E_{\mathrm{act}}^{(\mathrm{b})\leftarrow}$ is the activation energy for the reverse reaction. The CH_3–H binding energy in the gas phase is $\Delta E_{\mathrm{CH_3-H}}^{(\mathrm{g})} = -4.62$ eV. $d_{\mathrm{C-H}}^{\mathrm{TS}}$ is the dissociating-hydrogen–carbon distance in Å, whose value for gas-phase CH_4 is 1.09 Å.

4.2.2 (b) $CH_4 \rightarrow CH_3+H$

The dehydrogenation of methane was already studied in Sec. 3.4.1 for the Rh(111) surface and the Rh adatom on Rh(111). The same analysis will now be extended to the reaction occuring on the other metals considered.

In Sec. 3.4.1 the activation energy for a dissociation was decomposed into

$$E_{\mathrm{act}}^{(\mathrm{b})} = \Sigma E^{\mathrm{TS}} + E_{\mathrm{int}}^{\mathrm{TS}} - E_{\mathrm{CH_4}}^{\mathrm{IS}} - \Delta E_{\mathrm{CH_3-H}}^{(\mathrm{g})}, \tag{4.4}$$

where the same notation as in Eq. (3.11) is adopted. This is a late-TS reaction: the C–H bond length, $d_{\mathrm{C-H}}^{\mathrm{TS}}$, reported in Table 4.3, is elongated at the TS by at least 0.47 Å with respect to gas phase methane (see also Fig. 4.4). By the "general rules" presented in Sec. 3.4.1, one would expect the activation energy to be surface sensitive.

The predicted behaviour is indeed veryfied. The terms composing $E_{\mathrm{act}}^{(\mathrm{b})}$ according to Eq. (4.4) are reported Table 4.3. It emerges that the energy barrier increases significantly on the latest transition metals, due to the lower binding of the dissociation products. It's worth noticing that the binding energy sum at the TS, ΣE^{TS}, is strongly correlated to the same value at the FS, ΣE^{FS}. These considerations suggest that significant information on the reactivity towards methane dehydrogenation can be obtained from the knowledge of the adsorption energies of methyl and hydrogen only, and that a useful indicator is $E_{\mathrm{CH_3}} + E_{\mathrm{H}}$. In Fig. 4.7b $E_{\mathrm{act}}^{(\mathrm{b})}$ is plotted against this

quantity. The quality of the linear fit confirms this conclusion: one has $E_{\mathrm{act}}^{(\mathrm{b})} \approx E_{\mathrm{CH_3}} + E_{\mathrm{H}} + 5.40 \pm 0.10$ eV.[4]

One is not concerned with the reverse reaction in the present discussion, but for completeness it's interesting to notice that the association barrier is quite independent on the chemical composition (values of $E_{\mathrm{act}}^{(\mathrm{b})\leftarrow}$ in Table 4.3), as it was already found in Sec. 3.4.1 for changes in the geometrical structure of the reaction site.

4.2.3 (c) $\mathrm{CH_4}$+O→$\mathrm{CH_3}$+OH

Differently from reaction (b), the hydrogen transfer from methane to oxygen is not a dissociation reaction. Nevertheless, it could be formally considered as a methane dissociation occurring on the O/metal system. The same analysis as for reaction (b) could then be adopted simply by taking as substrate O/metal instead of the metal terrace. By means of the "general rules" illustrated in Sec. 3.4.1, we would again expect the activation energy to be sensitive to the substrate change. However, this is not the case: the energy barrier $E_{\mathrm{act}}^{(\mathrm{c})}$ lies in a ≈ 0.2 eV narrow range, whereas for the same systems variations in $E_{\mathrm{act}}^{(\mathrm{b})}$ as large as 1.5 eV have been observed.

The decomposition of the barrier according to Eq. (4.4) and the most relevant geometrical parameters can be found in Table 4.4. Two main differences with the previous case have to be discussed. First, for reaction (b) the dissociation products was forming stronger bonds (ΣE^{FS} decreases) on more reactive surfaces. This made the reaction more energetically favorable and also lowered the barrier since $\Sigma E^{\mathrm{TS}} \approx \Sigma E^{\mathrm{FS}}$ for late-TS reactions. In case (c), instead, ΣE^{FS} is rather constant. This is explained by observing that $\Sigma E^{\mathrm{FS}} = E_{\mathrm{CH_3}} + \tilde{E}_{\mathrm{H}}$, where $E_{\mathrm{CH_3}}$ is as usual the adsorption energy of methyl to the terrace, and $\tilde{E}_{\mathrm{H}}$ the one of H to the adsorbed oxygen. The latter term can be rewritten as $E_{\mathrm{OH}} - E_{\mathrm{O}} + \Delta E_{\mathrm{O–H}}^{(\mathrm{g})}$, where

[4] A fit of even higher quality would be obtained by considering the adsorption energy of $\mathrm{CH_3}$ in top site, which is closest to the position of methyl at the TS, instead of considering the most stable adsorption geometry for each substrate. However, this would imply a loss of generality for the use of the indicator to other systems, possibly having different geometries.

Substrate	$E_{\mathrm{act}}^{(\mathrm{c})}$	$E_{\mathrm{act}}^{(\mathrm{c})\leftarrow}$	$E_{\mathrm{CH_4}}^{\mathrm{IS}}$	ΣE^{TS}	$E_{\mathrm{int}}^{\mathrm{TS}}$	ΣE^{FS}	$E_{\mathrm{int}}^{\mathrm{FS}}$	$d_{\mathrm{C–H}}^{\mathrm{TS}}$	$d_{\mathrm{O–H}}^{\mathrm{TS}}$
Rh(111)	1.10	0.79	−0.10	−2.21	−1.40	−4.46	0.05	1.37	1.29
Pd(111)	1.21	1.03	−0.09	−2.21	−1.29	−4.49	−0.04	1.36	1.31
Ag(111)	1.06	1.01	−0.09	−2.06	−1.59	−4.61	−0.04	1.41	1.25
Cu(111)	1.31	0.71	−0.11	−1.66	−1.76	−4.42	0.28	1.46	1.22
Au(111)	1.23	1.13	−0.09	−1.77	−1.72	−4.56	−0.05	1.33	1.32

Table 4.4: Same as Table 4.3 for the activation energy of CH_4+O→CH_3+OH, interpreted as methane dehydrogenation on O/metal. Energies in eV. The CH_3–H binding energy in the gas phase is $\Delta E_{\mathrm{CH_3–H}}^{(\mathrm{g})} = -4.62$ eV. Distances in Å. The C–H distance in gas-phase CH_4 and O–H distance in gas phase OH are 1.09 Å and 1.00 Å, respectively.

$\Delta E_{\mathrm{O–H}}^{(\mathrm{g})} = E_{\mathrm{OH}}^{(\mathrm{g})} - E_{\mathrm{O}}^{(\mathrm{g})} - E_{\mathrm{H}}^{(\mathrm{g})} = -4.76$ eV.[5] Thus,

$$\Sigma E^{\mathrm{FS}} = E_{\mathrm{CH_3}} + E_{\mathrm{OH}} - E_{\mathrm{O}} + \text{constant}. \tag{4.5}$$

Apart from constant contribution arising from the CH_3–H bond breaking and the O–H bond making in the gas phase, during the reaction the double bond formed by oxygen with the substrate is broken, and substituted by two weaker single bonds (CH_3– and OH–surface), the sum of which approximatively compensates the original bond so that the energy balance is almost insensitive to the change of substrate. This explains qualitatively why the activation energy for process (c) is relatively insensitive to the substrate change, whereas much larger variations were observed for reaction (b) and (a).

The second difference concerns the geometry of the TS. Comparing the C–H distances $d_{\mathrm{C–H}}^{\mathrm{TS}}$ in the two cases, we see that the C–H bond is now much less elongated (≈ 0.3 Å instead of ≈ 0.5 Å or more). Moreover, $d_{\mathrm{C–H}}^{\mathrm{TS}}$ is of the order of the O–H distances $d_{\mathrm{O–H}}^{\mathrm{TS}}$, that is at the TS hydrogen is roughly half-way between being bound to methyl and oxygen, in contrast to the late-TS approximation certainly valid for process (b).

If one still assumes a late-TS, the decomposition of the FS energy in

[5] One has $\tilde{E}_{\mathrm{H}} = E_{\mathrm{H/O/metal}} - E_{\mathrm{H}}^{(\mathrm{g})} - E_{\mathrm{O/metal}} = \left(E_{\mathrm{OH/metal}} - E_{\mathrm{OH}}^{(\mathrm{g})} - E_{\mathrm{metal}}\right) - \left(E_{\mathrm{O/metal}} - E_{\mathrm{O}}^{(\mathrm{g})} - E_{\mathrm{metal}}\right) + \left(E_{\mathrm{OH}}^{(\mathrm{g})} - E_{\mathrm{O}}^{(\mathrm{g})} - E_{\mathrm{H}}^{(\mathrm{g})}\right) = E_{\mathrm{OH}} - E_{\mathrm{O}} + \Delta E_{\mathrm{O–H}}^{(\mathrm{g})}$.

Eq. (4.5) would suggest that

$$E_{\mathrm{act}}^{(\mathrm{c})} \propto E_{\mathrm{CH_3}} + E_{\mathrm{OH}} - E_{\mathrm{O}}. \tag{4.6}$$

To verify this statement, Fig. 4.7c reports the values of $E_{\mathrm{act}}^{(\mathrm{c})}$ versus $E_{\mathrm{CH_3}} + E_{\mathrm{OH}} - E_{\mathrm{O}}$. The linear fit through the points gives $E_{\mathrm{act}}^{(\mathrm{c})} \approx E_{\mathrm{CH_3}} + E_{\mathrm{OH}} - E_{\mathrm{O}} + 0.97 \pm 0.12$ eV. The same scale of the graph as Fig. 4.7a,b has been chosen to put in evidence that the range of variation of the abscissa and ordinate ($\approx$ 0.30 and 0.25 eV, respectively) is consistent with Eq. (4.6), but in this case too small to draw significant conclusions on the details and fine differences among the substrates. Nevertheless, the compensation of the double O–surface bond with the single C– and OH–surface ones, leading to the insensitivity of the activation energy, is an important result which can be expected to hold for a large class of materials. An enlargement of the graph is shown in Fig. 4.7c′. Apparently, the fit does not look as good as for reactions (a) and (b), but as a matter of fact the deviation from the linear estimate is not larger than in the other cases.

4.3 Search for a new catalyst

In the previous section indicators for reactions (a), (b), and (c) have been identified. These are easy-to-evaluate quantities which correlate with the activation energies for the five transition metal surfaces studied. This knowledge will now be used in the search for a better catalyst for direct methane-to-methanol conversion that is, for sake of the present model study, a substrate/reaction site for which methanol formation, process (a), is the favored one. It was indicated for reaction (a) that the activation energy is linearly correlated to the binding energy difference $E_{\mathrm{OH}} - E_{\mathrm{O}}$, and hence decreases on less reactive substrates since the O bond is generally stronger than the OH one. As for methane dissociation, reaction (b), it was seen that it is particularly unfavorable exactly on the less reactive substrates on which (a) is enhanced. Therefore the analysis of process (b) can be discarded since it will be competitive only in the cases where (a) is not, and comparison with (c) is sufficient. Finally, the hydrogen transfer to O, reaction (c), should depend on an indicator, $E_{\mathrm{CH_3}} + E_{\mathrm{OH}} - E_{\mathrm{O}}$ which is approximatively constant over

the wide range of materials considered. One can then expect its activation energy being roughly constant in the range 1.18 ± 0.09 eV—the average and standard deviation of $E_{\text{act}}^{(\text{c})}$ over the Rh, Pd, Ag, Cu, Au series.

Summarizing, one has

$$E_{\text{act}}^{(\text{a})} \approx E_{\text{OH}} - E_{\text{O}} + 0.02 \pm 0.08 \text{ eV}, \tag{4.7}$$

$$E_{\text{act}}^{(\text{c})} \approx 1.18 \pm 0.09 \text{ eV}, \tag{4.8}$$

from which it can be foreseen that the condition for which $E_{\text{act}}^{(\text{a})} < E_{\text{act}}^{(\text{c})}$—i.e., for which (a) is the favored process—is approximatively given by

$$\Delta_{\text{BE}} = E_{\text{OH}} - E_{\text{O}} < 1.16 \pm 0.17 \text{ eV}. \tag{4.9}$$

The notation Δ_{BE} has been chosen for the indicator. Candidate catalyst for methane-to-methanol direct synthesis can then be identified as a system having values of Δ_{BE} appreciably smaller than a threshold of ≈ 1 eV.[6] The determination of this indicator is roughly 50 times cheaper than the one of the activation energies,[7] and large sets of systems can be quickly investigated. Finally, the energy barriers can be determined only for the interesting substrates.

The approach described above has been developed and adopted in this thesis. The values of Δ_{BE} for several systems will now be discussed, together with the activation energies whenever it was worth evaluating them on the basis of the indicator. Results are reported in Table 4.5, where many values of E_{act} are missing exactly because the corresponding Δ_{BE} was higher than the threshold value.

4.3.1 Adatoms

Rh adatoms on Rh(111)

For Rh/Rh(111) $\Delta_{\text{BE}} = 1.59$ eV is far from the interesting range. Nevertheless, data for this system are available from the study of Chapter 3 and it

[6] For being practically usable, as an additional constraint the binding energy of O to the substrate should be more than half the atomization energy of O_2, or oxygen dissociative adsorption would occur to a small extent and only at very high pressures.

[7] It is assumed that a structural relaxation requires 50 SCF loops, and a NEB optimization 250 steps each composed by 10 SCF loops.

Substrate	E_{O}	E_{OH}	Δ_{BE}	$E_{\mathrm{act}}^{(\mathrm{a})}$	$E_{\mathrm{act}}^{(\mathrm{b})}$	$E_{\mathrm{act}}^{(\mathrm{c})}$
Rh(111)	−4.96	−2.88	2.08	2.06	0.73	1.10
Pd(111)	−4.20	−2.47	1.73	1.67	0.89	1.21
Ag(111)	−3.63	−2.57	1.06	1.19	2.29	1.06
Cu(111)	−4.83	−3.11	1.72	1.84	1.72	1.31
Au(111)	−3.12	−1.80	1.32	1.34	1.93	1.23
Rh/Rh(111)	−4.89	−3.30	1.59	1.64	0.41	1.23
Rh/Cu(111)	−4.86	−3.17	1.69	–	–	–
Rh/Ag(111)	−4.45	−3.19	1.26	–	–	–
Ag/Ag(111)	−3.55	−2.51	1.04	–	–	–
Ag(111) $-10\%\Delta_{XY}$	−3.15	−2.15	1.00	–	–	–
Ag(111) $-5\%\Delta_{XY}$	−3.43	−2.37	1.06	–	–	–
Ag(111) $+5\%\Delta_{XY}$	−3.85	−2.82	1.03	–	–	–
Ag(111) $+10\%\Delta_{XY}$	−4.09	−3.05	1.04	–	–	–
$\mathrm{O}_{1/4\mathrm{ML}}^{\text{on-surf}}$/Ag(111)	−2.50	−1.87	0.62	–	2.19	–
$\mathrm{O}_{1/4\mathrm{ML}}^{\text{on-surf-hcp}}$/Ag(111)	−2.41	−1.79	0.62	0.60	–	0.88
$\mathrm{O}_{1/2\mathrm{ML}}^{\text{on-surf}}$/Ag(111)	−1.50	−1.31	0.19	–	–	–
$\mathrm{O}_{3/4\mathrm{ML}}^{\text{on-surf}}$/Ag(111)	−1.04	−0.99	0.04	0.19	–	–
$\mathrm{O}_{1/4\mathrm{ML}}^{\text{sub-surf}}$/Ag(111)	−4.20	−2.33	1.87	–	–	–
$\mathrm{O}_{\approx 0.2\mathrm{ML}}^{\text{on-step}}$/Ag(210)	−3.91	−2.63	1.28	–	–	–

Table 4.5: Adsorption energy of O and OH, and activation energies of reactions (a), (b), and (c) for: (111) surfaces of elements; adatoms on (111) surfaces; strained Ag(111); high oxygen coverages on Ag(111). $\Delta_{\mathrm{BE}} = E_{\mathrm{OH}} - E_{\mathrm{O}}$ is the indicator for the reactivity chosen on the basis of the discussion in the text. Values in eV. Dashes indicate values of E_{act} which have not been evaluated, mostly because the corresponding Δ_{BE} was higher than the threshold value, Eq. (4.9).

is instructive to compare this case to the Rh(111) terrace to indicate what should be sought for. While oxygen binds in the hollow site on the clean surface (−4.96 eV), hydroxyl binds equally well in hollow or forming two Rh–O bonds in the bridge position (−2.88 eV in both sites). Close to the adatom, no hollow site is available and O has to bind in the bridge position between the adatom and a surface Rh, with a binding energy which is almost unchanged ($E_O = -4.89$ eV) independently of the narrowing of the metal *d*-band at the adatom (see also the discussion at page 38). OH, instead, can bind to the same bridge site lowering its energy to −3.25 eV (or on top of the adatom, −3.30 eV). Overall, when moving from the terrace site to the adatom, Δ_{BE} decreases by 0.49 eV. The activation energy for (a) decreases by almost the same amount, 0.42 eV.

It's worth noticing that the quest for a better catalyst for the (a) process is not simply the search for a "less reactive" metal, as it could be concluded superficially from the analysis of Fig. 4.6. In this case, the more reactive Rh adatom is indeed better.

Rh adatoms on other surfaces

Table 4.5 also reports the values of Δ_{BE} for reactive Rh adatom on less reactive Cu(111) surface, briefly discussed at page 34, and on even less reactive Ag(111). Corresponding activation energies have not been determined, since Δ_{BE} was found to be larger than the threshold value given by Eq. (4.9) (1.69 and 1.26 eV, respectively).

Ag adatoms on Ag(111)

With $\Delta_{BE} = 1.06$ eV, silver is the best among the (111) surfaces of elements studied. If this could be decreased by as much as ≈ 0.5 eV by moving to adatoms as it was found for Rh, the resulting Δ_{BE} would be well within the desirable range. However, almost the same value for the indicator as for Ag terrace was obtained ($\Delta_{BE} = 1.04$ eV), since both the binding energy of O and OH are very close to the ones on the (111) surface. The energy cost for binding O in the bridge site is so high that it prefers to bind in hollow displacing the adatom, thus in a four-coordinated position. The binding

energy is thus similar to the one on the terrace. For hydroxyl, no energy gain is obtained since the d band of the Ag adatom is narrower, but also completely filled and does not take active part in the bonding.

4.3.2 Strained (111) surfaces

The effect of surface strain has also been investigated, since variations of the surface lattice parameter are known to affect the adsorption energies [3].

From the experimental point of view, surface strain can be induced by depositing a thin layer over a surface with a different lattice constant or through ion implantation by a nobel gas. In these simulations, the model surface obtained by cutting along (111) a silver crystal stretched along $[1\bar{1}0]$ and $[10\bar{1}]$, and relaxed along [111] was simply considered.

As compared to fully relaxed Ag(111), the adsorption energy of O increases rather linearly when applying a compressive strain, and increases when the strain is tensile. Results reported in Table 4.5 indicate variations in E_{O} of the order of 0.05 eV per percent variation in the lattice parameter, in agreement with other DFT calculations [44]. Since the same behavior has been obtained for OH, the values of Δ_{BE} are constant in the large deformation interval considered, $\pm 10\%$ and therefore not useful for the present purpose.

4.3.3 High oxygen coverages

Another method to change the adsorption energy of a species to a given surface is to coadsorb a competing species. In the case of oxygen, this can be done with O itself by increasing the coverage. In addition to direct O–O electrostatic repulsion, the presence of oxygen reduces the electric charge available on the surface for bonding an additional O atom. Thus the adsorption energy of O decreases dramatically when the oxygen concentration on the surface is increased [44]. On the other hand the same effect can be expected to be lower when applyied to the adsorption of OH, since OH bonding involves a smaller charge transfer. Silver was chosen to test this approach due to its small value of Δ_{BE} already at low coverage.

The structures considered here are illustrated in Fig. 4.8, and consists of "active" oxygen atoms participating in the reaction and "passive" ones, playing only spectator roles. The binding energy of the active O to one of these structures is defined as $E_{\mathrm{O}} = E_{\mathrm{O/structure}} - E_{\mathrm{O}}^{(\mathrm{g})} - E_{\mathrm{structure}}$. Having used (2×2) surface unit cells to compute these quantities for the (111) surfaces, to be rigorous E_{O} is the energy difference between two phases having coverages $\theta = (x+1/4)$ ML and $\theta = x$ ML, x ML being provided by the passive oxygen atoms. For consistency with the notation adopted so far, the label chosen for indicating the substrate to which the active O adsorbs at $\theta = x$ML total coverage is "$\mathrm{O}_{(x\,-\,1/4)\mathrm{ML}}$/Ag(111)". For example, at full oxygen coverage, the active O has adsorbed on $\mathrm{O}_{3/4\mathrm{ML}}$/Ag(111) substrate.

When adsorbing all oxygen atoms in the fcc site, passing from the clean (111) surface to an oxygen coverage $\theta = \frac{1}{4}$, $\frac{1}{2}$, and $\frac{3}{4}$ ML, the active-O–surface bond is much weakened, passing from -3.63 to -2.50, -1.50, and -1.04 eV respectively. The corresponding OH bond, instead, is less destabilized and reduces from -2.57 to -1.87, -1.31, and -0.99 eV. On the $\mathrm{O}_{3/4\mathrm{ML}}^{\text{on-surf}}$/Ag(111) (Fig. 4.8d), the adsorption of OH is almost as favorable as the one of OH, and Δ_{BE} approaches zero (0.04 eV). The calculated activation energy for (a) is very low (0.19 eV) and confirms the linear relation with the indicator put forward in Sec. 4.2. On this substrate it is not possible to compare (a) and (c) processes because there is not enough space for adsorbing the FS of reaction (c). The comparison between the two processes can be done for $\theta = \frac{1}{4}$ ML, provided that the passive oxygen atom is located in the hcp hollow instead of the fcc one, or again there would not be space for reaction (c) to occur. This slightly different structure, labeled as $\mathrm{O}_{1/4\mathrm{ML}}^{\text{on-surf-hcp}}$/Ag(111) and depicted in Fig. 4.8b, provides almost the same values for E_{O} and E_{OH} at the active site (-2.41 and -1.79 eV, respectively), and Δ_{BE} coincides within 0.01 eV with the one for fcc passive oxygen, 0.62 eV. On this substrate, reaction (a) is already more favorable than (c), the activation energies being 0.60 and 0.88 eV, respectively.[8]

It's worth to remark at this point that structures with so high oxygen coverages in *on*-surface sites are not yet experimentally feasible. First, the

[8]Owing to different TS geometry, the activation energy for methane dissociation to CH_3 and H reported in Table 4.5 has been computed with passive oxygen in fcc.

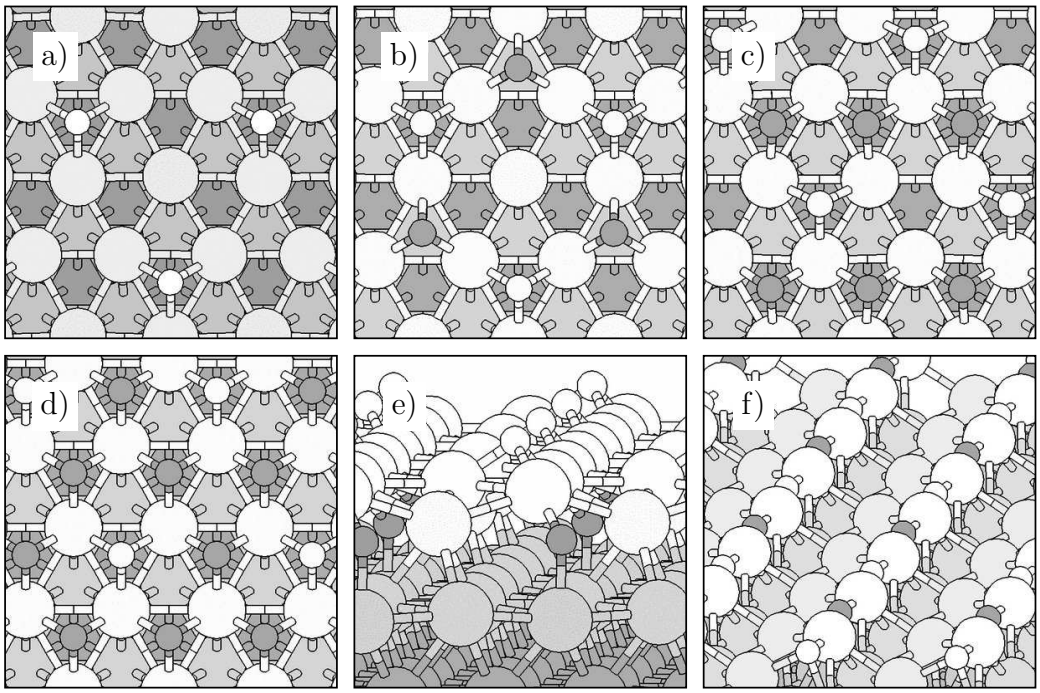

Figure 4.8: Atomic structures of oxygen-covered silver surfaces considered in the text: a) adsorption of O to the clean Ag(111) surface, resulting in a 1/4 monolayer of O; b) adsorption to $O^{\text{on-surf-hcp}}_{1/4\text{ML}}$/Ag(111) (2/4 monolayer total); c) adsorption to $O^{\text{on-surf}}_{2/4\text{ML}}$/Ag(111) (3/4 monolayer total); d) to $O^{\text{on-surf}}_{3/4\text{ML}}$/Ag(111) (4/4 monolayer total); e) to $O^{\text{sub-surf}}_{1/4\text{ML}}$/Ag(111), forming an Ag_2O-like structure (2/4 monolayer). A top view of this structure would be the same as in panel b); f) to Ag(210) steps decorated by oxygen [$O^{\text{on-step}}_{\approx 0.2\text{ML}}$/Ag(210)], forming [-Ag-O-] rows ($\approx$ 0.4 ML). Large and small spheres represent silver and oxygen atoms, respectively. The passive oxygen atoms, not participating in the reactions, are filled with a darker gray than the active oxygen atoms.

average adsorption energy for oxygen atom would be higher than half the dissociation energy of O_2 (approximatively for $\theta > 0.5$ ML), so that dissociative adsorption is not energetically favorable and large pressures are required. Second, oxygen would start occupying sub-surface sites, eventually forming silver oxyde. At $\theta = 0.5$ ML, it was found that a $0.25\text{ML}^{\text{sub-surf}}$+$0.25\text{ML}^{\text{on-surf}}$ combination (Fig. 4.8e) is more favorable than a pure 0.50ML on-surface structure (Fig. 4.8b) by 0.39 eV per oxygen atom, in close agreement with the value of 0.35 eV obtained by previous DFT calculations [45]. The $0.25\text{ML}^{\text{sub-surf}}$+$0.25\text{ML}^{\text{on-surf}}$ exhibits very similar atomic geometry and electronic structure to the observed [46, 47] Ag(111)-$p(4\times4)$-O surface ("surface oxide", $\theta = 0.375$), and for these reasons has been proposed as model of the latter [45]. It is therefore interesting to discuss the results for O/OH adsorption energy to an $\text{O}^{\text{sub-surf}}_{1/4\text{ML}}$/Ag(111) surface. Unfortunately, they are not so promising for what concerns the value of our indicator. Upon adsorption, an oxygen in the fcc site gains -4.20 eV, a bond stronger than on clean Ag(111) since the surface O also stabilizes the subsurface one. Unfortunately, no such stabilization occurs for hydroxyl adsorption ($E_{\text{OH}} = -2.33$ eV), and the value of $\Delta_{\text{BE}} = 1.87$ eV falls well above the crossover point.

This discussion on oxygen-covered Ag surfaces will be concluded by a quick mention to the results for another structure experimentally observed for which the coverage is relatively high—equivalent to $\theta \approx 0.4$ ML on the (111) terrace, that is the Ag(210) surface. This is composed by one-atom-wide (100) terraces and open (110) steps. Oxygen adsorbs decorating the steps with the formation of O-Ag-O rows (Fig. 4.8f), gaining 0.80 eV per oxygen atom with respect to $1/2O_2$ [48]. Adsorption energy of O and OH to this structure have been calculated assuming periodicity of two Ag lattice spacings in the in-row direction—thus species adsorbed to $\text{O}^{\text{on-step}}_{\approx 0.2\text{ML}}$/Ag(210) substrate. A value of $\Delta_{\text{BE}} = 1.28$ eV was obtained, out of the potentially interesting range.

4.3.4 Summary and outlook

Summarizing the results obtained in this chapter, indicators for the reactivity have been identified from the decomposition of the activation energies in

elemental terms for a few substrates. In particular, for direct methane-to-methanol conversion via reaction (a), the key quantity is $\Delta_{\mathrm{BE}} = E_{\mathrm{OH}} - E_{\mathrm{O}}$: for Δ_{BE} lower than ≈ 1 eV process (a) should be favored with respect to (b) and (c).

Δ_{BE} was evaluated for several model materials, and for those satisfying the above requirement also the activation energies were determined. Results collected in Fig. 4.9 clearly show the validity of the proposed approach: trends for the activation energy, which were obtained for values of $\Delta_{\mathrm{BE}} = 1$–2 eV, can be successfully extrapolated down to $\Delta_{\mathrm{BE}} \approx 0$, for which reaction (a) would occur with almost no barrier.

Realistic catalysts for methane-to-methanol conversion, direct pathway, could then be identified on the basis of the following guidelines:

(i) The substrate should not be too much reactive (i.e., it should not bind adsorbates too strongly), otherwise methane dissociation to CH_3 and H, and eventually further decomposition to CH or C, would be favored with respect to the formation of methanol: energy barriers for C–H bond breaking are generally small on reactive surfaces, and in particular smaller than those for the C–O bond formation necessary for methanol synthesis (Chap. 3).

(ii) Oxygen has to adsorb dissociatively at catalyst's surface, so that it is readily available for methanol formation.

(iii) On the other hand, oxygen should be weakly bound, while OH as stable as possible, so that the indicator $\Delta_{\mathrm{BE}} = E_{\mathrm{OH}} - E_{\mathrm{O}}$ proposed in this section is as small as possible: for Δ_{BE} lower than ≈ 1 eV, methanol formation, reaction (a), would be more probable than hydrogen transfer to adsorbed O, reaction (c).

(iv) Changing the geometry of the reaction site (e.g., see Sec. 4.3.1) or applying surface strain (Sec. 4.3.2) might not be sufficient to optimize the value of this indicator. The best results hitherto achieved were obtained by the co-adsorption of "promoter" species, for instance competitive electronegative adsorbates which destabilize O more than OH.

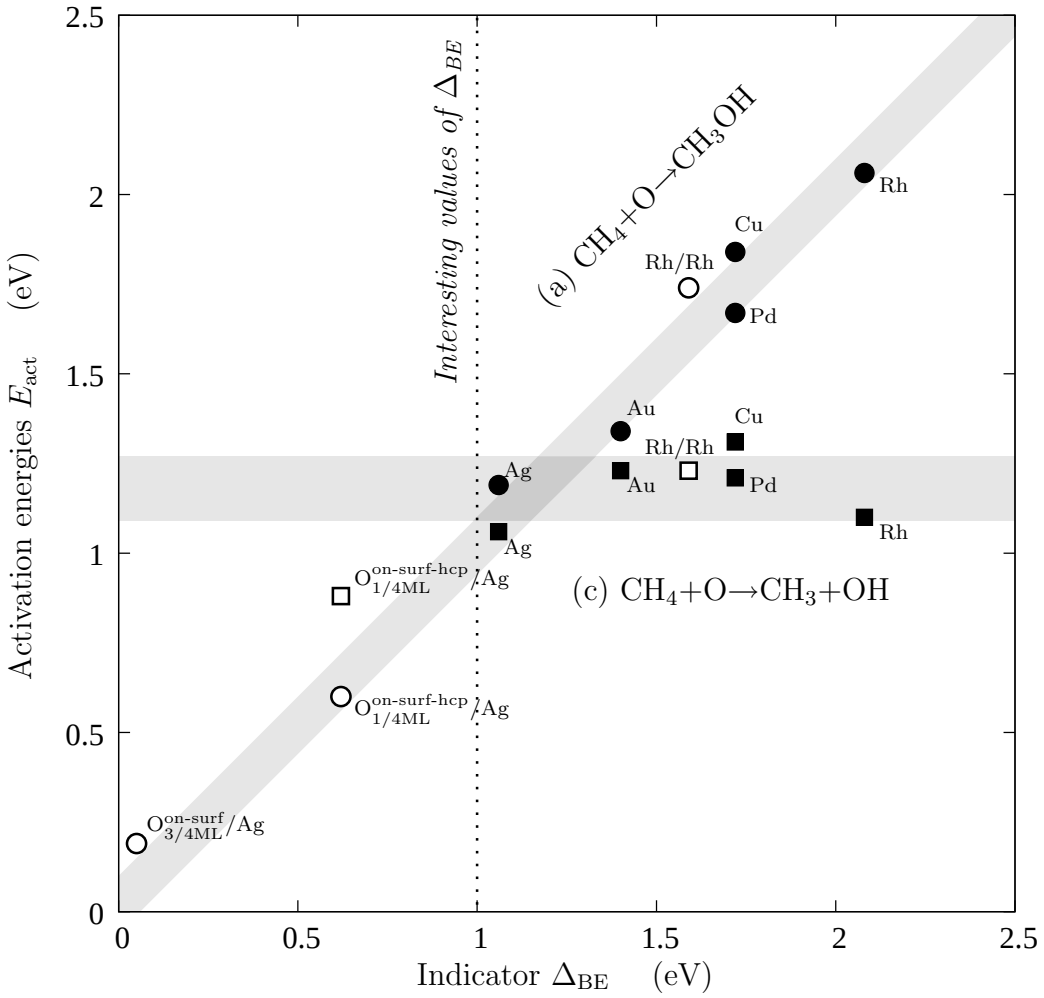

Figure 4.9: Activation energies for (a) methanol formation (circles) and (c) hydrogen transfer to the adsorbed oxygen (squares) as a function of the indicator $\Delta_{\mathrm{BE}} = E_{\mathrm{OH}} - E_{\mathrm{O}}$. Gray areas indicate the estimated activation energies on the basis of equations (4.7) and (4.8), within the standard deviation as evaluated from the data for Rh, Pd, Ag, Cu, and Au(111) (marked with filled symbols). Empty symbols refer to values of Δ_{BE} and corresponding E_{act} for the other systems discussed in the text. The vertical dotted line delimitate the range of interesting values of the indicator according to Eq. (4.9). Values in eV. (111) Miller indexes for the surface orientation are common for all the substrates and have been omitted.

Here the effect of additional oxygen itself was examined (Sec. 4.3.3) but other strongly electronegative species could have similar effect.

It is quite evident that conditions (i)-(iv) above are not easily satisfied simultaneously—consistently with the fact that a good catalyst for direct methane-to-methanol conversion has not yet been identified despite the great effort spent in this direction.

As for the systems considered here, the most interesting one is O/Ag(111). At 0.5 ML total coverage [CH_4+O/$O_{1/4ML}$/Ag(111), Fig. 4.8b], an impinging methane molecule would preferentially form methanol ($E_{act}^{(a)} = 0.60$ eV) rather than dissociate ($E_{act}^{(b)} = 2.19$ eV) or donate one H to adsorbed O ($E_{act}^{(c)} = 0.88$ eV). Since $E_{act}^{(b)}$ is much larger than the other activation energies, one should consider processes (a) and (c) only. The ratio between their reaction rates, $k^{(a)}$ and $k^{(c)}$, gives the selectively towards methanol formation in terms of the number of reacting methane molecules:

$$\frac{k^{(a)}}{k^{(c)}} = e^{-\left(E_{act}^{(a)} - E_{act}^{(c)}\right)/k_B T}. \tag{4.10}$$

Here, reaction rates have been evaluated according to Eq. (2.19) assuming the same prefactors. Eq. (4.10) says that, for highly selective methanol formation, low reaction temperatures are needed. E.g., if one requires that only one methane molecule form CH_3 and OH, every 1000 synthesizing CH_3OH, the temperature T must be lower than 470 K. Lower selectivities could be accepted, considering that after reaction (c) methanol could still be synthesized from CH_3 and OH. For this reason it would be interesting to study the follow-up 2nd-order processes. For example, preliminary calculations for Ag at 1/4 ML indicate that CH_3–OH recombination is favored with respect to the process of further methyl dehydrogenation [49].

Recall that for evaluating adsorption energies and activation barriers reported in this chapter (2×2) surface unit cells have been used. This means that O adsorption on $O_{1/4ML}$/Ag(111) inevitably results in a very large total coverage, 0.5 ML. As a matter of fact, it is possible that the interaction with the nearest neighbours only would be sufficient to destabilize an oxygen atom to give the wanted value of Δ_{BE}, so that results similar to the ones of O/$O_{1/4ML}$/Ag(111) could be obtained both for $E_{act}^{(a)}$ and $E_{act}^{(c)}$. A *local*

coverage higher than 0.25 ML could be reached, e.g., when a further atom adsorbs to the (2×2) structure. Therefore, it would not be necessary to adsorb 0.5 ML on-surface, a task which would require special techniques so far undeveloped since this structure is not thermodynamically stable, whereas 0.25 ML coverage is indeed stable for some values of temperature and oxygen partial pressure, P_{O_2}. Tuning T so that reaction (a) is significantly favored over (c), and adjusting P_{O_2} so as to fulfil the stability requirements, thermal diffusion or adsorption of further oxygen might produce local fluctuations in the oxygen density on the surface. These atoms would be less bound, and prone to react with impinging methane.

In this picture, the most competitive process could be oxygen migration to sub-surface sites. Migration below the first atomic layer would reduce the local density of surface oxygen, thus reducing the number of weakly-bound O atoms and stabilizing surface ones. Extended surface oxide would anyhow not form because at these values of P_{O_2}, T it would not be thermodynamically stable, and subsurface oxygen would eventually come back to surface. For the following, it is safe to assume the worse case, that is that O will not return on-surface until the local density is further reduced because of diffusion, desorption, or some other reason.

At 0.11 ML coverage, the activation energy for migration below the first atomic layer has been recently evaluated to be $E_{act}^{(surf–subsurf)} = 0.86$ eV [45].[9] This barrier is very close to the one for reaction (c) above, hence the temperature dependent exponential in the reaction rate is similar. However, the vibrational frequency could be rather larger than CH_4-surface collision frequencies, unless at very high partial pressure, P_{CH_4}. This suggests that a CH_4-rich environment is required, together with low temperatures [already necessary for making process (a) favored over (c)]. The reaction rates can be

[9] Since sub-surface oxygen atoms are stabilized with respect to on-surface ones at higher concentrations, it can be expected that this energy barrier decreases with coverage. An estimate of $E_{act}^{(surf–subsurf)}$ at the larger coverages considered here would worth be used, but was not available at the time of writing.

estimated as[10]

$$k^{(\mathrm{a})} = AP_{\mathrm{CH_4}}\sqrt{\frac{\pi}{2M_{\mathrm{CH_4}}k_{\mathrm{B}}T}}\mathrm{e}^{-E^{(\mathrm{a})}_{\mathrm{act}}/k_{\mathrm{B}}T}, \tag{4.11}$$

$$k^{(\text{surf-subsurf})} = \frac{\omega}{2\pi}\mathrm{e}^{-E^{(\text{surf-subsurf})}_{\mathrm{act}}/k_{\mathrm{B}}T}, \tag{4.12}$$

where A is the surface area corresponding to one adsorbed O atom and was approximated by half the (111) unit cell, $M_{\mathrm{CH_4}}$ is the mass of methane, and ω is the vibrational frequency of adsorbed O, of the order of 10 THz. It's easily seen that for $T = 300$–400 K and $P_{\mathrm{CH_4}} = 0.1$–1 bar the two rates are of the same order: this could be already enough, since sub-surface O would not accumulate but mostly come back to surface as discussed above.

The overall rate for the formation of methanol is given by

$$2\big[\mathrm{O_2}\text{ dissociation rate}\big]\frac{k^{(\mathrm{a})}}{k^{(\mathrm{a})} + k^{(\text{surf-subsurf})} + k^{(\text{other processes})}}. \tag{4.13}$$

Thus, whenever $k^{(\mathrm{a})}$ is not much smaller than the rate for the other processes which could lower the concentration of atomic O on the surface, the rate determining step for methanol formation would be the sticking of $\mathrm{O_2}$, which unfortunately is very low. For a larger rate, higher temperatures would be required. The presence of defects such as steps could also ease oxygen dissociation.

Because of uncertainties of calculated adsorption and activation energies, which affect exponentially reaction rates, it would be worthwhile investigating the reactivity and selectivity of silver (111) surface towards methanol synthesis by controlled ultra-high vacuum (UHV) experiments, at room temperature and coverages as large as possible, before attemping the realization of a reactor operating under real high-pressure conditions. Practical difficulties for the realization of such a system under UHV conditions are the low sticking of oxygen, and the low methane pressure which could be adopted. As for oxygen adsorption, one could dose oxidant molecules less stable than $\mathrm{O_2}$ such as $\mathrm{N_2O}$ or $\mathrm{O_3}$, or directly dose atomic oxygen with the use of plasma sources. The efficiency of surface-colliding $\mathrm{CH_4}$ might instead be increased

[10]For process (a) the reaction rate is computed by multiplying the frequency of impact of $\mathrm{CH_4}$ onto an adsorbed O times the exponential $\mathrm{e}^{-E^{(\mathrm{a})}_{\mathrm{act}}/k_{\mathrm{B}}T}$.

if a vibrationally excited molecular beam is adopted, since the frequency of C–H stretching mode in methane is quite large, ≈ 0.5 eV. This procedure, which could be achieved by illuminating the molecular beam with a suitable laser, would raise the energy of the initial state but presumably not the one of the transition states for processes (a) and (c), thus not disturbing selectivity measure.

After that, the effect of several other details could be investigated both by *ab initio* simulations and experimentally in order to optimize the catalyst. A great achievement in this matter would be the enhancement of the difference among the activation energy for process (a) and the competing ones, which would enable the use of larger temperatures—thus raising the reaction rate—without relevantly affecting selectivity. This could be realized by a number of methods such as: the use of different "promoter" atoms to tune the adsorption energy of surface oxygen; alternatively, binary alloys could be more resistant to surface oxide formation and be adopted as substrate instead of silver; surface strain might be a way to change the adsorption properties of O, without affecting the binding energy difference Δ_{BE}; additional O could adsorb to surface oxide, resulting in interesting weakly-bound oxygen species, before the formation of thick layers of Ag_2O, which is not easily observed and could be kinetically hindered. Similar routes for improvement are currently adopted, or have been proposed, for other silver catalyzed reactions [50, 51, 52].

Conclusions

In recent times the development of efficient methanol fuel cells and the ever-growing price of oil have attracted increasing technological interest to direct conversion of methane into methanol. This topic is relevant also to the theoretical condensed matter community, as the need for a proper catalyst can be helped by the atomistic modelling of adsorption and reaction phenomena at a catalyst's surface.

This thesis is focused on the simulation of processes leading to methanol on transition metal surfaces and of the competing ones making other chemicals (or producing catalyst's coking and inactivation). The case of heterogeneous catalysis was addressed through the *ab initio* numerical study of activation energies, reaction pathways, and energy barriers.

One of the major problems in chemical synthesis from methane on transition metal catalysts is the difficulty of breaking or at least weakening ("activating") a C–H bond, so that the resulting CH_3 radical may react with other species e.g., be oxygenated to eventually form methanol, without activating other C–H bonds. In fact, the first C–H bond cleavage commonly starts a dehydrogenation pathway leading to CH or atomic C poisoning the catalyst. Recently, both experimental and theoretical studies have indicated that under-coordinated sites might be a solution to the problem. In particular, this was suggested to be the case for the model catalyst composed of Rh adatoms on Rh(111) surfaces [Rh/Rh(111)].

Following these observations, reactions connecting methane to methanol on Rh(111) surfaces and Rh/Rh(111) have been studied in detail and have been reported in this thesis. The reaction pathways were identified for a set of elemental processes, and the rate-determining step of methane-to-methanol conversion was found to be the C–O bond formation. The corresponding

activation energies are however too high with respect to competing further dehydrogenation of methyl radical. The conclusion is that methanol formation cannot occur on these two substrates.

The question is then how much these results depend on specific choice of the substrate e.g., cutting orientation, or a defect other than the adatom. This question is of fundamental importance because no matter how large is the number of systems one can simulate, it cannot be excluded *a priori* that different results would be obtained in other cases, unless some general argument is provided. Such a topic has been analyzed in detail. Previous discussions reported in the literature regarding site sensitivity or insensitivity of association/dissociation reactions were reviewed and extended. The "general rule" for late transition-state reactions is that dissociation reactions are structure sensitive—that is, the activation energy depends significantly on the substrate—except for the case of strongly adsorbed reactants where compensations may occur. On the other hand association reactions are mostly structure insensitive. The above arguments translate into the indication that no Rh surface could be a good catalyst for methane-to-methanol conversion, since it was found that the rate-determining steps, which are association reactions, are site-insensitive.

To go beyond the trial-and-error procedure in the search of a better catalyst, the identification of guidelines is then desirable. This was achieved by the study of (111) surfaces of different transition metals. Given the difficulty experienced on Rh in synthesizing methanol after methane dehydrogenation, focus was put on the direct insertion of atomic O (thought as preadsorbed on the surface) into a C–H bond and on the competing processeses which share the same initial configuration. It was found that substrates which bind adsorbates less strongly could be better for methanol formation than more reactive ones. The contrary was observed for methane dehydrogenation, one of the competing processes, whereas for the other, hydrogen transfer to adsorbed O with OH synthesis, the activation energy was found to be almost constant for all the metals considered. On none of these substrates methanol formation was however the preferred process.

Significant insight was obtained by an analysis conceptually similar to the one mentioned above for site-sensitivity of dissociation and association

reactions. It was shown that activation energies are fairly correlated to linear combinations of adsorption energies of the radicals involved in the reaction ("indicators"), the specific combination to be established on a case by case basis depending on reaction specific characteristics, such as in particular the geometry of the transition state. The important point here is that these relations can be determined from the analysis of a small number of substrates only, and then extrapolated to a much wider class of materials. One thus easily obtains a first estimate of the energy barrier for a newly proposed system, by the evaluation of a few adsorption energies only.

The usefulness of this approach was then illustrated by its application to the search of a new catalyst for methanol synthesis, where the indicator is the binding energy difference between OH and O. From a rather large set of model systems, for which the evaluation of the activation energies would have been extremely expensive, the most promising substrates have been identified on the basis of the indicator. Energy barriers have then be determined for these systems only, saving much of the effort. The validity of the indicator chosen from a limited set of data was confirmated by the calculation of activation energies even for substrates of quite different properties.

On the basis of our results, a candidate catalyst could be suggested. This consists in a Ag(111) surface dosed with large amounts of oxygen, from 0.25 ML up to 0.5 ML. On this O/Ag substrate the activation energy for methanol formation would be significantly lower than for competing methane reactions. Even though 0.5 ML on-surface coverage has not yet been reported due to its instability towards surface oxide formation, oxygen adsorption and desorption are in a dynamical equilibrium and statistical fluctuations might produce *locally* the high coverage required. In this case oxygen sticking and dissociation is estimated to be the rate determining step of the overall process. An experimental procedure aimed at the confirmation of the relevance (activity and selectivity) of this system for methane-to-methanol conversion is suggested. At a later stage, additional issues could be addressed both theoretically and experimentally in order to optimize the catalyst, such as the use of different adsorbed species for destabilizing oxygen, or of suitable alloys subject to oxidation only at larger coverages, or adsorption over surface oxide.

It is worth remembering that the oxygen/silver system still presents several open questions, despite the numerous experimental and theoretical studies in the literature. It is well known from long time that, under different reaction conditions, silver is *the* catalyst for various partial oxidation reactions such as ethylene epoxidation (atmospheric pressure, T = 500–600 K) and methanol oxidation to formaldehyde (also at atmospheric pressure, T = 800–900 K), owing to exceptional selectivities. However, it is only in recent times that the scientific community has started understanding from the microscopical point of view catalytic properties of silver, thanks to the combination of experimental investigation with *ab initio* numerical simulations. I hope that results presented in my thesis will stimulate further study in this interesting subject.

Appendix A

Overview of other works by the author

This Appendix will give a short presentation of the works that I contributed to as a Ph. D. student at S.I.S.S.A./I.S.A.S.

Templated growth of metal-organic coordination chains at surfaces

Thomas Classen, Guido Fratesi, Giovanni Costantini, Stefano Fabris, Frank Louis Stadler, Cheolkyu Kim, Stefano de Gironcoli, Stefano Baroni, and Klaus Kern;
accepted for publication in Angewandte Chemie International Edition (cover article).

Abstract:
One dimensional metal-organic coordination chains (MOCCs) have been fabricated at the Cu(110) surface by self-organized growth. Using scanning tunneling microscopy (STM) we demonstrate that the anisotropy of the surface can be translated to one-dimensional MOCCs with both Cu and Fe as metallic centers and trimesic acid (TMA) as molecular linker. The atomistic and electronic structure of the chains is determined by comparing the STM results to density functional theory calculations (DFT). Our calculations predict a strong spin polarization for the Fe adatoms coordinated by the organic molecules.

Design of the reaction site: A model study of methane dehydrogenation on Rh/Cu(111)

Nicola Bonini, Anton Kokalj, Stefano de Gironcoli, Carlo Sbraccia, Guido Fratesi, and Stefano Baroni;
in preparation.

Abstract:
Tuning the relative reaction rates of the different steps of methane dehydrogenation would allow to optimally design many dream reactions such as, e.g. the direct conversion of methane to methanol. On metal catalysts, it is known that the reaction barrier for the first step, $CH_4 \rightarrow CH_3+H$, is larger than that for the second, $CH_3 \rightarrow CH_2+H$, indicating the difficulty of controlling the reaction. In this work we address by density-functional-theory calculations the problem of the dependence of the reaction barriers of the first two steps of methane dehydrogenation on the local (i) atomic structure and (ii) chemical composition of the reaction site. By the atomic-scale analysis of the two reactions we design a new reaction site on a model catalyst that effectively activates the dehydrogenation of methane, but the dehydrogenation of methyl is effectively hindered. It is shown that a proper geometry of a reaction site, such as an ad-atom defect, can reduce the barrier for the first reaction and increase the barrier for the second reaction. On the other hand, by tuning the chemical composition such that the reaction site involves only one reactive metal atom the barrier for the second reaction is substantially increased. These ideas are implemented on a model catalyst composed by isolated reactive Rh atoms on less reactive Cu(111).

Appendix B

Computational tools

All the results presented in this thesis have been obtained by *ab initio* simulations in the framework of density-functional theory (DFT, see Sec. 2.1.2). The Perdew-Burke-Ernzerhof (PBE) [19] generalized gradient approximation (GGA) has been adopted for the exchange and correlation functional. Peridically repeated slabs separated by a vacuum region of 10 Å or more have been chosen as model for the surfaces (see Fig B.1). The plane-wave ultrasoft pseudopotential method [21] was used as implemented in the PWscf code of the Quantum-ESPRESSO distribution [22]. Pseudopotentials derived from relativistic all-electron atomic calculations have been used for the heavier elements Rh, Pd, Ag, and Au. A kinetic energy cutoff of 27 Ryd and 60 special points for the Brillouin zone (BZ) integration [53] were considered in the bulk fcc unit cell. The same cutoff and equivalent **k**-point meshes were used for all the surface structures investigated, except for the (2×3) unit cell adopted in Sec. 3.3.2 for the study of O-H recombination on Rh+Rh(111), for which no **k**-point set equivalent to the chosen bulk mesh can be defined. Test calculations with a lower (25 Ryd) kinetic energy cutoff and a BZ sampling twice as coars as above have also been performed for all the metastable structures studied on the Rh(111) surface, and the root mean square error found for the adsorption energies was less than 0.07 eV.

Lattice parameter and bulk moduli of Rh, Pd, Ag, Cu, and Au, obtained using the above setup, are reported in Tab. B.1 and compared with the experimental values [54]. In agreement with typical results obtained within

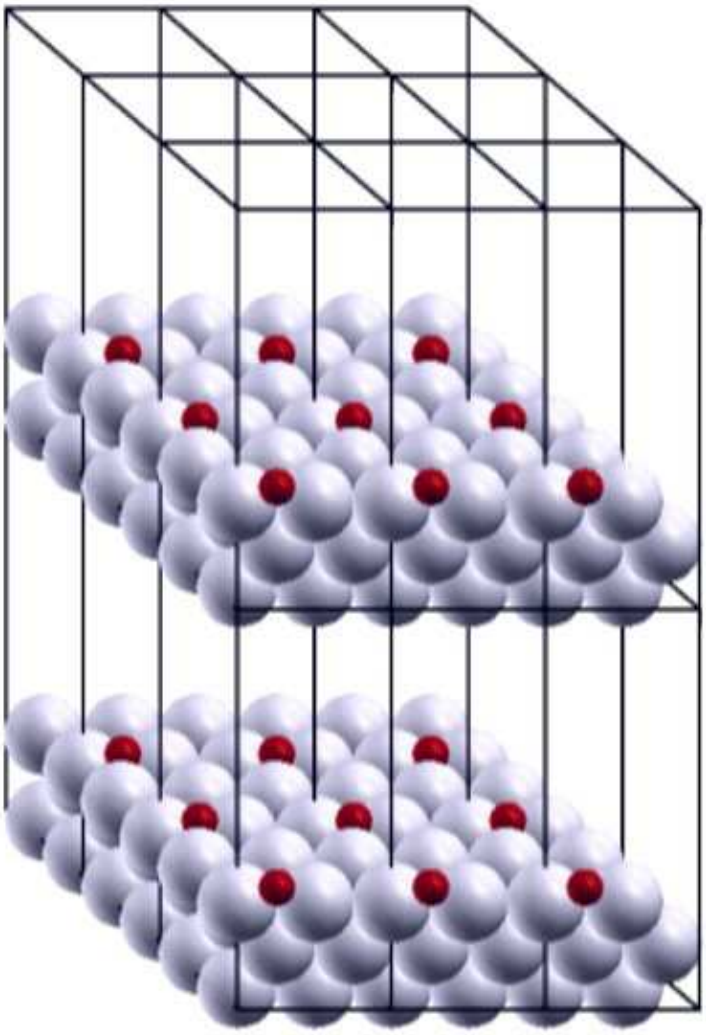

Figure B.1: Periodically repeated image of a typical supercell used for the calculations.

	Lattice parameter (Å)		Bulk modulus (GPa)	
	theory	exp.	theory	exp.
Rh	3.86	3.80	255	270
Pd	3.98	3.89	151	181
Ag	4.16	4.09	94	101
Cu	3.67	3.61	126	137
Au	4.17	4.08	138	173

Table B.1: Lattice parameters and bulk moduli of selected metals as obtained with the setup described in the text. Experimental values are taken from the book of Kittel [54].

GGA approximation theoretical lattice parameters are slightly overestimated and the bulk moduli underestimated with respect to experimental results.

Total energy of isolated molecules and atoms, needed as reference to compute adsorption energies, have been evaluated in a cubic cell of 20 bohr side length using only the Γ point only for Brillouin zone integration, and allowing for spin-polarization. The net reaction from methane and oxygen to methanol is found exothermic by 1.35 eV, in very good agreement with the experimental value (1.31 eV [55]) This agreement is somehow fortuitous since larger errors are obtained in other cases. For instance, the atomization energy of O_2 molecule is 6.12 eV according to our calculation, whereas the experimental value with zero point vibrations removed is 5.25 eV [26].

For the determination of the adsorption sites and energies, the bottom layers of the slabs were kept fixed at the bulk truncated positions, while the upper one(s) where allowed to relax. Molecules were placed on this side of the slabs and relaxed together with the upper layer until the forces on the atoms were less than 0.02 eV/Å. Structural optimizations have been performed using a quasi-Newton algorithm and a BFGS scheme available in the PWscf code [22]. The adsorption energy of a generic species A to a metal m is defined as

$$E_{\mathrm{A}} = E_{\mathrm{A/m}} - E_{\mathrm{A}}^{(\mathrm{g})} - E_{\mathrm{m}}, \tag{B.1}$$

where $E_{\mathrm{A/m}}$, $E_{\mathrm{A}}^{(\mathrm{g})}$, and E_{m} are the total energies of the A/m complex, gas

phase A, and the clean m surface in their relaxed atomistic configurations. Following the notation chosen, more negative values of E_{A} correspond to stronger bonds. In some cases, we found convenient to refer adsorption energies to the energy of desorbed methanol. This was done by computing

$$E'_{\mathrm{A}} = E_{\mathrm{A/m}} - E^{(\mathrm{g})}_{\mathrm{CH_3OH}} - E_{\mathrm{m}}, \tag{B.2}$$

provided that species A has the same atomic composition as CH_3OH.

Activation barriers for transitions from one metastable configuration to another have been computed using the climbing-image variant of the nudged elastic band (NEB) method [23] overviewed in Sec. 2.2.2, which allows to identify the transition state of a given process. Reaction paths were optimized by a molecular dynamics based algorithm until the L_∞ norm of the force vector at the transition states was less than 0.05 eV/Å.

The XCrySDen graphical package [56] was used for the rendering of all the atomistic structures presented in this thesis.

Bibliography

[1] P. Hohenberg and W. Kohn. Inhomogeneous electron gas. *Physical Review*, 136:B864–871, 1964.

[2] W. Kohn and L. J. Sham. Self-consistent equations including exchange and correlation effects. *Physical Review*, pages A1133–1138, 1965.

[3] B. Hammer and J. K. Nørskov. Theoretical surface science and catalysis – calculations and concepts. *Advances in Catalysis*, 45:71–129, 2000.

[4] BP statistical review of wold energy. Available on-line at http://www.bp.com/statisticalreview, June 2005.

[5] Jean-Paul Lange. Perspectives for manufacturing methanol at fuel value. *Industrial & Engineering Chemistry Research*, 36:4282–4290, 1997.

[6] A. S. Aricò, S. Srinivasan, and V. Antonucci. DMFCs: from fundamental aspects to technology development. *Fuel Cells*, 1:133–161, 2001.

[7] Bent Sørensen. *Hydrogen and fuel cells*. Elsevier Academic Press, 2005.

[8] Toward a hydrogen economy. Science special issue 305, August 2004.

[9] George A. Olah. Beyond oil and gas: the methanol economy. *Angewandte Chemie International Edition*, 2005.

[10] K. Aasberg-Petersen, J.-H. Bak Hansen, T. S. Christensen, I. Dybkjaer, P. Seier Christensen, C. Stub Nielsen, S. E. L. Winter Madsen, and J. R. Rostrup-Nielsen. Technologies for large-scale gas conversion. *Applied Catalysis A: General*, 221:379–387, 2001.

[11] Alexander Ya. Rozovskii and Galina I. Lin. Fundamentals of methanol synthesis and decomposition. *Topics in Catalysis*, 22:137–150, 2003.

[12] Qijian Zhang, Dehua He, Jinlu Li, Boqing Xu, Yu Liang, and Qiming Zhu. Comparatively high yeld methanol production from gas phase partial oxidation of methane. *Applied Catalysis A: General*, 224:201–207, 2002.

[13] H. D. Gesser and N. R. Hunter. The direct conversion of methane to methanol (DMTM). In E. E. Wolf, editor, *Methanol conversion by oxidative processes*, chapter 12, pages 403–425. Van Nostrand Reinhold, 1992.

[14] Detlef Schröder and Helmut Schwarz. FeO^+ activates methane. *Angewandte Chemie International Edition*, 29:1433–1434, 1990.

[15] Yoshito Shiota and Kazunari Yoshizawa. Methane-to-methanol conversion by first-row transition-metal oxide ions: ScO^+, TiO^+, VO^+, CrO^+, MnO^+, FeO^+, CoO^+, NiO^+, and Cu^+. *Journal of the American Chemical Society*, 122:12317–12326, 2000.

[16] Yoshito Shiota and Kazunari Yoshizawa. A spin-orbit coupling study on the spin inversion processes in the direct methane-to-methanol conversion by FeO^+. *Journal of Chemical Physics*, 118:5872–5879, 2003.

[17] Roy A. Periana, Douglas J. Taube, Scott Gamble, Henry Taube, Takashi Satoh, and Hiroshi Fujii. Platinum catalysts for the high-yeld oxidation of methane to a methanol derivative. *Science*, 280:560–564, 1998.

[18] Lijin Shu, Jeremy C. Nesheim, Karl Kauffmann, Eckard Münck, John D. Lipscomb, and Lawrence Que Jr. An $Fe_2^{IV}O_2$ diamond core structure for the key intermediate Q of methane monooxygenase. *Science*, 275:515–518, 1997.

[19] John. P. Perdew, Kieron Burke, and Matthias Ernzerhof. Generalized gradient approximation made simple. *Physical Review Letters*, 77:3865–3868, 1996.

[20] Stefano Baroni, Stefano de Gironcoli, Andrea Dal Corso, and Paolo Giannozzi. Phonons and related crystal properties from density-functional perturbation theory. *Reviews of Modern Physics*, 73:515–562, 2001.

[21] David Vanderbilt. Soft self-consistent pseudopotentials in a generalized eigenvalue formalism. *Physical Review B*, 41:7892–7895, 1990.

[22] Quantum-ESPRESSO (opEn-Source Package for Research in Electronic Structure, Simulation, and Optimization, http://www.pwscf.org) is an initiative of DEMOCRITOS national simulation centre (http://www.democritos.it) for the development of open-source scientific software.

[23] H. Johnsson, G. Mills, and K. W. Jacobsen. Nudged elastic band method for finding minimum energy paths of transitions. In B. J. Berne, G. Ciccotti, and D. F. Coker, editors, *Classical and quantum dynamics in condensed phase simulations*, chapter 16, pages 385–404. World Scientific, Singapore, 1998.

[24] Carlo Sbraccia. *Computer simulation of thermally activated processes*. PhD thesis, S.I.S.S.A./I.S.A.S., February 2005. Available on-line at http://www.sissa.it/.

[25] Graeme Henkelman, Blas P. Uberuaga, and Hannes Jónsson. A climbing image nudged elastic band method for finding saddle points and minimum energy paths. *Journal of Chemical Physics*, 113:9901–9904, 2000.

[26] John A. Pople, Martin Head-Gordon, Douglas J. Fox, Krishnan Raghavachari, and Larry A. Curtiss. Gaussian-1 theory: A general precedure for prediction of molecular energies. *Journal of Chemical Physics*, 90:5622–5629, 1989.

[27] R. M. Watwe, H. S. Bengaard, J. R. Rostrup-Nielsen, J. A. Dumesic, and J. K. Nørskov. Theoretical studies of stability and reactivity of CH_x species on Ni(111). *Journal of Catalysis*, 189:16–30, 2000.

[28] A. Michaelides and P. Hu. Insight into microscopic reaction pathways in heterogeneous catalysis. *Journal of the American Chemical Society*, 122:9866–9867, 2000.

[29] I. M. Ciobîcă, F. Frechard, R. A. van Santen, A. W. Kleyn, and J. Hafner. A DFT study of transition states for C–H activation on the Ru(0001) surface. *Journal of Physical Chemistry B*, 104:3364–3369, 2000.

[30] C. J. Zhang and P. Hu. Methane transformation to carbon and hydrogen on Pd(100): Pathways and energetics from density functional theory calculations. *Journal of Chemical Physics*, 116:322–327, 2002.

[31] C. J. Zhang and P. Hu. The possibility of single C–H bond activation in CH_4 on a MoO_3-supported Pt catalyst: A density functional theory study. *Journal of Chemical Physics*, 116:4281–4285, 2002.

[32] Anton Kokalj, Nicola Bonini, Carlo Sbraccia, Stefano de Gironcoli, and Stefano Baroni. Engineering the reactivity of metal catalysts: a model study of methane dehydrogenation on Rh(111). *Journal of the American Chemical Society*, 126:16732–16733, 2004.

[33] P. A. Thiel, J. T. Yates Jr., and W. H. Weinberg. The interaction of oxygen with the Rh(111) surface. *Surface Science*, 82:22–44, 1979.

[34] Kevin A. Peterlinz and Steven J. Sibener. Absorption, adsorption, and desorption studies of the oxygen/Rh(111) system using O_2, NO, and NO_2. *Journal of Chemical Physics*, 99:2817–2825, 1995.

[35] S. Schwengmann, H. Over, V. De Renzi, and G. Ertl. The atomic geometry of the O and CO+O phases on Rh(111). *Surface Science*, 375:91–106, 1997.

[36] M. V. Ganduglia-Pirovano and M. Scheffler. Structural and electronic properties of chemisorbed oxygen on Rh(111). *Physical Review B*, 59:15533–15543, 1999.

[37] M. Veronica Ganduglia-Pirovano, Karsten Reuter, and Matthias Scheffler. Stability of subsurface oxygen at Rh(111). *Physical Review B*, 65:245426, 2002.

[38] J. Gustafson, A. Mikkelsen, M. Borg, E. Lundgren, L. Köhler, G. Kresse, M. Schmid, P. Varga, Yuhara J, X. Torrelles, C. Quirós, and J. N. Andersen. Self-limited growth of a thin oxide layer on Rh(111). *Physical Review Letters*, 92:126102, 2004.

[39] L. Köhler, G. Kresse, M. Schmid, E. Lundgren, J. Gustafson, A. Mikkelsen, Yuhara M. Borg J, J. N. Andersen, M. Marsman, and P. Varga. High-coverage oxygen structures on Rh(111): Adsorbate repulsion and site preference is not enough. *Physical Review Letters*, 93:266103, 2004.

[40] Zhi-Pan Liu and P. Hu. General rules for predicting where a catalytic reaction should occur on metal surfaces: a density functional theory study of C–H and C–O bond breaking/making on flat, stepped, and kinked metal surfaces. *Journal of the American Chemical Society*, 125:1058–1967, 2003.

[41] A. Michaelides and P. Hu. Methyl chemisorption on Ni(111) and C–H–M multicentre bonding: a density functional theory study. *Surface Science*, 437:362–376, 1999.

[42] Gui-Chang Wang, Jun Li, Xiu-Fang Xu, Rui-Fang Li, and Junji Nakamura. The relationship between adsorption energies of methyl on metals and the metallic electronic properties: A first-principles DFT study. *Journal of Computational Chemistry*, 26:871–878, 2005.

[43] Gui-Chang Wang, Yu-Hua Zhou, and Junji Nakamura. Characterization of methoxy adsorption on some transition metals: A first principles density functional theory study. *Journal of Chemical Physics*, 122:044707, 2005.

[44] Wei-Xue Li, Catherine Stampfl, and Matthias Scheffler. Oxygen adsorption on Ag(111): A density-fucntional theory investigation. *Physical Review B*, 65:075407, 2002.

[45] Wei-Xue Li, Catherine Stampfl, and Matthias Scheffler. Subsurface oxygen and surface oxide formation at Ag(111): A density-functional theory investigation. *Physical Review B*, 67:045408, 2003.

[46] V. I. Bukhtiyarov, V. V. Kaichev, and I. P. Prosvirin. Oxygen adsorption on Ag(111): X-ray photoelectron spectroscopy (XPS), angular dependent x-ray photoelectron spectroscopy (ADXPS) and temperature-programmed desorption (TPD) studies. *Journal of Chemical Physics*, 111:2169–2175, 1999.

[47] C. I. Carlisle, D. A. King, M.-L. Bocquet, J. Cerdá, and P. Sautet. Imaging the surface and the interface atoms of an oxide film on Ag{111} by scanning tunneling microscopy: Experiment and theory. *Physical Review Letters*, 84:3899–3902, 2000.

[48] N. Bonini, A. Kokalj, A. Dal Corso, S. de Gironcoli, , and S. Baroni. Structure and dynamics of oxygen adsorbed on Ag(100) vicinal surfaces. *Physical Review B*, 69:195401, 2004.

[49] Paola Gava, Guido Fratesi, and Stefano de Gironcoli. (unpublished).

[50] Suljo Linic and Mark A. Barteau. On the mechanism of Cs promotion in ethylene epoxidation on Ag. *Journal of the American Chemical Society*, 126:8086–8087, 2004.

[51] Suljo Linic, Jerome Jankowiak, and Mark A. Barteau. Selectivity driven design of bimetallic ethylene epoxidation catalysts from first principles. *Journal of Catalysis*, 224:489–493, 2004.

[52] Richard M. Lambert, Federico J. Williams, Rachael L. Cropley, and Alejandra Palermo. Heterogeneous alkene epoxidation: past, present, and future. *Journal of Molecular Catalysis A: Chemical*, 228:27–33, 2005.

[53] Hendrik J. Monkhorst and James D. Pack. Special points for Brillouin-zone integrations. *Physical Review B*, 13:5188–5192, 1976.

[54] Charles Kittel. *Introduction to solid state physics, 5th ed.* Wiley, New York, 1976.

[55] P.J. Linstrom and W.G. Mallard, editors. *NIST Chemistry WebBook, NIST Standard Reference Database Number 69.* National Institute of Standards and Technology, Gaithersburg MD, 20899, June 2005. (http://webbook.nist.gov).

[56] A. Kokalj. Computer graphics and graphical user interfaces as tools in simulations of matter at the atomic scale. *Computational Materials Science*, 28:155–168, 2003. Code available from http://www.xcrysden.org/.

Acknowledgments

This *acknowledgments* section would not be adequate if I would not start by thanking my supervisor Stefano for the many interesting discussions we had, and for his exceptional ability to inspire thoughts and suggestions on a large variety of topics, ranging from fundamentals of theoretical condensed matter physics to applications and computational issues.

During my first year at S.I.S.S.A., for the *Magister Philosophiæ* project whose outcome is outlined at page 91, I also benefited from supervision and frequent interaction with Stefano Fabris and Stefano Baroni. Even after that period, we kept in touch and in several occasions they shared their experience with me.

For several discussions, and paricularly when physical and chemical intuition was fundamental, Giacinto Scoles has been a formidable reference point.

Considerable amount of information and material on methane reactions on Rh(111) and Rh/Rh(111) has been provided to me by Nicola Bonini and Anton Kokalj, who started studying these systems before me.

When learning NEB, I profited from the neighborhood of Carlo Sbraccia who implemented the method in the ESPRESSO package. Moreover, it's important to remember the many people who worked and are still working to make this simulation software available to the scientific community. As for "job running", Stefano Cozzini and Moreno Baricevic from the HPC section at S.I.S.S.A. have helped a lot.

I'm debtful to Nicola and Carlo also for the possibility of always knocking on their door for the everyday small questions and problems.

I would also like to remember those who have not been directly related to the work I just presented, but who made S.I.S.S.A. a stimulating scientific

and recreational milieu for me, sharing discussions on our research topics often closely related—yet remarkably different—and sometimes on others not scientific at all: in particular, Demian, Adriano, Michel, Walter, Daniele, and Monica.

Finally, I could not forget to thank my parents, without whom all this would never have taken place, at least not for me, and my girlfriend Anna who is always making my life happier.